



2009

INVESTIGATION OF SURFACE FINE GRAINED LAMINAE, STREAMBED, AND STREAMBANK PROCESSES USING A WATERSHED SCALE HYDROLOGIC AND SEDIMENT TRANSPORT MODEL

Joseph Paul Russo

University of Kentucky, joseph.paul.russo@gmail.com

[Click here to let us know how access to this document benefits you.](#)

Recommended Citation

Russo, Joseph Paul, "INVESTIGATION OF SURFACE FINE GRAINED LAMINAE, STREAMBED, AND STREAMBANK PROCESSES USING A WATERSHED SCALE HYDROLOGIC AND SEDIMENT TRANSPORT MODEL" (2009). *University of Kentucky Doctoral Dissertations*. 750.

https://uknowledge.uky.edu/gradschool_diss/750

This Dissertation is brought to you for free and open access by the Graduate School at UKnowledge. It has been accepted for inclusion in University of Kentucky Doctoral Dissertations by an authorized administrator of UKnowledge. For more information, please contact UKnowledge@lsv.uky.edu.

ABSTRACT OF THESIS

INVESTIGATION OF SURFACE FINE GRAINED LAMINAE, STREAMBED, AND STREAMBANK PROCESSES USING A WATERSHED SCALE HYDROLOGIC AND SEDIMENT TRANSPORT MODEL

Sediment transport at the watershed scale in the Bluegrass Region of Kentucky is dominated by surface fine grained laminae, streambed, and streambank erosion; high in-stream sediment storage; and surface erosion processes. All these processes can be impacted by agricultural, urban, and suburban land-uses as well as hydrologic forcing. Understanding sediment transport processes at the watershed scale is a need for budgeting and controlling sediment pollution, and watershed modeling enables investigation of the cumulative effect of sediment processes and the parameters controlling these processes upon the entire sediment budget for a watershed. Sediment transport is being modeled by coupling the hydrologic model Hydrologic Simulations Program-FORTRAN (HSPF) with an in-house conceptually based hydraulic and sediment transport model. The total yield at the watershed outlet as well as the source fractions from surface fine grained lamina, streambed, and streambank sources; deposition; and biological generation within the streambed are predicted with the sediment transport model. Urbanization scenarios are then run on the calibrated model so as to predict the sediment budget for the South Elkhorn watershed for present and future conditions.

KEYWORDS: sediment transport modeling, surface fine grained lamina, erosion, HSPF, watershed

Joseph Russo

12-18-2009

INVESTIGATION OF SURFACE FINE GRAINED LAMINAE, STREAMBED, AND
STREAMBANK PROCESSES USING A WATERSHED SCALE HYDROLOGIC
AND SEDIMENT TRANSPORT MODEL

By

Joseph Paul Russo

James Fox

Director of Thesis

Kamyar Mahboub

Director of Graduate Studies

12-18-2009

RULES FOR THE USE OF THESES

Unpublished theses submitted for the Master's degree and deposited in the University of Kentucky Library are as a rule open for inspection, but are to be used only with due regard to the rights of the authors. Bibliographical references may be noted, but quotations or summaries of parts may be published only with the permission of the author, and with the usual scholarly acknowledgments.

Extensive copying or publication of the thesis in whole or in part also requires the consent of the Dean of the Graduate School of the University of Kentucky.

A library that borrows this thesis for use by its patrons is expected to secure the signature of each user.

Name

Date

THESIS

Joseph Paul Russo

The Graduate School
University of Kentucky

2009

INVESTIGATION OF SURFACE FINE GRAINED LAMINAE, STREAMBED, AND
STREAMBANK PROCESSES USING A WATERSHED SCALE HYDROLOGIC
AND SEDIMENT TRANSPORT MODEL

THESIS

A thesis submitted in partial fulfillment of the requirements
for the degree of Master of Science in Civil Engineering
in the College of Engineering at the University of Kentucky

By

Joseph Paul Russo

Lexington, Kentucky

Director: Dr. James Fox, Professor of Civil Engineering

Lexington, Kentucky

2009

Copyright © Joseph Paul Russo 2009

I dedicate this thesis to the love of my life, Jessica.

Acknowledgements

This work benefited from the input of several people. First and foremost, I would like to thank my Thesis Chair, Dr. James Fox, for his continued support, encouragement, and insight. I would like to thank the other members of my Thesis Committee: Dr. Scott Yost and Dr. Yin-Tin Wang. All three of these instructors aided my research and graduate education greatly. I would also like to thank Dr. Chandramouli Viswanathan for his help and guidance.

Several institutions provided invaluable help to my Master's Research. I would like to thank the University of Kentucky's Department of Civil Engineering for providing educational support, the University of Kentucky's Environmental Research and Training Laboratory, under the management of Tricia Coakley, for the use of their laboratory and guidance, and the funding sources for my Master's Research including the United States Geologic Survey via the 104b program maintained by the Kentucky Water Resources Research Institute.

I would like to thank my fellow research colleagues Darren Martin, Allen Cantrell, Sruti Pulugurtha, Daniel Doss, and Forrest Holdsworth for providing help, insight, and friendship throughout my research endeavors.

Finally, I would like to thank my friends and family who have helped me to reach this goal.

TABLE OF CONTENTS

Acknowledgements.....	iii
List of Tables	vii
List of Figures	viii
Chapter 1: Introduction and Research Objectives	1
1.1 Environmental Concerns Associated with Fine Sediments.....	1
1.2 In-stream Sediment Transport Processes in Lowland Watersheds	3
1.3 Modeling In-stream Sediment Transport Processes at the Watershed Scale	7
1.4 Impact of Urbanization Upon In-stream Sediment Transport Processes	11
1.5 Objective	13
1.6 Significance of Results from this Research.....	16
1.7 Contents of the Thesis.....	18
Chapter 2: Sediment Transport Modeling Review	21
2.1 Empirical, Conceptual and Physics-based Watershed Erosion Models	21
2.2 Lumped or Distributed Watershed Erosion Models.....	23
2.3 Temporal Scale of Watershed Erosion Models.....	24
2.4 In-stream Sediment Transport Models	24
2.5 Reaction-based Stream Models.....	26
2.6 In-stream Processes within Sediment Transport Models	27
Chapter 3: Model Framework and Formulation	29
3.1 Model Framework.....	29
3.2 Hydrologic Watershed Model Formulation	30
3.3 In-stream Sediment Transport Model	45
3.3.1 Hydraulic Variables	45
3.3.2 Sediment Mass Balance Stream-Reach	46
3.3.3 Sediment Transport Capacity and Residual Capacity	48
3.3.4 Fluvial Erosion	50
3.3.5 Unsteady Fluvial Shear Stresses.....	50
3.3.6 Budgeting Sediment Sources.....	52
3.3.7 Bank Erosion	53
3.3.8 SFGL Erosion.....	55

3.3.9 Bed Erosion	57
3.3.10 Deposition.....	58
3.3.11 Sediment Routing	62
Chapter 4: Study Watershed	64
Chapter 5: HSPF Watershed Model Calibration, Validation, and Sensitivity Analysis...	69
5.1 Model Set Up	69
5.2 Model Calibration	72
5.3 Model Sensitivity	81
5.4 Model Validation.....	83
Chapter 6: In-Stream Model Calibration	88
6.1 Model Set Up, Input Data and Parameterization.....	88
6.2 Calibration Data Collection and Calculations.....	101
6.2.1 Suspended Sediment Samples	101
6.2.2 Sediment Yield Data Analysis.....	104
6.3 Model Calibration	108
6.4 Model Sensitivity	112
6.5 Model Validation.....	124
6.6 Discussion	125
Chapter 7: Sediment Transport Model Results.....	126
7.1 Results of Current Conditions	126
7.1.1 Sediment Yield	126
7.1.2 Sediment Yield Source Fractions	129
7.1.3 Temporal Change in the Streambed	130
7.1.4 Temporal Change in the SFGL.....	132
7.1.5 Bank Erosion	133
7.2 No Loading from Uplands/Tributaries	134
7.2.1 Sediment Yield	135
7.2.2 Sediment Yield Source Fractions	136
7.2.3 Temporal Change in the Streambed	137
7.2.4 Temporal Change in the SFGL.....	138
7.2.5 Bank Erosion	139

7.3 Double Loading from Upland/Tributaries.....	140
7.3.1 Sediment Yield	140
7.3.2 Sediment Yield Source Fractions	141
7.3.3 Temporal Change in the Streambeds.....	143
7.3.4 Temporal Change in the SFGL.....	144
7.3.5 Bank Erosion	144
7.4 Discussion of Results for the Three Year Period	145
Chapter 8: Urbanization Results	149
8.1 Frequency analysis Results for the Simulation Periods	154
8.2 Sediment Budget Results for the Simulation Periods	156
8.3 Bed Supply for the Simulation Period	162
8.4 Discussion	165
Chapter 9: Conclusions.....	170
Appendix A.....	173
References.....	180
Vita.....	191

List of Tables

Table 1: <i>Table of Input and Calibration Data for HSPF and origin.</i>	70
Table 2: <i>Table of commonly accepted hydrologic model calibration statistics.</i>	74
Table 3: <i>Table of HSPF parameters and their range of values.</i>	77
Table 4: <i>Table of HSPF parameters and their calibrated values for a large delineation.</i>	78
Table 5: <i>Table of the upper zone nominal storage monthly calibrated values for a large delineation.</i>	78
Table 6: <i>Table of the interception monthly calibrated values for a large delineation.</i>	79
Table 7: <i>Table of the lower zone evapotranspiration parameters and their monthly calibrated values for a large delineation.</i>	79
Table 8: <i>Table of observed and simulated flow statistics for the year 2007 and 2008.</i>	84
Table 9: <i>Table of observed and simulated flow statistics for calendar seasons.</i>	84
Table 10: <i>Table of observed and simulated flow frequencies for the year 2007.</i>	86
Table 11: <i>Table of observed and simulated flow frequencies for the year 2008.</i>	86
Table 12: <i>Table of observed and simulated daily flow t-test for 2007.</i>	87
Table 13: <i>Table of observed and simulated daily flows t-test for 2008.</i>	87
Table 14: <i>Table of input data and parameter values for the sediment transport model.</i> .	89
Table 15: <i>Table of mean Total Suspended Solids loading (Coulter et al. 2004).</i>	99
Table 16: <i>Table of sediment yield for each storm event.</i>	108
Table 17: <i>Table of general guidelines for sediment component evaluation (Donigian, 2002).</i>	109
Table 18: <i>Table of observed and simulated sediment yield statistics.</i>	110
Table 19: <i>Table of sensitivity parameters and range of values.</i>	115
Table 20: <i>Table of return interval (days), stream flow (cms), sediment flux (kg/s), and total daily yield (kg).</i>	128
Table 21: <i>Table of source fractions and annual yields for the three year calibration and validation period.</i>	130
Table 22: <i>Table of source fractions and annual yields for each source.</i>	137
Table 23: <i>Table of source fractions and annual yields for each source under increased upland/triburary loading.</i>	142
Table 24: <i>Table of impervious areas for each estimated urbanization rate.</i>	151
Table 25: <i>Table of input data and parameter values for the re-calibrated sediment transport model.</i>	153
Table 26: <i>Frequency analysis of observed and simulated streamflows.</i>	154
Table 27: <i>Table of streamflow and sediment flux frequency analysis for the simulation periods.</i>	155
Table 28: <i>Table of annual sediment yields and source fractions for each sediment source for each simulation run.</i>	157

List of Figures

Figure 1: <i>Conceptual Stream Channel and Sediment Transport Processes</i>	4
Figure 2: <i>Modeling framework for watershed modeling of in-stream sediment processes.</i>	30
Figure 3: <i>Conceptual diagram of a pervious land segment for HSPF.</i>	35
Figure 4: <i>Conceptualization of stream reach mass balance hydraulic processes.</i>	42
Figure 5: <i>Conceptualization of stream reach mass balance for sediment transport processes.</i>	47
Figure 6: <i>Figure of Bank Erosion.</i>	53
Figure 7: <i>Conceptualization of SFGL and Bed Erosion Model.</i>	56
Figure 8: <i>Figure 7.9 from H. Chang (1988) on page 149. "Vanoni nomograph."</i>	61
Figure 9: <i>Figure of z^* versus deposition coefficient.</i>	62
Figure 10: <i>Location map for the study watershed.</i>	64
Figure 11: <i>Map of the South Elkhorn Watershed, Lexington Ky.</i>	65
Figure 12: <i>(a) 1992 urban area, (b) 2001 urban area, (c) 1992 NLCD, and (d) 2001 NLCD.</i>	67
Figure 13: <i>Chart of HSPF parameters and their sensitivity to a large delineation.</i>	82
Figure 14: <i>Observed and simulated flows for 2007.</i>	85
Figure 15: <i>Observed and simulated flows for 2008.</i>	85
Figure 16: <i>Graph of peak storm flow and sediment yield showing 2.50 cms as the boundary between high and low flows.</i>	91
Figure 17: <i>Graph of $C\tau$. Where the horizontal axis represents the depth to width ratio and the vertical axis is the shear stress coefficient.</i>	97
Figure 18: <i>TSS concentration (points) and flow rate (solid black) data for a) December 2, 2007, b) February 21, 2008, c) April 10, 2008, d) May 15, 2008, e) July 30, 2008, and f) July 31, 2008, and g) October 7, 2008.</i>	103
Figure 19: <i>Figure of sediment flow over time for the storm events a) December 2, 2007, b) February 21, 2008, c) April 10, 2008, d) May 15, 2008, e) July 30, 2008, and f) July 31, 2008, and g) October 7, 2008.</i>	107
Figure 20: <i>Graphs of observed and modeled sediment yield for the storm events on a) December 2, 2007, b) February 21, 2008, c) April 10, 2008, d) May 15, 2008, e) July 30, 2008, and f) July 31, 2008, and g) October 7, 2008.</i>	111
Figure 21: <i>Chart of in-stream sediment model parameters and their sensitivity.</i>	116
Figure 22: <i>Chart of deposition coefficient and settling velocity sensitivity.</i>	118
Figure 23: <i>Chart of eroding sediment fractions with changes in t_d parameter with (a) tributary loading and (b) no tributary loading.</i>	119
Figure 24: <i>Chart of eroding sediment fractions with changes in $D_{sfgl\ max}$ parameter with (a) tributary loading and (b) no tributary loading.</i>	120
Figure 25: <i>Chart of eroding sediment fractions with changes in $\tau_{cr\ (sfgl)}$ parameter.</i>	122
Figure 26: <i>Chart of eroding sediment fractions with changes in $\tau_{cr\ (bed)}$ parameter.</i>	123

Figure 27: <i>Chart of eroding sediment fractions with changes in $\tau_{cr (bank)}$ parameter.</i>	124
Figure 28: <i>Figure of Sediment Flux (kg/s) for the three year calibration and validation period.</i>	127
Figure 29: <i>Figure of stream flow (cms) for the three year calibration and validation period.</i>	127
Figure 30: <i>Sediment budget (metric tons per year) in the South Elkhorn watershed for the three year calibration and validation period.</i>	129
Figure 31: <i>Graph of bed supply (kg) and bed depth (cm) for the three year calibration and validation period.</i>	131
Figure 32: <i>Graph of SFGL supply (kg) and bed depth (cm) for the three year calibration and validation period.</i>	132
Figure 33: <i>Figure of bank erosion mass (kg) and bank depth eroded (m) for the three year calibration and validation period.</i>	134
Figure 34: <i>Sediment flux with no upland/tributary input.</i>	136
Figure 35: <i>Sediment budget for one year in the South Elkhorn watershed under no upland/tributary loading conditions.</i>	137
Figure 36: <i>Graph of bed supply (kg) and bed depth (cm) under no upland/tributary loading conditions.</i>	138
Figure 37: <i>Graph of SFGL supply (kg) and bed depth (cm) under no upland/tributary loading conditions.</i>	139
Figure 38: <i>Figure of bank erosion mass (kg) and bank depth eroded (m) under no upland/tributary loading conditions.</i>	140
Figure 39: <i>Sediment flux (kg/s) with increased upland/tributary loading.</i>	141
Figure 40: <i>Sediment budget for one year in the South Elkhorn watershed under increased upland/tributary contribution conditions.</i>	142
Figure 41: <i>Graph of bed supply (kg) and bed depth (cm) under increased upland/tributary loading conditions.</i>	143
Figure 42: <i>Graph of SFGL supply (kg) and bed depth (cm) under increased upland/tributary loading conditions.</i>	144
Figure 43: <i>Figure of bank erosion mass (kg) and bank depth eroded (mm) under increased upland/tributary loading conditions.</i>	145
Figure 44: <i>Map of conceptual Urban/Agricultural borders at 20 years for each estimated urbanization rate.</i>	150
Figure 45: <i>Figure of Sediment Budgets for the simulation periods.</i>	161
Figure 46: <i>Figure of bed supply for simulation runs.</i>	165

Chapter 1: Introduction and Research Objectives

1.1 Environmental Concerns Associated with Fine Sediments

Fine sediment is defined here to include in-stream, previously eroded and transported particulate inorganic and organic matter with a size range of 0.7 to 500 μm . Fine sediment erosion, transport, and fate are of great environmental concern. Unlike chemical pollutants which can be addressed directly via effluent controls and regulations for sources, sediment is a naturally occurring and vital biological component of stream, river, lake and reservoir ecosystems. Sediment provides a matrix for the microbial community in-stream, and provides a habitat for aquatic plants and other benthic organisms, and sediment erosion and scour are a part of the landscape formation process (Stone and Droppo, 1994; Lehmann et al, 1997; Turkington et al, 2005). However, excess fine sediment can be a pollutant which can disrupt aquatic ecosystems as well as impact human health and infrastructure (Wood and Armitage; 1997).

Fine sediment can harmfully impact biological components of stream ecosystems including fish, algae and macrophytes, and benthic invertebrates (USEPA 2004). Excessive concentrations of fine sediments can impact fish species by a number of mechanisms including: blinding fish and impairing their ability to hunt; reducing their growth rate; reducing their tolerance to disease; reducing their spawning habitats; adversely affecting the growth of their eggs and juveniles; modifying their natural migration patterns; reducing the abundance of available food; and clogging their gills causing suffocation (Wood and Armitage, 1997; FISRWG, 1998; USEPA, 1999; Richardson and Jowett, 2002; Spiro and Stigliani, 2003). At the base of the food chain,

excess suspended fine sediments can impact algal communities by reducing the penetration of light into the water column, and thus inhibiting the ability for photosynthetic plants to grow (Wood and Armitage; 1997). Sediment can harmfully impact algae as well as macrophytes by a number of mechanisms including: reducing the organic content of cells; damaging cellular bodies, leaves and stems due to abrasion of transported sediments; preventing attachment of organic substrate to algal cells; and by smothering and eliminating periphyton and aquatic macrophyte in extreme instances (Wood and Armitage; 1997). Sediment impacts the benthic invertebrates within the bed of stream or river by the following mechanisms including: altering substrate composition and changing the suitability of the substrate for some taxa; increasing drift due to sediment deposition or substrate instability; harmfully affecting respiration due to the deposition of silt on respiration structures or low oxygen concentrations associated with silt deposits; and harmfully affecting feeding activities by impeding filter feeding due to an increase in suspended sediment concentrations (Wood and Armitage; 1997).

In addition to harmfully impacting ecosystem function, fine sediment can harmfully impact human health and infrastructure. High sediment levels can disrupt intake to water treatment plants, and sediments can fill reservoirs, reducing their capacity for water supply needs (Morris and Fan, 1997). Excess fine sediments can change bed forms, and affect the aesthetics of recreational waters (EPA, 1999; Richardson and Jowett, 2002). From the uplands, pesticides, fertilizers, organic matter, and heavy metals and other potentially hazardous substances can attach themselves onto the soil particles and eventually wash into the stream (Thoms, 1987; Lartiges et al., 2000; Zappou, 2001). Fine silt and clay sized particles are of particular importance for this concern because of

their large surface area, geochemical properties, and ability to absorb and transport these pollutants (Wood and Armitage; 1997; Long et al., 1998; Owens et al, 2001). Erosion and sediment transport process effect the final pollutant and sediment loading for an affected stream, and understanding sediment erosion, transport, and fate processes is a vital step toward controlling sediment pollution.

1.2 In-stream Sediment Transport Processes in Lowland Watersheds

This thesis focuses on in-stream sediment transport processes in lowland watersheds. A lowland watershed is defined as a watershed having mild watershed and stream gradients that cause significant storage of fine sediments in the stream channel and frequent erosion of streambanks (Walling et al. 2006; Davis 2008). In-stream processes refer to sediment transport within the stream corridor and includes streambank erosion, streambed erosion and storage, and erosion, deposition and development of the streambed surface or surface fine-grained laminae (SFGL). Figure 1 shows a conceptualized stream channel and the involved sediment transport processes.

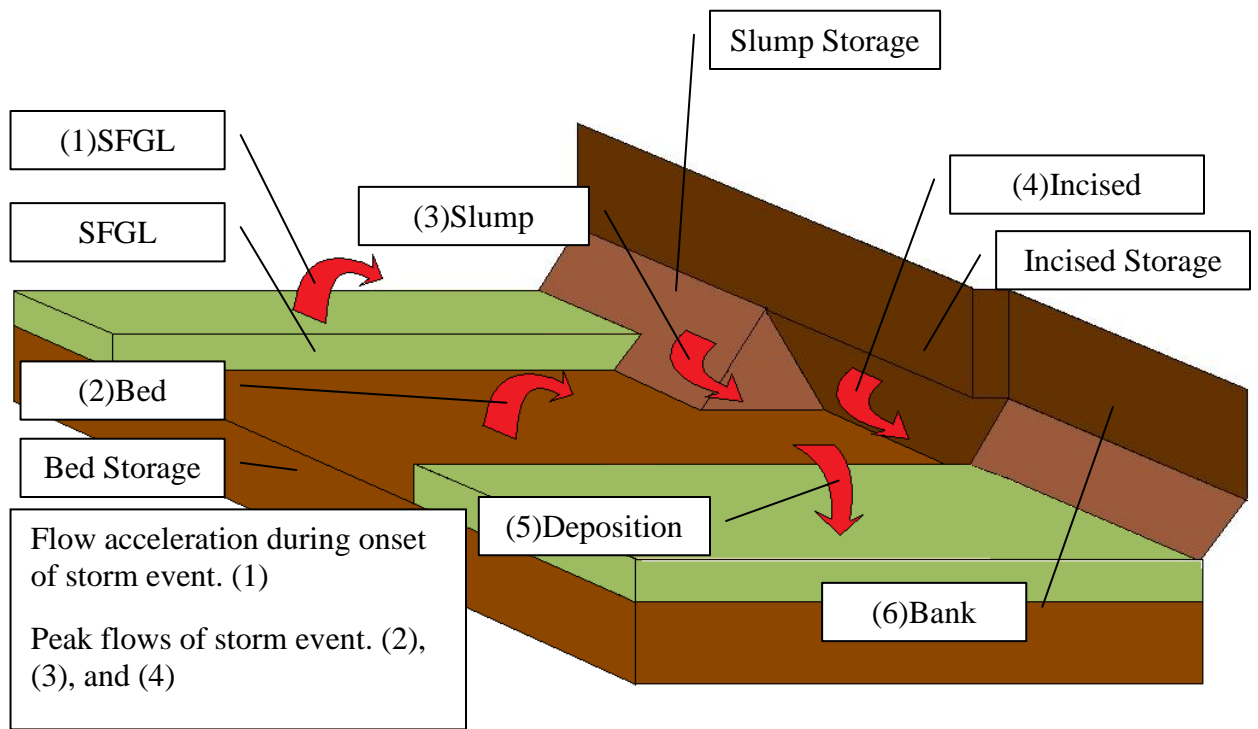


Figure 1: *Conceptual Stream Channel and Sediment Transport Processes*

Figure 1 shows erosion from three sediment sources, the surface fine grained lamina, the slump banks, and the incised banks. Streambanks fail and erode by two mechanisms, hydraulic erosion and mass wasting (Millar and Quick, 1997; Julian and Torres, 2006). Fluvial erosion occurs during the rising limb of the hydrograph when flow acceleration induces high shear stresses that overcome the critical shear stress or resistance of sediment particles and the erosion of fine sediment occurs (Papanicolaou and Hilldale, 2002). The second mechanism is mass wasting. Mass wasting is initiated due to fluvial erosion during periods of prolonged rainfall when streambank toe material becomes entrained and eroded, which results in undercutting of the bank (Millar and Quick, 1998; Simon et al., 2000; Cancienne et al, 2008; Simon et al, 2009; Shields et al, 2009). Thereafter, water content and bulk density of the streambanks become high from the prolonged rainfall resulting in a decrease in sediment particle cohesion and increase in pore pressure (Millar and Quick, 1998; Simon et al., 2000; Cancienne et al, 2008;

Simon et al, 2009; Shields et al, 2009). Mass wasting failure finally occurs during hydrograph recession when the confining pressure of the flow is lost and the streambank either slumps (i.e., sloughing) or fails as a cantilever (Millar and Quick, 1998; Simon et al., 2000; Cancienne et al, 2008; Simon et al, 2009; Shields et al, 2009). Figure 1 shows the erosion of incised banks during the peak flows of a storm event, and the mass failure of the banks during the recession of the hydrograph which regenerates the storage of slump bank material.

Sediment can be temporarily stored in the streambed of a stream or river. In-stream deposited sediments are temporarily stored during low and moderate flow conditions until a subsequent hydrologic event repeats the sediment transport processes and removes the sediment (Walling and Amos, 1999; Smith et al, 2003). The result of the sediment transport processes is the existence of a dynamic streambed defined by intermittent sediment erosion and temporary sediment storage in the lowland watershed system. This can be seen in Figure 1 as the storage of sediment in the slump bank, bed and surface fine grained lamina material.

It should be pointed out that hydrodynamic forces are the most important mechanism involved in sediment transport because hydrodynamic processes provide the force needed to erode the streambank and streambed (Dietrich et al., 1999; Liu et al., 2002; Aksoy and Kavvas, 2005). Transport mechanisms can be described as detachment by shear stress, detachment by impact from large particles in the stream striking the bed, transport by flow, and deposition by decreasing transport capacity (Aksoy and Kavvas, 2005). For these reasons, hydrodynamic and hydraulic forcing need to be represented when modeling in-stream sediment transport.

In addition to hydrodynamic forces, biological processes become pronounced within the biologically active aerobic surface fine-grain lamina (SFGL). The SFGL exists at approximately the top 1 cm of the streambed surface and can be defined as a high water content, “fluffy”, “buoyant” layer with substantial inter-particle–inter-floc spaces–pores with a density of approximately 1.1 g/cm^3 where biological processes are persistent (Droppo and Stone, 1994; Droppo and Amos, 2001). The SFGL is composed of recently deposited fine inorganic and organic sediment matter as well as heterotrophic bacteria, autotrophic algae, fungi, macrophytes (aquatic plants) and benthic macroinvertebrates (e.g., crayfish, aquatic worms). Thus, the SFGL has been termed a location for biofilm development due to the growth of microorganisms within the SFGL. Biofilm development causes the stabilization or ‘biostabilization’ of the streambed defined as the increasing of the critical shear stress or stabilization of the SFGL due to biofilm development in the SFGL that causes individual particles to stick together (Droppo and Amos, 2001). Biofilm development and biostabilization in the SFGL is heavily dependent upon the live bodies of microorganisms that produce biomass composed of their excretions or mucilage of the microbes. This substance has been termed extracellular polymeric substances (EPS) in the literature and is a thick gluey substance composed of exopolysaccharides (polymers consisting of sugar that is excreted by microorganisms) that binds soil aggregates together (Decho, 1990). EPS has been considered the most important factor in biostabilization of the SFGL and as a biofilm growth media (Worner, et. al., 2002; Lartiges et. al., 2000; Droppo et. al., 1997; Thornton, 2002). While the SFGL is loosely structured and dynamic, the heterotrophic bacteria, algal grazers, and macrophytes excrete EPS that provide a ‘stickiness’ or

cohesiveness to the SFGL, providing a matrix that fosters interrelated biogeochemical processes including: (1) the decomposition of sediment particulate organic matter derived from erosion sources by heterotrophic bacteria within the SFGL; and (2) the growth of microbial and algal biomass through breakdown of particulate nutrients and organic matter within the SFGL as well as uptake of nutrients and dissolved carbon from the water column (Stehr et al., 1995; Kies et al., 1996; Lartiges et al., 2000; Thornton, 2002; Worner et al., 2002; Zimmerman-Timm, 2002). The development of biological processes within the SFGL is further impacted by benthic macroinvertebrates that perturb the sediment surface increasing its porosity and ability to support aerobic growth and decomposition processes.

1.3 Modeling In-stream Sediment Transport Processes at the Watershed Scale

In this thesis, a watershed modeling approach is taken to study, estimate and predict in-stream sediment transport processes at the watershed scale. Streambank erosion, streambed erosion and temporary storage, and biofilm development in the SFGL are modeled at the watershed scale. There is a need for performing watershed erosion and sediment transport modeling across an entire watershed in order that future land-use scenarios can be investigated and optimized (Brun and Band, 2000; Watts et al., 2003; Luo et al., 2006; Hunter and Walton, 2008; Cho et al., 2009). Watershed modeling involves understanding the processes of water and sediment transport and representing those processes with equations that can be run *via* a computer. A computer model is much less expensive and less difficult than constantly measuring sediment transport (Kuhnle, 1996). Once a computer model is built it can be used to predict the effects of future events on the environment, such as the effect increased impervious area will have

on sediment yield, and proper controls can then be created to prevent such problems from occurring (Bora and Bera, 2003; Zappou, 2001).

Hydrologically driven watershed scale erosion and sediment transport models can fall into one of three categories including empirical, physics-based, and conceptual-based models. An empirical model is a purely data driven model, which requires many years of collected data to accurately predict future results (Aksoy and Kavass, 2005; Merritt et al, 2003). Physical models model sediment transport based on physical laws, with coefficients usually obtained from laboratory experiments (Aksoy and Kavass,2005; Merritt et al, 2003). Conceptual watershed models usually lump the uplands together into hydrological response units, or sub catchments, and derive average spatial values for these catchments so as to simplify the calculation process (Aksoy and Kavass,2005; Merritt et al, 2003).

In-stream processes can be cumbersome (i.e., require high data inputs and dense computational domain) to model at the watershed scale due to the variability of their sediment make-up across a watershed and fluid turbulence complexity throughout a stream segment. For example, even small watersheds contain several miles of streambanks which can be heterogeneous and estimating erosion rates for these streambanks is compounded due to the varying degrees of vegetation coverage, exposure to sidewall shear stresses, mass failure, and root density which can make quantifying an erosion rate/yield difficult.

A recent critical review of the literature found that hydrologically driven watershed scale erosion and sediment transport models do not typically represent the

processes involved with in-stream sediment transport. Many watershed scale studies include streambank erosion in their modeling, but the majority of these studies include streambank erosion source terms in their model with a long-term, empirical relationship created by estimating bank erosion rates with erosion pins or aerial photographs and computing an average rate of streambank retreat per year (Kinsey-Henderson et al., 2005; Smith and Dragovich, 2008; Simon, 2008; Wilkinson et al., 2009). Other researchers have performed in-depth studies of streambank erosion and a process-based understanding and physics-based modeling tools to evaluate stream-corridor erosion, e.g., the CONCEPTS model (Langendoen et al., 2001), has advanced greatly in recent years; however, these models are typically limited to modeling single banks and typically do not perform watershed scale modeling (Langendoen et al., 2001; Mosselman, 1998; Simon et al., 2000). Jakeman et al. (1999) modeled streambank erosion conceptually on an event basis and coupled streambank erosion with a watershed scale model but was limited to a constant lateral source term. Watershed scale modeling of streambed sediment transport has also been limited, as streambed and streambank processes are typically combined into one term in watershed scale models, e.g. the INCA-Sed models (Jarrit and Lawrence; 2006). Large scale stream-reach models include streambed erosion and deposition processes (Duan and Nanda, 2006; Lui et al., 2002; Viney and Sivapalan, 1999; Jarritt and Lawrence, 2007), however this application is limited for watershed scale models. Allen et al., 2008 used a modified SWAT hydrologic and hydraulic model to simulate channel evolution at the catchment scale, but erosion was considered to only occur from bed sources. No studies were found in the literature that modeled SFGL processes for a

watershed and this represents a further need for development within the environmental water resources community.

Based on the above review, it was found that hydrologically driven watershed prediction models typically do not accurately represent in-stream sediment transport processes including streambank erosion, streambed erosion and temporary storage, and biofilm development in the SFGL. The modeling limitation is partially due to the fact that while empirical equations of streambank erosion are available, accurate process-based bank erosion models are less developed, particularly for composite watershed modeling applications where simple, computationally inexpensive subroutines with low data requirements are desirable (Borah and Bera, 2003; Merritt et al., 2003; Kalin et al., 2003). There is a need to build erosion models that are conceptually simple, but capture all the necessary in-stream sediment processes with simple data requirements while providing a representation of the dominant underlying processes.

In the present thesis, an existing conceptual hydrologic watershed model is coupled with a new conceptual model of in-stream sediment transport processes. A conceptual modeling framework is adopted with the intent to advance modeling of in-stream processes in order to make estimates and predictions of in-stream results for watersheds while not being overly burdened by data requirements that can be difficult to obtain at the watershed scale. It will be shown that hydrologic, hydraulic, sediment transport, and biologic equations used in the conceptual models are process based. These equations will be lumped across the subcatchment scale in order to reduce data and computational requirements. It is the intent that the modeling framework is flexible

enough to allow low data requirements but process-based enough that the equations can be discretized when high data requirements are available in future research.

1.4 Impact of Urbanization Upon In-stream Sediment Transport Processes

Urbanization is defined as disruptive upland development, most notable the construction of impervious areas. In order to understand the impact of urbanization upon in-stream sediment processes, it is important to explain the connectivity between the uplands of a basin and the stream corridor. Hydrodynamics is the driving mechanism impacting sediment transport in the stream or river, and the flow can be significantly affected by land-use change in the uplands (Kuhnle et al., 1996; Trimble, 1997). Kuhnle et al. (1996) studied land-use change in watersheds and noted that the major benefit in changing from erodible to non-erodible lands within high infiltration capacity is not the reduction in sediment load from the uplands, but that the change in land reduced the peak flows from the watershed and reduced channel erosion. Trimble (2008) noted a similar trend when studying an urbanizing watershed—the urbanizing of the watershed caused a significant increase in sediment yield from increased channel flows.

While urbanization might be focused in the uplands of a watershed, urbanization is an indirect forcing of in-stream sediment transport processes. Urbanization causes impervious surfaces such as parking lots or roadways that do not infiltrate water from heavy rainfall events, thus increasing runoff and causing flooding. Urbanization indirectly increases in-stream sediment transport, i.e., erosion of streambeds and streambanks, by increasing the frequency and volume of storm flows, which causes the stream corridor to widen to accommodate the new flow volumes (Wolman, 1967; Nelson and Booth, 2002; Davis, 2008). In addition to higher volumes, water originated from

urban areas can be starved for sediment. The upland sediment supply is low thus the flow has more energy to erode the streambed and streambanks. The results is that the stream corridor erodes and works to adjust to a new geomorphologic equilibrium (Allen et al., 2008).

Review of the literature shows that a number of studies have reported the increase of erosion and sediment transport processes in the stream corridor due to urbanization. Trimble (1997) highlights the idea that erosion of the stream corridor can be a major source of sediment yield from urbanizing areas, and the study found that nearly two thirds of the sediment yield originated from the stream channel in a San Diego Creek. Nelson and Booth (2002) characterized the role of human activity associated with urbanization in a watershed on the western slopes of the Cascade Mountains and demonstrated the enhanced stream-channel erosion accounted for 20% of the sediment yield, even in their steep watershed that included massive landslides in the uplands. Fraley et al. (2009) studied the impact of urbanization upon in-stream processes in the Valley Creek Watershed near Philadelphia, Pennsylvania and found that 49% of the sediment yield originated from the stream corridor.

While the above studies have been important to understand the linkages between urbanization and the stream, fewer studies have focused on discriminating the individual processes within the stream corridor, including streambank erosion, streambed erosion and storage, and erosion, deposition and development of the SFGL. Few, if any, studies have modeled all of these processes at the watershed scale in the context of an urbanizing watershed. It has been noted that urbanizing watersheds have higher streambank erosion as compared to than non-urban watersheds (Smith and Dragovich, 2008) due to the

stream widening mechanisms detailed above. Fraley et al. (2009) found that although streambank erosion was a potentially dominant source of sediment by comparison with annual suspended sediment load, streambed sediment storage and potential for remobilization is of the same order of magnitude as the mass of sediment derived from streambank erosion. Sediment yield from construction in an urbanizing watershed can be up to several hundred times greater than forest watersheds (Wolman, 1967) and particularly in lowland watersheds, sediment loads during development can become stored in-stream—sometimes termed ‘legacy sediments’—and it is well recognized that sediment loading originated from the sediment stored in the bed are important even decades after urban development takes place. No studies were found in the literature that investigated or modeled the impact of urbanization upon the SFGL.

In this thesis, emphasis is placed upon the impact of urbanization upon in-stream sediment processes including streambank erosion, streambed erosion and storage, and erosion, deposition and development of the SFGL. Urbanization rates are projected forward for the study watershed in order to see how these processes might be altered in the future as predicted with the watershed modeling framework.

1.5 Objective

The health of stream ecosystems are very much dependent upon upland and upstream conditions. Pollutants that are present in the uplands of our communities will eventually be washed into our streams, lakes, or groundwater if controls are not in place, and the runoff of the uplands controls the erosion, transport, and fate of contaminants, sediment, and organic matter in these aquatic systems. Sedimentation has been identified as the predominant impairment affecting rivers and streams within the Commonwealth of

Kentucky (KYDOW 2006). The presented research works towards the coupling of a computationally simple yet representative watershed scale erosion and sediment transport model which includes multiple in-stream sediment processes. It is expected that the coupling these models is so that in-stream processes, such as streambank erosion, can be more accurately modeled at the watershed scale.

The overarching objective of this thesis was to gain a better understanding of in-stream sediment transport processes at the watershed scale by using a modeling tool that can simulate multiple in-stream sediment processes present watershed conditions and under varying urbanization rates. To meet the overarching objective, the following specific objectives of this thesis were:

1. To review watershed and river models capable of estimating and prediction erosion and in-stream transport.
2. To formulate a conceptual-based watershed scale model capable of estimating and predicting in-stream processes including the ability to provide results of fine sediment flux from the stream corridor of a watershed; the flux of sediment derived from the streambanks, streambed, and SFGL; the temporal change within the stored sediment in the streambed; the temporal fate of the SFGL in terms of storage and biofilm re-development; the recession rate of the bank; and the increased volume of water to the stream channel.
3. To select and describe a study watershed for application of the watershed modeling tool.
4. To describe the methods for collection and calculation of flow and sediment data needed for calibration of the watershed modeling tool.

5. To perform a sensitivity analysis of the parameters impact upon the in-stream processes represented within the model.
6. To calibrate and provide results of the model simulation for the study watershed for present conditions and specifically provide results of: (i) fine sediment flux from the stream corridor of a watershed over time; (ii) the flux of sediment derived from the streambanks, streambed, and SFGL over time; (iii) the temporal change within the stored sediment in the streambed over time; (iv) the temporal fate of the SFGL in terms of storage and biofilm re-development over time; (v) the recession rate of the banks; and (vi) the increase in water volume to the stream channel.
7. To make predictions using the model for varying urbanization rates within the watershed and specifically provide predictions regarding: (i) fine sediment flux from the stream corridor of a watershed in the future; (ii) the flux of sediment derived from the streambanks, streambed, and SFGL in the future; (iii) the temporal change within the stored sediment in the streambed in the future; (iv) the temporal fate of the SFGL in terms of storage and biofilm re-development in the future; (v) the recession rate of the banks; and (vi) the increase in water volume to the stream channel.

1.6 Significance of Results from this Research

The results of this research have significance in several areas, most notable, the change from reactive watershed management to proactive watershed management. The fine sediment flux from the watershed over time; the flux of sediment derived from the streambanks, streambed, and SFGL over time; the temporal change within the stored sediment in the streambed over time; the temporal fate of the SFGL in terms of storage and biofilm re-development over time; the recession rate of the banks, and the increase in water volume to the stream channel can all be used to assess future water quality problems from urbanization. Most fine sediment water quality programs involve the sampling of surface waters for fine sediments and then the analysis determines if the water quality standards have been breached after the pollution has already taken place (USEPA, 1999). With the knowledge of fine sediment fluxes, storage of sediments, fate and development of the SFGL, bank retreat, and water volume proper controls can be implemented at the specific source and location of the erosion before the source becomes problematic.

A Total Maximum Daily Load (TMDL) is a tool used to implement water quality standard (USEPA, 1999). A sediment TMDL establishes the allowable sediment loading a water body may receive without violating water quality standards thereby providing a basis for pollution control. Many guidelines are already available for chemical pollutants, but much information is still lacking on the fate, transport, and impact of sediments on waterbodies (USEPA, 1999). TMDL's require a cause and effect relationship between a pollutant and a source to be identified. Sources of fine sediment pollution must be identified for the water quality protocol to be of any effect, as sampling

surface water and determining a sediment concentration is accomplished easily but identifying the source of sediments causing the pollution is difficult. The results of this study can be used to help solve these difficulties. A sediment transport modeling tool can be used to assess if quality standards will be breached before urbanization occurs, thus eliminating the reactive nature of the sampling approach and creating a proactive modeling approach.

Watershed and in-stream modeling serve a useful tool for fine sediment pollution. Urbanization can be modeled before construction begins to predict if water quality standards will be breached, and if they are which sediment source is causing the pollution. Fine sediment flux at the watershed outlet can be used to determine if sediment TMDL's are being breached, and bank and bed erosion fractions at the outlet and in-stream cell can be used to estimate which sources are being affected, and where these sources are located. This is useful from a city development perspective in that erosive controls can be implemented at the source of the erosion before the source becomes problematic.

In-stream bank retreat is directly related to in-stream erosion. The estimation of bank retreat can be used to assess to loss of developable land, and determine which, if any, structures near the stream are being threatened by bank retreat. Knowledge of the areas that will be affected by bank retreat allows developers to implement erosive controls before these areas become problematic.

The storage of sediment in depositional areas, including bed and surface fine grained lamina sources, is an important process to understand. The burial of sediments

and their removal rates are important when assessing the sediment delivery ratio, which is needed to create a TMDL for the for a watershed and creating a complete sediment budget (USEPA, 1999; Walling et al., 2006). Understanding how sediment deposition changes with urbanization is an important part of assessing potential sedimentation problems.

The contribution of Carbon to the atmosphere from eroded sediments and their impact on the global carbon budget is unknown (Van Oost et al., 2007). Organic matter decays in the water column, but much carbon is buried in anaerobic depositional areas in the stream and is not exposed to the atmosphere (Chapra,1997). The storage and turnover rates of deposited sediments in the bed and the surface fine grained lamina and the flux of the material eroding and depositing to these sources is a key component in the decomposition and growth of organic matter occurring in these sediment. In order to estimate the contribution of carbon of eroded material to the global Carbon budget, turnover rates and fluxes of these storage areas must be known. The rate of growth and turnover, as well as erosion depth can be used as part of a biogeochemical model to estimate the ultimate contribution of Carbon from these eroded sediments. These rates from computer modeling are useful not only for current watershed prediction of Carbon contribution, but also how Carbon contribution changes with urbanization.

1.7 Contents of the Thesis

Chapter 1 provides an outline of environmental problems associated with fine sediments, the processes controlling sediment transport, a review of the limitations of watershed scale erosion models, an outline of the problems associated with urbanization

as it relates to fine sediment transport, the objective of this study, and the significance of this research.

Chapter 2 provides a literature review of sediment transport models, definitions for sediment transport models, and descriptions of sediment transport models.

Chapter 3 provides the model framework and formulation for the hydrologic, hydraulic, and sediment transport model.

Chapter 4 provides information about the study watershed, including location, topology, and land cover. Information about the sources of sediment as well as the data needed for the urbanization analysis is also provided.

Chapter 5 provides the hydrologic model set up procedure, sensitivity analysis, calibration, validation, and results for the calibration/validation period in comparison with the observed results.

Chapter 6 provides the hydraulic model set up procedure, sensitivity analysis, calibration, validation, and results for the calibration/validation period in comparison with the observed results. Information of the procedure, testing, analysis, and consolidation of field data needed to run the hydrologic and hydraulic models is also provided.

Chapter 8 provides the results from the urbanization study, including the fine sediment flux from the watershed over time; the flux of sediment derived from the streambanks, streambed, and SFGL over time; the temporal change within the stored sediment in the streambed over time; the temporal fate of the SFGL in terms of storage and biofilm re-development over time; the recession rate of the banks, and the increase in water volume to the stream channel. A discussion of the results is also provided.

Chapter 9 provides the conclusions of this thesis.

Chapter 2: Sediment Transport Modeling Review

Most models and modeling strategies applied by researchers only focus on the specific processes involved in the transport and fate of pollutants in a watershed. In reality, many interacting processes are involved, but the purpose of modeling is to understand the processes involved in each individual area of study concerning the chosen pollutants. By modeling the dominant and most important processes, the model becomes simpler. If the results of the model does not compare well with observed data, then the model does not include all the necessary processes. This modeling strategy creates the simplest and best model possible and a greater understanding of the processes involved without over parameterizing the model with processes that do not affect the pollutant of concern (Merritt et al., 2003). Predictions can then be made on that area of study once the model is calibrated and validated.

2.1 Empirical, Conceptual and Physics-based Watershed Erosion Models

Empirical models are purely data driven models, conceptual models lump areas of homogeneity together and simulate processes across them as a whole, and physics-based models employ equations based on physical laws and observations (Aksoy and Kavvas, 2005). All three types of models have their utility and their limitations.

An empirical model is a purely data driven model, which requires many years of collected data to accurately predict future results (Merritt et al., 2003). A major shortcoming of empirical models is that empirical models are only applicable to the study area in which the data was collected (Aksoy and Kavvas, 2005; Merritt et al., 2003). Empirical upland erosion models do not model the processes of sediment erosion, but

instead relate a known independent variable (such as rainfall), to an unknown dependent variable (such as sediment yield) (Zoppou, 2001). They can perform well if properly calibrated, but use of an empirical model outside of the study area for which it was designed should be done so only if no other modeling resources are available. If the geomorphology of the study area changes, then the model is no longer valid because the conditions with which the data was collected no longer exist (Merritt et al., 2003). Empirical models should be avoided for regions with changing conditions because they do not simulate the processes involved (Jarritt and Lawrence, 2007). Empirical models are very easy to set up and use, and are very useful for areas where calibration and parameter data is limited or not available, and because of their simplicity and ease with which they can be used they are often employed to provide a “first guess” at understanding a process (Merritt et al., 2003).

Conceptual models employ a lumped modeling approach where an input is related to an output *via* an process-based equation. Conceptual models lump homogeneous areas together, represent these areas as a series of storage systems, and then calculate applicable processes across these areas as a whole with equations that describe the processes involved but lack the specifics of detailed process interactions at specific spatial locations, which would require detailed data on the modeling areas (Zoppou, 2001; Merritt et al., 2003; Aksoy and Kavvass, 2005). Conceptual models can be calibrated for different watersheds and study areas because they simulate the processes involved and not just the results like empirical models, but also do not have the massive data requirements of physics-based models (Merritt et al., 2003). The equations used in the model may not accurately represent the environment and its processes as well as

physic-based equations, but conceptual models provide more insight into the processes involved than empirical models (Merritt et al., 2003).

Physical models model sediment transport based on physical laws, with coefficients usually obtained from laboratory experiments (Merritt et al., 2003). Standard equations used in such models are the equations of conservation of mass and momentum for flow and conservation of mass for sediment. Physical models can be very accurate at the laboratory scale (usually a hill slope), but coefficients rarely transfer well from one hill slope to another unless the hill slope are very similar spatially (similar soil, slope, land cover, etc.) (Letcher et al., 2002; Merritt et al., 2003; Panday and Huyakorn, 2004; Adams and Elliot, 2006). Unfortunately, physical models are not usually representative of all watersheds because the coefficients used for creating the model are only valid for a small laboratory scale basin and these are often calibrated or “lumped” together at larger spatial scales which creates more uncertainty (Letcher et al., 2002; Merritt et al., 2003). Most physically based models contain documentation that they are only meant to be applied to a specific region or land type because of these coefficients. At the correct spatial scale, physics-based models are the most accurate at modeling specific processes, and are useful for studying these processes.

2.2 Lumped or Distributed Watershed Erosion Models

Watershed models can represent the watershed as either lumped land areas or as a grid of distributed points. Distributed models break the watershed up into grid cells spatially and calculations are run on the grid on a cell by cell basis (Viney and Sivapalan, 1999; Zoppou, 2001; Merritt et al., 2003; Panday and Huyakorn 2004; Wilkinson et al., 2009). Distributed models handle spatial variability better than lumped models, but tend

to be more complex and need a large number of parameters that have to either be measured or estimated (Merritt et al., 2003; Kalin et al., 2003). Lumped models simplify the environment by combining spatially similar regions together into a hydraulic response unit and averaging attributes of that region, as previously mentioned. An example would be combining all urban landcover together in one region and averaging slope values over the whole region to derive one approximate slope value used to describe that region in the model.

2.3 Temporal Scale of Watershed Erosion Models

Time scale is another important factor in choosing a watershed model. Many watershed models only operate at a daily time step. Such models are appropriate for estimating yearly trends but are inappropriate when analyzing the properties of individual events, while other watershed models only simulate a single storm event which is useful when analyzing design storm events, but do not have the dexterity needed to model continuous rainfall (Zappou 2001; Bora and Bera, 2003). Most models that have been developed do not provide accurate watershed scale, event based predictions of sediment load, and most models suffer from having unrealistic input requirements, over-parameterization, and inappropriate model assumptions (Merritt et al., 2003).

2.4 In-stream Sediment Transport Models

An in-stream sediment transport model is a model that describes sediment transport processes in the environment (i.e. bed aggradation/degradation, settling of solids, scour around structures, est.) through either physically based or computational means. (Papanicolaou et al., 2008). Most in-stream models have a physically based hydraulic component and a conceptual sediment erosion component. An in-stream model

requires initial boundary conditions (such as flow and initial concentration) and these values must either be an input measured by the modelers, or a hydrologic model must be coupled with the in-stream model (Green et al., 1999; Zoppou, 2001; Bockelmann, et al., 2004; Papanicolaou et al., 2008).

The majority of in-stream sediment transport models have a physically based hydraulic component, so the number of dimensions a model employs is very important, and the appropriate type of model should be chosen based on the individual requirements of the system being modeled. One dimensional models are easy to set up and require a minimal computational power, but most can only predict basic parameters, such as mean velocity, mean flow, and sediment transport load. Most one dimensional models are formulated in a rectilinear coordinate system and solve the differential conservative equations of mass and momentum flow along with the sediment mass continuity equation (Dietrich et al., 1999; Bora and Bera, 2003; Zoppou, 2001; Papanicolaou et al., 2008). Two dimensional models are more computationally intensive than one dimensional models, but provide more detailed information. Most two dimensional models are depth averaged that can provide information on streamwise and transverse components. Most two dimensional models solve the depth averaged continuity and Navier Stokes equation and the sediment mass balance equation, and are applicable in most circumstances when three dimensional flow is weak (i.e. the vertical component is not very dominant) (Mosselman, 1998; Hardy et al., 2000; Duan and Nanda, 2006; Papanicolaou et al., 2008). Three Dimensional models are used in these circumstances when three dimensional flow is very dominant, such as around bridge piers. Most three dimensional models solve the continuity and Navier Stokes equation, along with the sediment mass

balance equation and require massive computational power, but will return more accurate and representative information on what is really occurring (Wu et al., 1998; Papanicolaou et al., 2008). When choosing a model structure, it is important to simplify the problem as much as possible, but not to over simplify and choose a model that does not accurately reflect the environment being modeled (Viney and Sivapalan, 1999; Bora and Bera, 2003). In-stream two dimensional models are very popular among modelers who only wish to view the processes occurring at a specific reach of the watershed no longer than a few hundred feet. Three dimensional models have yet to become popular because of the computational requirements and the relatively small scale which they can be applied, but may become more popular as computer capabilities increase (Papanicolaou et al., 2008).

2.5 Reaction-based Stream Models

A reaction based model is a model that describes sediment and chemical transport and decomposition reactions. It differs from a traditional water quality model in that a reaction based model describes the decomposition process of all organic compounds with numerous decomposition rates, as well as both equilibrium (reversible) and reaction (non-reversible) processes. A traditional water quality model views the microbial community as a single phase and uses a Monod like equation that relates organic matter decomposition to a function of substrate concentrations (Zhang et al., 2007; Zhang et al., 2008). An example of a Monod like relationship would be relating microbial growth as an exponential function of dissolved oxygen. The equation may take into account growth kinetics of the microbial population, but the growth is still a function of substrate concentration. Reaction based modeling considers the reaction rates of the each chemical reaction involved in a microbe decaying a piece of organic matter (Zhang et al., 2007).

This process is complicated and requires great computing power, but does accurately describe the process of decomposition instead of the Monod model which is conceptual but requires much less computational power.

2.6 In-stream Processes within Sediment Transport Models

Most in-stream sediment transport studies found do not include multiple sources in their model, but instead limit erosion to a single source (Wu et al., 1998; Lui et al., 2002; Duan and Nanda 2006; Papanicolaou et al., 2008). Detailed bank erosion models, including CONCEPTS and BSTEM, have been created which account for fluvial undercutting, bank height, bank slope, unit weight of soil, and moisture content of bank when determining if a bank failure will occur at a specific streambank location within a watershed (Mosselman, 1998; Simon and Collison, 2002; Cancienne et al., 2008; Langendoen and Simon, 2008; Simon et al., 2000; Simon et al., 2009). These models predict the failure of bank material due to subaerial processes and fluvial erosion, but no studies found have applied these models outside the reach or stream bank scale.

The majority of watershed scale studies that included bank source terms in their in-stream model did so with an empirical relationship by estimating bank erosion rates with erosion pins or aerial photographs and computing an average rate of bank retreat per year (Kinsey-Henderson et al., 2005; Smith and Dragovich, 2008; Simon, 2008; Wilkinson et al., 2009). The only study found which modeled bank erosion conceptual on an event basis and coupled with a watershed scale model was Jakeman et al. (1999) which included bank erosion as a constant lateral source term. Other watershed scale stream-reach models only include bed erosion (Duan and Nanda, 2006; Lui et al., 2002; Viney and Sivapalan, 1999; Jarritt and Lawrence, 2007). No studies found included

multiple bed sources and only one study found investigated the decomposition of sediment (Zhang et al., 2008).

The accurate modeling of in-stream sediment sources has a scale limitation. Current sediment transport studies that model bank erosion sources are either not at the watershed scale or present an empirical representation of bank erosion. This thesis research formulated a model to overcome these existing limitations so that the effect of land use change on in-stream erosion can be studied.

Chapter 3: Model Framework and Formulation

3.1 Model Framework

The modeling framework is shown in Figure 2. The modeling framework couples in-stream sediment processes that include: streambed and streambank erosion; temporary sediment storage in the SFGL; in-stream sediment accumulation, biofilm development in the SFGL; and intermittent sediment erosion during a hydrologic event in the lowland watershed system. To meet this goal, a Watershed Hydrologic Model is used to evaluate flowrate for the watershed and is based on the hydrology of the watershed system. The flow conditions are used as forcing for the sediment transport model that includes the relationships for erosion from streambanks, deposition and resuspension at the streambed SFGL and transport. Convergence of the coupled modeling framework is performed through iteration using calibration data that includes: flowrate from the watershed outlet and sediment yield at the watershed outlet.

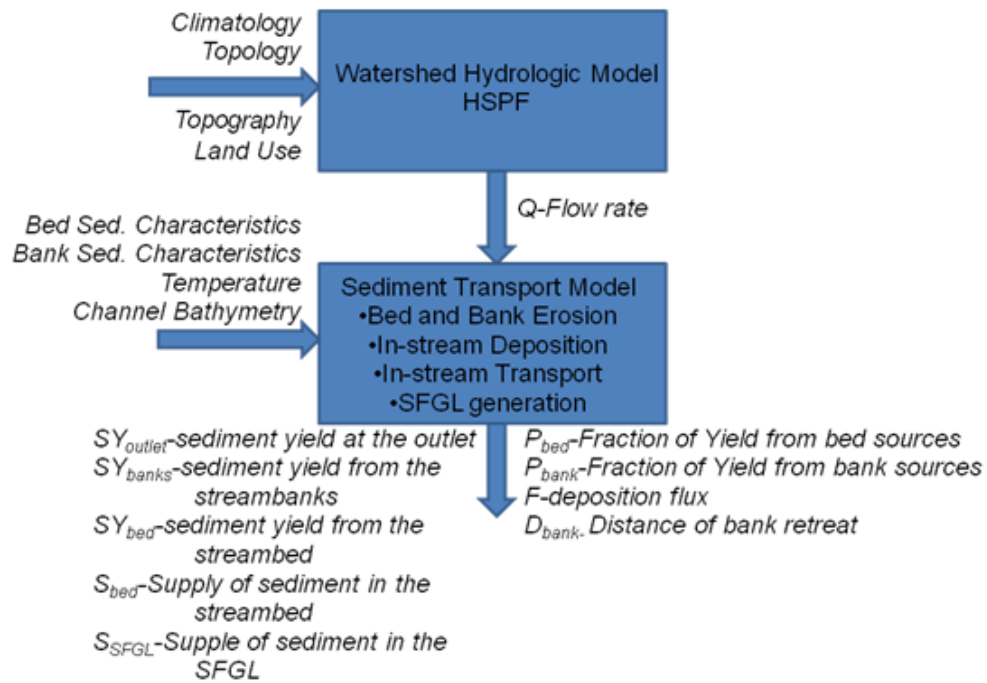


Figure 2: Modeling framework for watershed modeling of in-stream sediment processes.

3.2 Hydrologic Watershed Model Formulation

The Hydrologic Simulation Program Fortran was chosen as an off-the-shelf hydrologic tool that is applicable to mid-sized watersheds (~100km) and conceptually based. HSPF is a conceptually based watershed modeling tool that uses a storage routing approach to budget flow conditions over space and time. A conceptual watershed modeling approach was chosen to maintain connectivity to the underlying physics of the problem while avoiding the immense input data needs of a fine resolution, distributed process-based model, which was deemed impractical at the 100 km² scale. HSPF has the advantage of long term multiple year simulations, which was the focus of this work.

The hydrologic simulations program-FORTRAN (HSPF) is a comprehensive, conceptually based, watershed scale, lump parameter, continuous hydrologic model. HSPF is part of the US EPA Better Assessment and Science Integrating Point and Non-Point Sources (BASINS) modeling system (USEPA, 2001). The BASINS modeling system is a multipurpose environmental analysis framework designed to facilitate the examination of environmental information. BASINS integrates a Geographic Information System (GIS) with several EPA environmental models (HSPF, SWAT, PLOAD, and QUAL2E) and a large database of environmental data for a user friendly modeling experience. HSPF is considered one of the most comprehensive and flexible watershed models to date because of its ability to simulate runoff and contaminant processes from a variety of land covers, link these upland processes with in-stream hydraulic, fate, and decomposition processes, and run these simulations at a variable time step (Merritt et al., 2003).

HSPF simulates upland processes by subdividing the uplands into hydrologic response units (HRU) unique to a specific land cover. HSPF recognizes six different HRUs: urban, agricultural land, forest, pasture, barren, and water. The sub-catchment is sub-divided into these six HRUs with each HRU representing a fraction of the area of the entire sub-catchment. Runoff processes are simulated on these HRUs for the sub-catchment and the results summed. Overland flow is treated as a turbulent flow process and is simulated using the Chezy-Manning equation and an empirical expression which relates outflow depth to detention storage. Infiltration, upper zone and lower zone storage, and groundwater recession are simulated as a function of land use. The outputs as surface flow, interflow, and groundwater flow are routed to a stream-reach. For the

present application, input for HSPF are a time series of precipitation, potential evapotranspiration, air temperature, wind speed, solar radiation, dew point temperature, and cloud cover and output are time series of stream flows (Bickenel et al, 2001).

HSPF is a useful modeling tool, but not without its limitations. HSPF simulates one-dimensional flow and is applicable to streams and well-mixed reservoir reaches with no tidal influence. Several studies have reported HSPF's inability to accurately model a storm hydrograph (Ackerman et al., 2005; Mohamoud, 2007; Lian et al., 2007). HSPF models in-stream hydraulic behavior using a kinematic wave method and does not account for momentum or the in-stream storage of water (Bickenell et al., 2001). Although enhancement of the stage-discharge curves with in-stream geometry can enhance the channel representation and accuracy (Staley et al., 2006; Mohamoud, 2007), the model is still limited by its underlying routing equations. However, this limitation is more applicable to large watersheds. Storage and momentum do not become important until the modeled watershed becomes very large (Lian et al. 2007), and studies which modeled stream flow for smaller watersheds, usually less than 1000 km², in general show a good correlation with observed stream flow data (Bergman et al., 2002; Johnson et al., 2003; Mishra and Singh, 2007; Mohamoud, 2007;).

Studies that use HSPF can be divided into two different categories: 1) Studies which use the entire HSPF software package to model hydraulic processes and in-stream contaminants (Brun and Band, 2000; Bergman et al., 2002; Singh et al., 2005; Ackerman et al., 2005; Mishra et al., 2007, Hunter and Walton, 2008), and 2) Studies which use HSPF to simulate upland processes, but coupled it with either another off the shelf model or developed a proprietary model to simulate processes which are important for the study

watershed (Johnson et al., 2003; Xu et al., 2007; Lian et al., 2007; Jeon et al., 2007; Cho et al. 2009). Many studies have used HSPF to study the effects of land use changes (Brun and Band, 2000; Luo et al., 2006; Cho et al. 2009; Hunter and Walton, 2008). Land use change simulations for HSPF commonly consist of altering the surface cover of the sub-basins, which can be done by modifying the land cover areas of the HRU's. Other changes applied to the model are alterations to the temperature, evapotranspiration, and precipitation time series data to simulate climate changes.

Calibration parameters include the monthly lower zone nominal storage, monthly upper zone nominal storage, baseflow recession constant, interflow inflow parameter, interflow recession constant, the monthly lower zone evapotranspiration parameter, infiltration rate, and monthly interception storage. Because the supply of moisture to the system is given by the precipitation time series, the precipitation must be larger than flow at the outlet and the parameters calibrated in HSPF must control the losses and loss rates in the system throughout the year. Figure 3 shows a conceptual diagram of a pervious land segment used by HSPF where S_{SUR} is the overland surface detention storage, S_{UZSN} is the upper zone nominal soil storage, S_{LZSN} is the lower zone nominal storage, S_{GW} is the storage of inactive groundwater, $P_{(i)}$ is the precipitation during time step i , I is the infiltration rate of the moisture into the soil column, I_{low} is the lower zone percolation, I_{deep} is the deep percolation into inactive groundwater, D_R is direct runoff, D_{INTFW} is interflow outflow, and D_{GW} is groundwater outflow. A complete list of parameters can be found in Appendix A.

The basic mass balance equation for HSPF is shown in Equation 1.

$$D_{out(i)} = P_{s(i)} - D_{evap(i)} - I_{deep(i)} - \Delta S_i, \quad (\text{Eq. 1})$$

where D_{out} is the total outflow for the time step i which is the sum of direct runoff (D_R), interflow (D_{INTFW}), and baseflow (D_{GW}), $P_{s(i)}$ is the precipitation for the time step, $D_{evap(i)}$ is the evapotranspiration for the time step which is the sum of evaporation from moisture storage sources including baseflow, interception storage, upper zone storage, groundwater storage, and lower zone storage, $I_{deep(i)}$ is the deep percolation for the time step, and ΔS_i is the change in the soil moisture storage for the time step which is the change in the sum of the overland storage, upper zone storage, lower zone storage, and baseflow storage. Changes in soil moisture storages and vegetation characteristics affect the actual evapotranspiration by making more or less moisture available to evaporate or transpire, and the infiltration parameter affects the storm volume by allowing more or less moisture to fill soil storage in the upper and lower zones. Both soil moisture and infiltration parameters have a major impact on percolation and are important in obtaining an annual water balance (Donigian, 2002). Seasonal and monthly balances occur concurrently with baseflow balance because seasonal balances often require water precipitated during the wet seasons to be released during dryer seasons. If severe variations in seasonal and monthly volumes are evident, soil storage, evapotranspiration, or interception can be adjusted on a monthly basis. Finally, individual storm events are examined and the timing and peaks of the event adjusted through surface detention and interflow parameters.

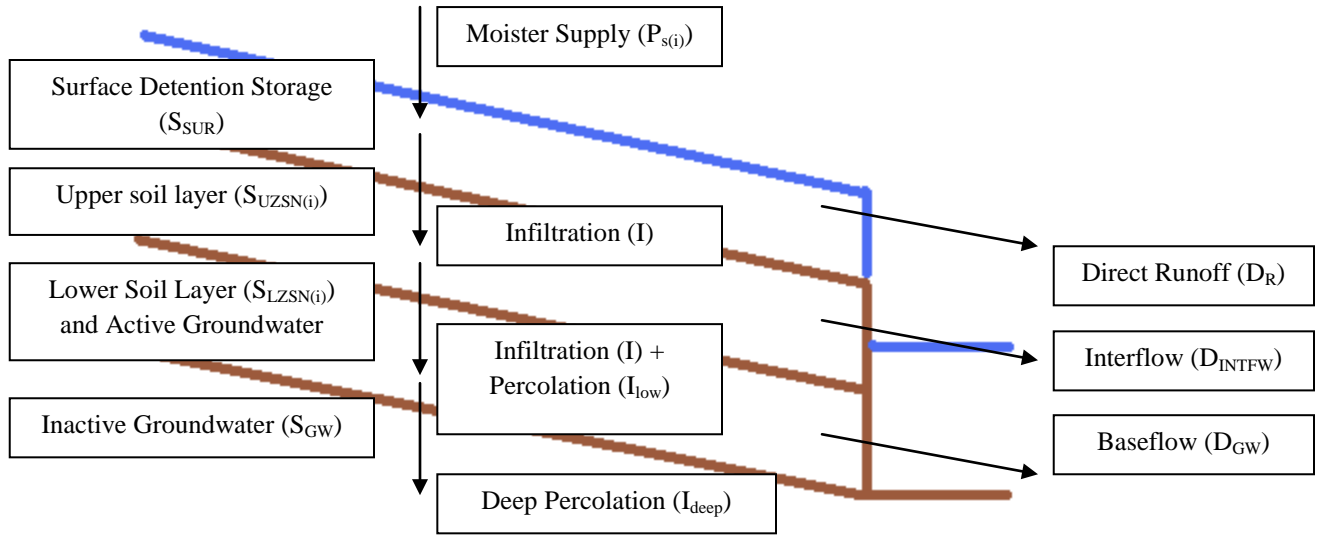


Figure 3: Conceptual diagram of a pervious land segment for HSPF.

Moisture is supplied to a land segment via precipitation time series. The separation of this supply between surface processes and subsurface processes are controlled by the infiltration capacity of the land segment. Mean infiltration capacity for a land segment is given by the equation

$$I_{avg} = C_1 \left[\frac{I}{R_{LZSN}(i)} \right]^{C_2}, \quad (\text{Eq. 2})$$

$$R_{LZSN}(i) = \frac{S_{LZS}(i)}{S_{LZSN}}, \quad (\text{Eq. 3})$$

and the following equations are used to simulated the separation of the moisture supply

$$I_{max} = R_{infiltr} I_{avg}, \quad (\text{Eq. 4})$$

$$I_{min} = I_{avg} - (I_{max} - I_{avg}), \quad (\text{Eq. 5})$$

$$R_{SUR} = C_{intf_w} (2.0^{R_{LZSN}(i)}), \quad (\text{Eq. 6})$$

where I_{avg} is the average infiltration capacity over the land segment (m/s), C_1 is a factor to account for frozen ground effects (unitless), I is the nominal infiltration rate supplied by the user (INFILT) (m/s), I_{max} and I_{min} are the maximum and minimum infiltration capacity for the land segment (m/s), $S_{LZS(i)}$ is the lower zone storage (m), S_{LZSN} is the nominal lower zone storage supplies by the user (LZSN) (m), $R_{infiltr}$ is the ratio of the maximum to the mean infiltration capacity for the land segment (m/m), and R_{SUR} is a ratio used to determine the separation of surface runoff, interflow, and infiltration (unitless), and C_{intfw} is an interflow inflow parameter supplied by the user (INTFW) (unitless). R_{SUR} is multiplied by I_{max} and I_{min} to obtain the ordinates used to separate surface runoff, interflow, and infiltration from the current water supply on the land segment. Depths of precipitation (P_i) that fall below I_{min} infiltrate to the lower zone storage where evapotranspiration processes are simulated, depths below I_{max} but above I_{min} are available for potential interflow inflow and upper zone storage, and depths above I_{max} are available for surface runoff and surface storage.

Overland flow is treated as a turbulent flow process and is simulated using the Chezy Manning equation and an empirical relationship between outflow depth and detention storage. The basic overland flow equation is given as

$$D_R = \Delta t \left[\frac{1020}{nL} \right] D_E^{1.67} S^{0.5}, \quad (\text{Eq. 7})$$

where D_R is the depth of runoff (m), Δt is the time step (s), n is manning coefficient, L is the length of the overland flow plane (m), S is the slope of the overland flow plane (m/m), and D_E is the empirical relationship between outflow depth and detention storage (m) which is determined by the equation

$$D_E = 1.6S_{S(i)}, \quad (\text{Eq. 8})$$

if $S_{SUR(i)}$ is less than $S_{SURN(i)}$ or

$$D_E = S_{SUR(i)} \left(1 + 0.6 \left[\frac{S_{SUR(i)}}{S_{SURN(i)}} \right] \right), \quad (\text{Eq. 9})$$

if $S_{SUR(i)}$ is greater or equal to $S_{SURN(i)}$ where $S_{SURN(i)}$ is calculated with the equation

$$S_{SURN(i)} = 0.00982 \left(\frac{nL}{S^{0.5}} \right)^{0.6} (P_{rate(i)})^{0.6}, \quad (\text{Eq. 10})$$

where $S_{SUR(i)}$ is the storage of water on the land segment (m), and $S_{SURN(i)}$ is the equilibrium storage of water on the land segment for the current moisture supply rate. $P_{rate(i)}$ is the moisture supply rate to the surface and is estimated by subtracting the surface storage at the start of the interval ($S_{SUR(i-1/2)}$) from the potential surface detention which was determined using Equations (1-6) as the moisture that falls above the maximum infiltration.

Moisture that is infiltrated is separated between interflow and groundwater storage. Interflow outflow is represented as a linear relation between storage such that

$$D_{I(i)} = f(IRC)_1 I_{in(i-\frac{1}{2})} - f(IRC)_2 I_{s(i-\frac{1}{2})}, \quad (\text{Eq. 11})$$

where $D_{I(i)}$ is the interflow outflow for the time step i , IRC is the interflow recession constant which is the ratio of the current interflow outflow to the value 24 hours earlier, $f(IRC)_1$ and $f(IRC)_2$ are empirical functions of IRC , $I_{in(i-1/2)}$ is the interflow inflow rate at the start of the timestep, and $I_{s(i)}$ is the storage of the interflow at the start of the interval.

The functions $f(IRC)_1$ and $f(IRC)_2$ are given by the equations

$$f(IRC)_2 = 1 - (e^{(-\log^{-1}(IRC))\Delta t/24}), \quad (\text{Eq. 12})$$

$$f(IRC)_1 = 1 - \left(\frac{f(IRC)_2}{(-\log^{-1}(IRC))\Delta t/24} \right), \quad (\text{Eq. 13})$$

Water stored in the upper zone may infiltrate to the lower soil layers and its monthly rate is calculated by the equation

$$I_{lower} = 0.1(I)(C_{frozen})(S_{UZSN})(R_{UZSN(i)} - R_{LZSN(i)})^3, \quad (\text{Eq. 14})$$

where I_{lower} is the infiltration to the lower zone, I is the infiltration rate of the soil supplied by the user (INFILT), C_{frozen} is a coefficient to account for frozen ground if any, S_{UZSN} is the parameter to account for the upper zone nominal storage (UZSN), and R_{UZSN} and R_{LZSN} are the ratio of the upper zone storage to the upper zone nominal storage (UZSN) and the ratio of the lower zone storage to the lower zone nominal storage (LZSN) respectively. R_{UZSN} takes the same form as Equation (3)

$$R_{UZSN(i)} = \frac{S_{UZS(i)}}{S_{UZSN}}, \quad (\text{Eq. 15})$$

where $S_{UZS(i)}$ is the upper zone storage (m) and S_{UZSN} is the nominal lower zone storage supplies by the user (UZSN) (m). The fraction of lower zone inflow, which is the sum of direct infiltration, percolation, lower zone lateral inflow, and irrigation application, that enters the lower zone storage is based on the lower zone storage ratio R_{LZSN} .

$$R_{lzfract} = 1 - R_{LZSN(i)} \left(\frac{1}{2+1.5|R_{LZSN(i)}-1|} \right)^{1.5|R_{LZSN(i)}-1|+1}, \quad (\text{Eq. 16})$$

$$R_{lzfract} = \left(\frac{1}{2+1.5|R_{LZSN(i)}-1|} \right)^{1.5|R_{LZSN(i)}-1|+1}, \quad (\text{Eq. 17})$$

The fraction of direct infiltration plus percolation from the upper zone which does not go to the lower zone will be inflow to either inactive or active groundwater. The fraction that does not enter inactive groundwater is assumed plus all lateral inflows and irrigation application make up the total inflow to the active groundwater storage. The groundwater outflow is based on a simplified model that assumes that the discharge of an aquifer is proportional to the product of the cross sectional area and the energy gradient of the flow. A representative cross section is assumed to be related to the groundwater storage level and the energy gradient is estimated as a basic gradient based on past ground water activity

$$D_{GW} = C_{GW1} S_{GW(i-\frac{1}{2})} \left(1 + C_{GW2} C_{GWslope} \right), \quad (\text{Eq. 18})$$

$$C_{GW1} = 1 - C_{GWrec}^{\Delta t/24}, \quad (\text{Eq. 19})$$

Where D_{GW} is the outflow depth for ground water (m), C_{GWI} is groundwater outflow recession parameter (KGW) (s^{-1}), $S_{GW(i-1/2)}$ is the active groundwater storage at the start of the time step (AGWS) (m), C_{GW2} is a user input parameter that can be used make groundwater outflow to storage relation nonlinear (KVARY) (m^{-1}), $C_{GWslope}$ is a user input parameter index to groundwater slope (AGWS) (m), and C_{GWrec} is a daily recession constant of groundwater flow which is used if C_{GW2} or $C_{GWslope}$ is zero which is a user input parameter defined as the ratio of current groundwater discharge to that 24 hours earlier (AGWRC).

Evapotranspiration accounts for over half the losses in most watersheds and its simulation is very important to the annual water budget. Potential evapotranspiration is the maximum evapotranspiration which can be expected in a time interval and is supplied via time series to HSPF. Actual evapotranspiration is then estimated based on the availability of water from five sources. These sources, described in the order in which they try to satisfy the potential evapotranspiration, are baseflow, interception storage, upper zone storage, groundwater storage, and lower zone storage.

The active groundwater outflow or baseflow subroutine simulates the effect of riparian vegetation withdrawing groundwater. The fraction of potential evapotranspiration which can be satisfied from baseflow is a user input. For interception storage, there is no limitation on the evapotranspiration. If water is available it will satisfy the potential evapotranspiration. There is no special upper zone evapotranspiration parameter, but it is based upon the ratio $R_{UZSN(i)}$. If this ratio is greater than 2 then evapotranspiration occurs until the potential evapotranspiration is satisfied or until the ratio drops at or below 2. Like evapotranspiration from baseflow, actual evapotranspiration from active groundwater is regulated by a user input parameter which supplies the fraction of remaining evapotranspiration which can be satisfied from active groundwater storage. Finally, lower zone storage will attempt to satisfy the evapotranspiration, but this is much more involved because it is based off of the land cover, depth of root vegetation, density of cover, stage of plant growth and moisture characteristics of the soil layer. The lower zone evapotranspiration parameter (C_{LZET}) (LZET), is a monthly input parameter supplied by the user. If this parameter is near one then the potential evapotranspiration can be satisfied by the entirety of the lower zone

storage. However, this is usually not the case. The maximum depth of lower zone evapotranspiration is given by the equation

$$D_{lzevap} = \frac{0.25}{1-C_{LZET}} (R_{LZSN(i)}) \left(\frac{\Delta t}{24}\right), \quad (\text{Eq. 20})$$

where D_{lzevap} is the maximum lower zone evapotranspiration (m) when the remaining potential evapotranspiration is less than D_{lzevap} . If potential evapotranspiration is greater than D_{lzevap} , then the depth of evapotranspiration in the lower zone is equal to D_{lzevap} .

For impervious areas, the hydrologic routines are the same as for pervious land segments except there is no infiltration and soil processes. Values for the input parameters are given for each land cover type, including wetland, urban, forest, upland shrub, grassland, cropland, pasture, and impervious areas. When land use change scenarios are run, these values will not be changed, but the percent of area in the watershed which contain the above mentioned hydrologic response units will change.

HSPF is a conceptually based watershed modeling tool that uses a storage routing approach to budget flow conditions over space and time. The stream-reach component of HSPF is modeled as

$$V_{\left(i+\frac{1}{2}\right)}^{(j)} = V_{\left(i-\frac{1}{2}\right)}^{(j)} + Q_{in(i)}^{(j)}\Delta t + P_{(i)}^{(j)} - E_{v(i)}^{(j)} - [k_s Q_{out\left(i-\frac{1}{2}\right)}^{(j)} + (1-k_s)Q_{out\left(i+\frac{1}{2}\right)}^{(j)}]\Delta t, \quad (\text{Eq. 21})$$

$$Q_{in(i)}^{(j)} = k_s Q_{out\left(i-\frac{1}{2}\right)}^{(j-1)} + (1-k_s)Q_{out\left(i-\frac{1}{2}\right)}^{(j-1)}, \quad (\text{Eq. 22})$$

where (j) represents the stream-reach and (i) represents the time step. $V^{(j)}_{(i+1/2)}$ is the volume of water in the stream-reach at the end of the time step [m^3], $V^{(j)}_{(i-1/2)}$ is the volume of water in the stream-reach at the beginning of the time step [m^3], $Q_{in}^{(j)}_{(i)}$ is the flow rate into the stream-reach from upstream and upland sources throughout the time step [m^3/s], $P^{(j)}_{(i)}$ is the precipitation into the stream-reach throughout the time step [m^3], $E_v^{(j)}_{(i)}$ is the evaporation from the reach during the time-step [m^3], $Q_{out}^{(j)}_{(i-1/2)}$ is the flow rate out of the reach at the beginning of the time step [m^3/s], $Q_{out}^{(j)}_{(i+1/2)}$ is the flow rate out of the reach at the end of the time step [m^3/s], Δt is the time step [s], and k_s is the flood wave coefficient. Figure 4 shows a conceptualization of the stream reach mass balance for hydraulic processes.

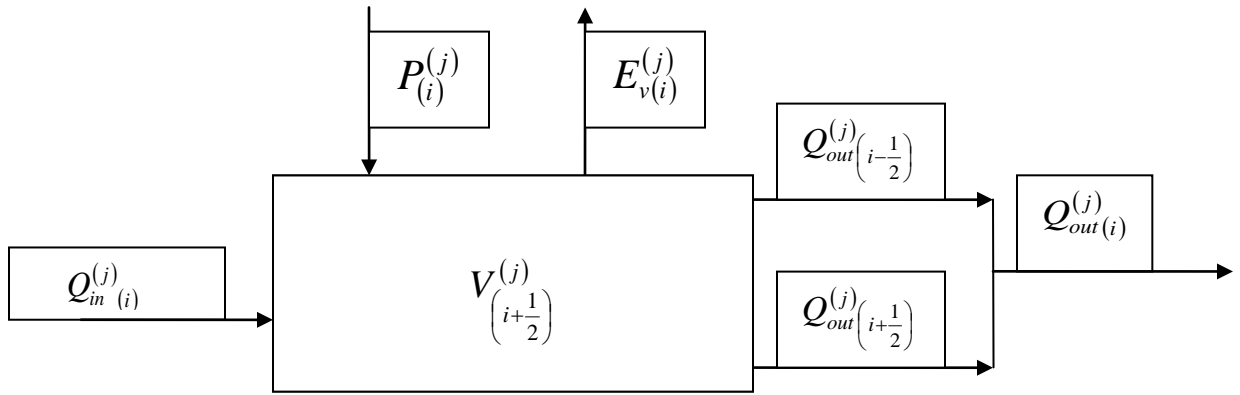


Figure 4: Conceptualization of stream reach mass balance hydraulic processes.

All water entering the stream reach from surface and subsurface sources arrives through $Q_{in}^{(j)}_{(i)}$ as an additional time series added to the outflow from the upstream stream-reach. Water is routed from upland sources using a modified version of the Chezy-Manning equation. Precipitation, $P^{(j)}_{(i)}$, and evaporation, $E_v^{(j)}_{(i)}$, are estimated by

the user and supplied via time series in units of depth per interval. These values are multiplied by the time step and surface area of the reach to obtain a volume for the mass balance calculation in Equation (21).

HSPF models flood waves by first running all surface runoff, hydraulic, and routing modules for the upmost catchment of the watershed, termed sub-catchment (j), for the entire simulation period. The outflow time series from sub-catchment (j) is a weighted average based on k_s and is used as the inflow time series for the next downstream reach, termed sub-catchment ($j+1$), during time step ($i+1$) for the entire simulation period. All runoff, hydraulic, and routing modules are then run on this reach and the outflow time series from this reach is used as the input time series for the next downstream reach. Thus, information travels downstream only. There are two unknowns in Equation (21), including $V_{(i+1/2)}^{(j)}$ and $Q_{out}^{(j)}(i)$. To solve this problem, a hydraulic routing relationship is introduced as

$$Q_{out}^{(j)}(i) = f(V_{(i)}^{(j)}). \quad (\text{Eq. 23})$$

Equation (23) represents a table used to document, in discrete numerical form, a functional relationship between two or more variables. In HSPF, the FTABLE describes the hydraulics of a stream reach by defining the functional relationship between water depth, surface area, volume, and outflow in the stream reach. Equation (23) may either be input by the user or estimated by the program using geometric, spatial, and geomorphic information about the reach including (1) cross sectional data, (2) channel slopes, (3) Manning's roughness coefficient, (4) and regional curve data if applicable.

To route the flows for a time step, a segment is selected from Equation (23) and its point of intersection with Equation (21) is determined. If this point is outside the selected segment, then the code will select the adjacent segment in the direction in which the point of intersection lies and the process is iterated until the point lies within the segment under consideration.

3.3 In-stream Sediment Transport Model

3.3.1 Hydraulic Variables

In-stream hydraulic variables were calculated using Q results from HSPF and stream bathymetry, and thereafter used to drive the sediment model. Hydraulic radius is predicted from the flow depth using Manning's Equations and cross sectional geometry for the stream-reach.

$$Q_{(i)}^{(j)} = \frac{1}{n} \left(\frac{(A_{(i)}^{(j)})^{5/3}}{(P_{(i)}^{(j)})^{2/3}} \right) S_{(i)}^{1/2}, \quad (\text{Eq. 24})$$

The area of the cross section $A_{(i)}^{(j)}$, wetted perimeter of the cross section $P_{(i)}^{(j)}$, and hydraulic radius of the fluid $R_{(i)}^{(j)}$ are estimated as a function of the average of the flow depth $H_{(i)}^{(j)}$ at the start of the time step and the flow depth at the end of the time step

$$A_{(i)}^{(j)} = f(H_{(i)}^{(j)}), \quad (\text{Eq. 25})$$

$$R_{(i)}^{(j)} = f(H_{(i)}^{(j)}), \quad (\text{Eq. 26})$$

$$P_{(i)}^{(j)} = \frac{A_{(i)}^{(j)}}{R_{(i)}^{(j)}}, \quad (\text{Eq. 27})$$

$$B_{(i)}^{(j)} = B_{(i-1)}^{(j)} + E_{d(i)}^{(j)}, \quad (\text{Eq. 28})$$

$$H_{(i)}^{(j)} = (k_s) \left(H_{(i-\frac{1}{2})}^{(j)} \right) + (1 - k_s) \left(H_{(i+\frac{1}{2})}^{(j)} \right), \quad (\text{Eq. 29})$$

where $H^{(j)}_{(i-1/2)}$ and $H^{(j)}_{(i+1/2)}$ are the flow depths at the beginning and end of the interval respectively, $B^{(j)}_{(i)}$ is the width of the channel, $E_d^{(j)}_{(i)}$ is the bank retreat for the time step, and k_s is the flood wave coefficient. The cross sectional area and hydraulic radius are function of the flow depth and are unique to the stream-reach.

In addition to the above equations for calculation of hydraulic variables, a correction was added to the model to account for flooding conditions when the water surface crested bankfull conditions in the stream. Manning's equation was discretized for a non-uniform cross-section typical of flooding conditions, and uniform depth in the channel was solved by optimization of Manning's equation for both the main channel and floodplain.

3.3.2 Sediment Mass Balance Stream-Reach

The sediment transport model is formulated to include the representation of in-stream sediment processes typical of a lowland watershed including streambank erosion, streambed erosion and storage, and erosion, deposition and development of the streambed surface or surface fine-grained laminae (SFGL). The sediment model is divided into transport and storage terms including the sediment transport model that also accounts fraction of sediment derived from different sources and the model subroutine that represents the change in the SFGL and streambed over time due to biofilm development.

The sediment transport component of the model is formulated to estimate sediment flux from a sub-catchment following a sediment mass balance approach, is driven by the hydrologic outputs and is also conceptual in nature. Figure 5 shows a

conceptualization of a stream reach mass balance for sediment transport processes. The sediment transport model is given as

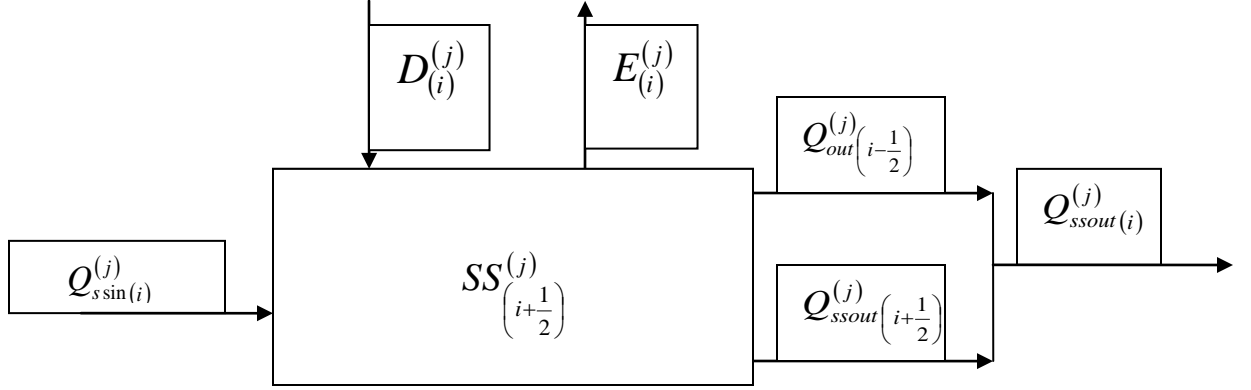


Figure 5: Conceptualization of stream reach mass balance for sediment transport processes.

$$SS_{\left(i+\frac{1}{2}\right)}^{(j)} = SS_{\left(i-\frac{1}{2}\right)}^{(j)} + \sum_{k=1}^N E_{(i)(k)}^{(j)} - D_{(i)}^{(j)} + Q_{ssin(i)}^{(j)}\Delta t - Q_{ssout(i)}^{(j)}\Delta t, \quad (\text{Eq. 30})$$

where (j) represents the stream-reach, (i) represents the time step, (k) represents the source term, and N represents the number of sediment sources. $SS_{(i+1/2)}^{(j)}$ is the mass of sediment in suspension at the end of the time step [kg], $SS_{(i-1/2)}^{(j)}$ is the mass of sediment in suspension at the start of the time step [kg], $E_{(i)(k)}^{(j)}$ represents the mass of eroded sediment [kg], $D_{(i)}^{(j)}$ is the deposited mass of sediments [kg], $Q_{ssin(i)}^{(j)}$ is the sediment flow rate into the stream reach during the time step [kg/s], and $Q_{ssout(i)}^{(j)}$ is the sediment flow rate out of the reach during the time step [kg/s].

3.3.3 Sediment Transport Capacity and Residual Capacity

Erosion and deposition are considered to be mutually exclusive and cannot occur simultaneously in a stream-reach during a time step. The occurrence of erosion or deposition is modeled based on the relationship between the sediment transport carrying capacity of the flow during the time step and the sediment load currently being carried by the stream reach during the time step. Transport capacity is modeled as

$$T_{c(i)}^{(j)} = C_{tc} \left(\tau_{f(i)}^{(j)} \right)^{1.5} L_{reach}^{(j)} \Delta t, \quad (\text{Eq.31})$$

where C_{tc} is a calibration coefficient [$\text{m}^{1/2} \cdot \text{s}^2 / \text{kg}^{1/2}$], $\tau_{f(i)}^{(j)}$ is the shear stress of the fluid at the location of the sediment source [N/m^2], L_{reach} is the length of the stream reach, and $T_{c(i)}^{(j)}$ is the average transport capacity across the reach during the time step [kg]. The exponent in Equation (31) is the transport capacity exponent and is assumed to be 1.5 given the relationship between shear stress and energy. During the sediment model calibration, two distinct transport capacity patterns were noticed between low and high flows. This distinction is believed to be from the spatial heterogeneity of the reach. The channel has a pool-rifle profile where the gradient of an individual pool-rifle profile is close to zero at low flows, but at high flows the average slope of the reach is representative because the individual steps of the reach are overtopped by the stage of the flow. Another possible reason for the difference in the transport capacity regime could be from a difference in the density of the baseflow sediments versus higher flow storm sediments. Lower flow sediments have a lower density than deeper eroded and more compacted higher flow sediments. The transport capacity was separated into two different equations, each taking the form of Equation (31) with a different coefficient to

account for the difference between the carrying capacity of low flow and high flows.

Erosion occurs for the conditions within the time-step when

$$T_{c(i)}^{(j)} > SS_{\left(i-\frac{1}{2}\right)}^{(j)}, \quad (\text{Eq.32})$$

while deposition occurs in the reach during the time step when

$$T_{c(i)}^{(j)} < SS_{\left(i-\frac{1}{2}\right)}^{(j)}. \quad (\text{Eq.33})$$

It is recognized that the flow will pick up and transport the most easily erodible sediment before transporting the less erodible or buried sediment sources. This preferential order for erosion and transport is modeled using the residual transport capacity. To model the residual transport capacity, the sediment sources are ordered with the most easily eroded sediment sources coming first. The residual transport capacity for the next sediment source is the difference between the transport capacity of the flow and the mass of eroded sediments from all previous sediment sources. The residual transport capacity is modeled as

$$T_{cr(i)(l)}^{(j)} = T_{cr(i)(l-1)}^{(j)} - E_{(i)(l)}^{(j)}, \quad (\text{Eq. 34})$$

$$E_{(i)(l)}^{(j)} = \sum_{k=1}^N E_{(i)(k)}^{(j)}, \quad (\text{Eq. 35})$$

where (l) is the source order, $T_{cr(i)(l)}^{(j)}$ is the residual transport capacity for the source order [kg], $T_{cr(i)(l-1)}^{(j)}$ is the residual transport capacity satisfied from the previous sediment source [kg], and $E_{(i)(l)}^{(j)}$ is the summation of the eroded mass for every source with the

source order (l) [kg]. The sources are ordered as 1) the surface fine grained lamina, 2) the slump banks and streambed, and 3) the incised banks.

3.3.4 Fluvial Erosion

Erosion is modeled by considering that multiple sources can be eroded either sequentially or concurrently and that the mass of sediment eroded can be shear limited, transport capacity limited, or supply limited. Erosion sources considered in the stream corridor are the surface fine grained lamina, streambed, streambanks. The mass of eroded sediments is dependent upon the fluid shear at the sediment source, the transport capacity of the flow, and the supply of erodible sediments available.

For each source, if the fluid shear stress at the sediment source is greater than its critical shear stress, erosion of the sediment source is then modeled by the equation

$$E_{(i)l}^{(j)} = \min \left[\left(a_{(k)} \left(\tau_{f(i)}^{(j)} - \tau_{cr(k)} \right)^{b_{(k)}} SA_{(k)} \Delta t \right) \left(T_{cr(i)l}^{(j)} \right), \left(S_{(i)k}^{(j)} \right) \right], \quad (\text{Eq.36})$$

where $E_{(i)l}^{(j)}$ represents the eroded mass for the sediment source for the time step [kg], $a_{(k)}$ is a coefficient, $b_{(k)}$ is an exponent, τ_f is the shear stress of the fluid at the centroid of the erosion source [N/m²], τ_{cr} is the critical shear stress for the erosion source [N/m²], $T_{cr(i)l}^{(j)}$ is the residual transport capacity for the sediment source [kg], $SA_{(k)}$ is the surface area of the sediment source [m²], and $S_{(i)k}^{(j)}$ is the sediment supply of the erosion source [kg].

3.3.5 Unsteady Fluvial Shear Stresses

The shear stress of the channel is modeled as to account for unsteady uniform flow. Using the Navier-Stokes equation, Equation (37), for description of a Newtonian

fluid in the direction of streamflow (x), where the lateral direction is defined as (y) and the vertical direction as (z), the bed shear stress equation is derived.

$$\rho \left(\frac{\delta u}{\delta t} + u \frac{\delta u}{\delta x} + v \frac{\delta u}{\delta y} + w \frac{\delta u}{\delta z} \right) = \frac{\delta P}{\delta x} - \rho g S + \frac{\delta \tau_{xy}}{\delta x} + \frac{\delta \tau_{yx}}{\delta y} + \frac{\delta \tau_{zx}}{\delta z}, \quad (\text{Eq. 37})$$

By assuming no significant velocity changes in the streamwise (x), lateral (y), or vertical (z) direction for a cell, no significant pressures changes across a cell in the streamwise direction, and assuming shear stress only changes with water depth, Equation (37) simplifies. Equation (38) shows the results of this simplification, and Equation (39) shows the equation after rearranging and integrating over the water depth. Equation (40) shows the final equation used in the numerical model with hydraulic radius substituted for water depth.

$$\rho \left(\frac{\delta u}{\delta t} \right) = -\rho g S + \frac{\delta \tau_{zx}}{\delta z}, \quad (\text{Eq. 38})$$

$$\tau_{zx} = \rho g S z + \rho \left(\frac{\delta u}{\delta t} \right) z, \quad (\text{Eq. 39})$$

$$\tau_{f(i)}^{(j)} = C_{\tau(1)} \left[\rho g R_{(i)}^{(j)} S^{(i)} + C_{\tau(2)} \rho \left(\frac{U_{(i-1/2)}^{(j)} - U_{(i+1/2)}^{(j)}}{\Delta t} \right) R_{(i)}^{(j)} \right], \quad (\text{Eq. 40})$$

where $\tau_{f(i)}^{(j)}$ is the shear stress of the fluid at the location of the sediment source [N/m^2], $C_{\tau(1)}$ is the shear stress coefficient to account for the difference between the bed and bank shear, ρ is the density of the fluid [g/m^3], $R_{(i)}^{(j)}$ is the hydraulic radius of the fluid at the sediment source [m], $C_{\tau(2)}$ is the flow acceleration coefficient, $U_{(i-1/2)}^{(j)}$ is the velocity of the streamflow at the beginning of the time step [m/s], and $U_{(i+1/2)}^{(j)}$ is the velocity at the

end of the time step [m/s], and $S^{(j)}$ is the energy slope which is assumed to be the slope of the channel bed.

3.3.6 Budgeting Sediment Sources

In addition to simulating sediment flux from each sub-catchment, the sediment flux is partitioned to its source origin using a mass balance. The mass fraction of eroded material which satisfies the transport capacity is determined using the equation

$$F_{(i)(k)}^{(j)} = \frac{E_{(i)(k)}^{(j)}}{\sum_{k=1}^N E_{(i)(k)}^{(j)}}, \quad (\text{Eq. 41})$$

Where the denominator shows the summation of eroded material from all sediment sources, the numerator shows eroded mass for a single sediment source, and $F_{(i)(k)}^{(j)}$ is the fraction of eroded material from a particular sediment source. The stream is assumed to be well mixed, and the mass fraction of material currently in suspension from an individual sediment source is the same as the fraction of material being discharged and deposited. This mass fraction is predicted with the equation

$$P_{(i)(k)}^{(j)} = \frac{P_{(i-1)(k)}^{(j)} SS_{(i-\frac{1}{2})}^{(j)} + F_{(i)(k)}^{(j)} \sum_{k=1}^N E_{(i)(k)}^{(j)} - F_{(i)(k)}^{(j)} D_{(i)}^{(j)} + P_{(i)(k)}^{(j-1)} Q_{ssin(i)}^{(j)} \Delta t}{SS_{(i-\frac{1}{2})}^{(j)} + \sum_{k=1}^N E_{(i)(k)}^{(j)} - D_{(i)}^{(j)} + Q_{ssin(i)}^{(j)} \Delta t}, \quad (\text{Eq. 42})$$

where $P_{(i)(k)}^{(j)}$ is the fraction of material from a sediment source (k), the numerator represents the total mass of material in suspension from that source, and the denominator represents the total mass of material in suspension.

3.3.7 Bank Erosion

In formulating the model, it was considered that streambank erosion can occur due to a subsequent processes of fluvial erosion at the toe of the streambank during high shear followed by slumping of sediment from high on the bank or mass failure (Millar and Quick, 1997). In the present scenario of lowland watersheds, the primary mechanism observed was fluvial erosion of the toe followed by slumping to produce sloughed sediment on the streambank.

All material eroded from the streambanks is assumed to be removed through fluvial shearing from the slump bank source. Mass failure, or sloughing of the banks, is not assumed to contribute directly to the in-stream sediment supply, but instead is assumed to regenerate the supply of erodible sediments to the slump material every time step. Material that is eroded from the slump is assumed to regenerate instantaneously with material from the upslope sloughing off to regenerate the eroded mass and maintain the channel side slope. Figure 6 shows a conceptualization of the bank erosion model.

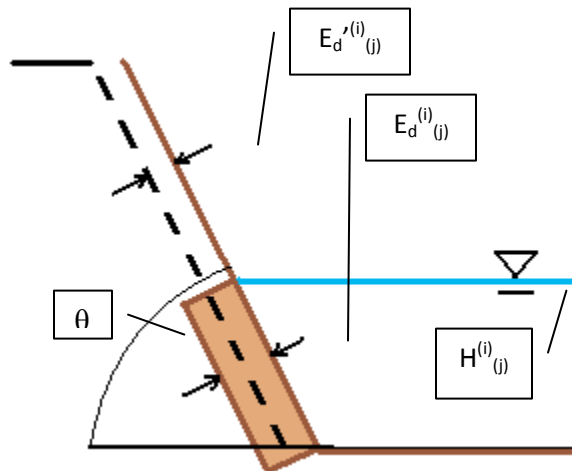


Figure 6: *Figure of Bank Erosion.*

Bank erosion is modeled using Equation (43),

$$E_{(i)(bank)}^{(j)} = \min \left[\left(a_{(bank)} \left(\tau_{f(i)}^{(j)} - \tau_{cr(bank)} \right) \right)^{b(k)} SA_{E(i)}^{(j)} \Delta t \right] \left(T_{cr(i)(bank)}^{(j)} \right), \quad (\text{Eq. 43})$$

Where $E_{(i)(bank)}^{(j)}$ is the eroded mass from the bank for a time step, and $SA_{E(i)}^{(j)}$ is the surface area of the eroded bank estimated using the equation

$$SA_{E(i)}^{(j)} = L_{reach}^{(j)} \frac{H_{(i)}^{(j)}}{\sin(\theta)}, \quad (\text{Eq. 44})$$

Where $L_{reach(j)}$ is the length of the stream reach for the cell, $H_{(i)}^{(j)}$ is the water depth for the time step, and θ is the bank angle. No supply term is included because bank sediment is assumed to be infinite laterally.

The eroded depth of slump material for the time step is predicted using the equation

$$E_{d(i)(bank)}^{(j)} = \frac{E_{(i)}^{(j)}}{(SA_{B(i)}^{(j)}) \rho_B}, \quad (\text{Eq. 45})$$

Where $E_{d(i)}^{(j)}$ is the depth of eroding bank material, ρ_B is the density of the bank material, and $SA_B^{(j)}$ is the surface area of the entire bankfull depth.

$$SA_B^{(j)} = L_{reach}^{(j)} \frac{H_{bankfull(i)}^{(j)}}{\sin(\theta)}, \quad (\text{Eq. 46})$$

where $H_{bankfull(i)}^{(j)}$ is the bankfull depth. Bankfull depth was predicted using measured channel cross sections and also acts as an upper limit for the erodible bank surface area.

The lateral recession rate of the bank is estimated using the equation

$$E'_{d(i)}^{(j)} = \frac{E_{d(i)}^{(j)}}{\cos(90-\theta)}, \quad (\text{Eq. 47})$$

where $E'_{d(i)}^{(j)}$ is the lateral bank recession rate. Channel width is then updated

$$W_{reach(i)}^{(j)} = W_{reach(i-1)}^{(j)} + E'_{d(i)}^{(j)}, \quad (\text{Eq. 48})$$

Where $W_{reach(j)}^{(j)}$ is the width of the channel for the current time step, and $W_{reach(j-1)}^{(j)}$ is the width of the channel for the previous time step.

3.3.8 SFGL Erosion

Supply of the surface fine grain lamina is controlled by two processes 1) Deposition on the falling limb of the hydrograph and 2) Generation of the surface fine grain lamina through biological activity at the streambed. The SFGL is divided into two storage areas; the mass of loose unconsolidated bed material that exist for a maximum depth of 1 cm, and the mass of biofilm growing in this top 1 cm matrix of loose unconsolidated sediments. Erosion from these sources is modeled as a single erosion term for the two storage SFGL system with the fraction of material eroding from each storage coming from a mass fraction of the bed material and the biofilm material to the whole SFGL storage. Figure 7 shows a conceptualization of the SFGL erosion model.

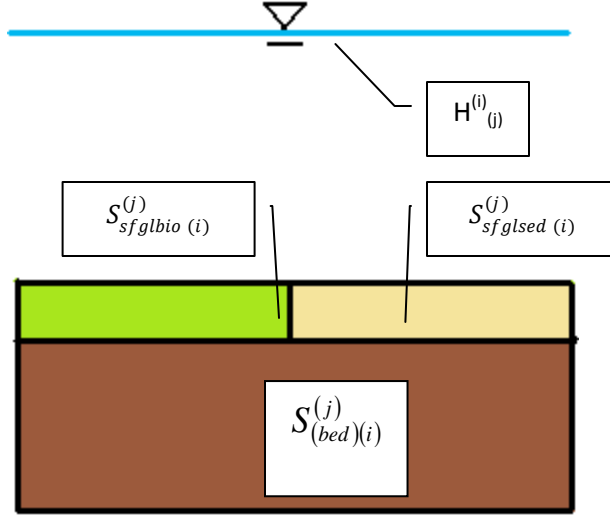


Figure 7: Conceptualization of SFGL and Bed Erosion Model.

SFGL erosion is modeled using Equation (49).

$$E_{(i)(sfgl)}^{(j)} = \min \left[\left(a_{(sfgl)} \left(\tau_f^{(j)} - \tau_{cr(sfgl)} \right)^{b(k)} SA_{(sfgl)} \Delta t \right) \left(T_{cr(i)(sfgl)}^{(j)} \right) \left(S_{(i)(sfgl)}^{(j)} \right) \right], \quad (\text{Eq. 49})$$

The supply of erodible sediment from the SFGL sediment source is modeled as

$$S_{sfgl sed}^{(j)}(i) = \min \left[S_{sfgl sed}^{(j)}(i-1) - E_{sfgl sed}^{(j)}(i) + D_{sfgl sed}^{(j)}(i) + G_{sfgl sed}, S_{sfgl sed}^{(j)}(max) \right], \quad (\text{Eq. 50})$$

Where $S_{sfgl sed}^{(j)}(i-1)$ is the supply of sediment in the SFGL from the previous time step, $E_{sfgl sed}^{(j)}(i)$ is the erosion of sediments from the SFGL, $D_{sfgl sed}^{(j)}(i)$ is the sediment fraction of depositing material to the surface fine grained lamina, $G_{sfgl sed}$ is the generation of sediment to the SFGL from bioturbation, and $S_{sfgl sed(max)}^{(j)}$ is the maximum supply of the surface fine grained lamina. The SFGL is assumed to form on top of bed material, and thus the surface area of the SFGL is assumed to be equal to that of the bed and is estimated as

$$SA_{(sfgl)(i)}^{(j)} = SA_{(bed)(i)}^{(j)} = W_{reach(i)}^{(j)} L_{reach}^{(j)}, \quad (\text{Eq. 51})$$

The sediment supply of the SFGL provides a matrix for the growth of microorganisms.

The supply fine grained biological material to the SFGL is given by the equation

$$S_{sfglbio(i)}^{(j)} = \min \left[S_{sfglbio(i-1)}^{(j)} - E_{sfglbio(i)}^{(j)} + D_{sfglbio(i)}^{(j)} + G_{sfgl(sed)}, S_{sfgl(sed)}^{(j)}, S_{sfgl(sed)(max)}^{(j)} \right], \quad (\text{Eq. 52})$$

Where $S_{sfglbio(i-1)}^{(j)}$ is the supply of biofilm in the SFGL from the previous time step, $E_{sfgl(sed)}^{(j)}$ is the erosion of biofilm, $D_{sfglbio(i)}^{(j)}$ is the fraction of depositing material that comes from eroded biofilm, $G_{sfgl(sed)}$ is the generation of the biofilm over time from biological growth, and $S_{sfglbio(max)}^{(j)}$ is the maximum supply of biological material in the SFGL.

The fraction of sediments eroding from each SFGL store is calculated with a mass fraction assuming sediments and biofilm material are homogeneously dispersed throughout the entire SFGL.

$$E_{sfgl(sed)(i)}^{(j)} = E_{sfgl(i)}^{(j)} \left[\frac{S_{sfgl(sed)}^{(j)}}{S_{sfgl(sed)}^{(j)} + S_{sfglbio(i)}^{(j)}} \right], \quad (\text{Eq. 53})$$

$$E_{sfgl(bio)(i)}^{(j)} = E_{sfgl(i)}^{(j)} \left[\frac{S_{sfglbio(i)}^{(j)}}{S_{sfgl(sed)}^{(j)} + S_{sfglbio(i)}^{(j)}} \right], \quad (\text{Eq. 54})$$

3.3.9 Bed Erosion

Streambed erosion sources are modeled as segments of constant surface area, so that the only spatial change occurring with erosion or deposition is a change in depth.

Bed erosion is simulated only after the supply of SFGL has been fully eroded using Equation (55).

$$E_{(i)(bed)}^{(j)} = \min \left[\left(a_{(bed)} \left(\tau_{f(i)}^{(j)} - \tau_{cr(bed)} \right)^{b(k)} SA_{(bed)} \Delta t \right) \left(T_{cr(i)(bed)}^{(j)} \right) \left(S_{(i)(bed)}^{(j)} \right) \right], \quad (\text{Eq. 55})$$

The supply of bed sediment is given by the equation

$$S_{(i)(bed)}^{(j)} = S_{(i-1)(bed)}^{(j)} + D_{(i-1)(bed)}^{(j)} - E_{(i-1)(bed)}^{(j)} - G_{sfgl(sed)}, \quad (\text{Eq. 56})$$

Where $S_{(i-1)(bed)}^{(j)}$ is the supply of bed sediments from the previous time step, $D_{(i)(bed)}^{(j)}$ is the deposition to the bed, $E_{(i)(bed)}^{(j)}$ is the erosion from the bed, and $G_{sfgl(sed)}$ is the removal of fine sediments from the bed and into the SFGL from bioturbation.

3.3.10 Deposition

Fine sediment is assumed to deposit as either part of the surface fine grain lamina, or in the streambed. Deposition occurs to the surface fine grained lamina first, only when the maximum SFGL storage is reached does deposition contribute to the bed storage. If material is depositing to the SFGL, then deposition to the sediment supply of the SFGL and the biofilm supply of the SFGL are estimated with a mass fraction.

The fraction of biofilm depositing during a time step is estimated as the fraction of biofilm currently in suspension over the total sediment load in suspension.

$$D_{sfgl(bio)(i)}^{(j)} = D_{sfgl(i)}^{(j)} \left[\frac{S_{sfglbio(i-1)}^{(j)} + E_{sfglbio(i)}^{(j)}}{SS_{(i)}^{(j)}} \right], \quad (\text{Eq. 57})$$

$$D_{sfgl(sed)(i)}^{(j)} = D_{sfgl(i)}^{(j)} - D_{sfgl(bio)(i)}^{(j)}, \quad (\text{Eq. 58})$$

where $D_{sfgl(i)}^{(j)}$ is the deposition associated with the SFGL [kg/s.m^2], the numerator of the fraction in Equation (57) is the current supply of biofilm in suspension, and the denominator is the total mass of sediments currently in suspension.

Deposition is modeled as a function of the particle settling velocity and the transport capacity deficit

$$D_{(i)}^{(j)} = \frac{\omega_s \Delta t}{k_p H_{(i)}^{(j)}} \left(SS_{(i-1/2)}^{(j)} - T_c^{(j)} \right), \quad (\text{Eq.59})$$

where $D_{(i)}^{(j)}$ is the total deposition for the time step [kg], ω_s is the settling velocity of the <63 micron fraction [m/s], k_p is a deposition coefficient based on the concentration profile, $H_{(i)}^{(j)}$ is the water depth [m], $T_c^{(j)}$ is the transport capacity of the reach [kg], and $SS_{(i-1/2)}^{(j)}$ is the mass of sediment being transported by the reach at the start of the time step [kg]. .

k_p is calculated every time step. This coefficient describes the vertical centroid of the concentration profile. The concentration profile is given by the equation

$$C(y) = C_a \left[\left(\frac{D-y}{y} \right) \left(\frac{a}{D-a} \right) \right]^{z_*} \quad (\text{Eq. 60})$$

where C_a is a reference concentration and a is a reference level. z_* is the Rouse number defined as

$$z_* = \frac{\omega_s}{\kappa U_*} \quad (\text{Eq. 61})$$

where w_s is sediment fall velocity in m/s, κ is the dimensionless von Karman constant equal to approximately 0.40, and U^* is the shear velocity in m/s. U^* is defined as

$$U_* = (gHS)^{1/2} \quad (\text{Eq. 62})$$

The reference level a is treated as the transition from bed load to suspended load and occurs on the order of 5% of the flow depth (Chang 1988). C_a typically corresponds to this reference level. To find k_p , concentration curves with values of z^* varying between 0.03 and 4 were numerically integrating over the entire profile depth. Numerical integration was performed by discretizing the depth into 2000 increments, multiplying the concentration given by Equation (60) by the current relative depth increment, summing the concentration and relative depth product, and dividing by the concentration sum to determine a concentration weighted average relative depth. Relative depth is defined by the equation

$$H_{rel} = \frac{y - a}{D - a} \quad (\text{Eq. 63})$$

where y is the depth increment, a is the reference level, and D is the arbitrary water depth chosen for this integration. Figure 8 shows an example of concentration curves with varying values of z^* . The vertical axis represents the relative depth, and the horizontal average the relative concentration.

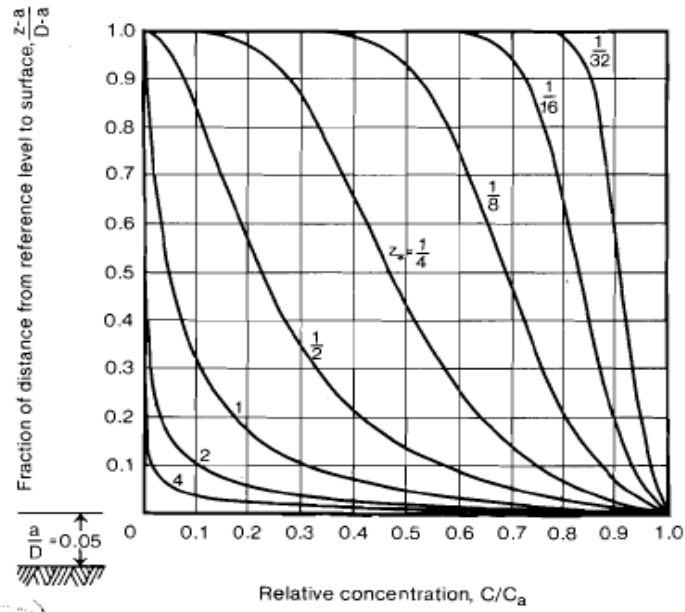


Figure 8: Figure 7.9 from H. Chang (1988) on page 149. "Vanoni nomograph."

The average relative depth for each concentration curve was then plotted with its associated z^* . The relationship between z^* and the average relative depth is the function used to determine k_p for the time step. The relationship was found to be Equation (64). Figure 9 shows the graph of z^* to the average relative depth.

$$k_p = 0.5e^{-0.98z^*}, \quad (\text{Eq. 64})$$

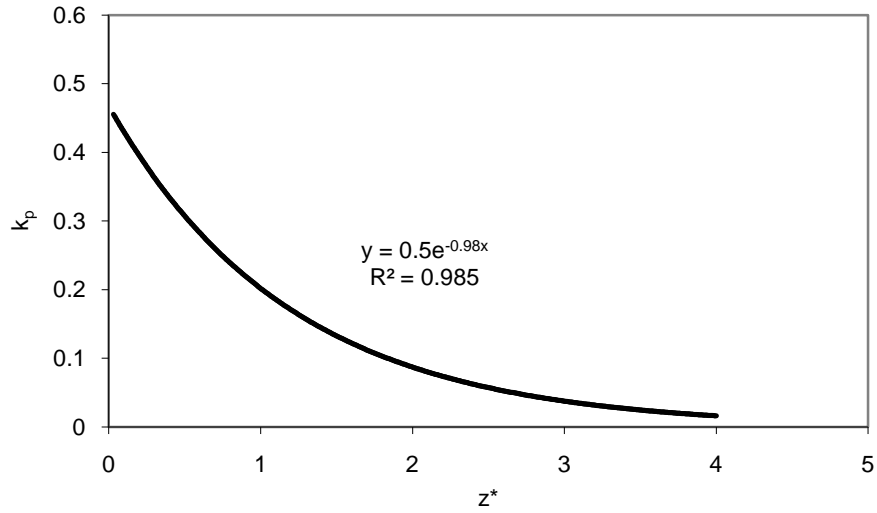


Figure 9: Figure of z^* versus deposition coefficient.

3.3.11 Sediment Routing

Sediment routing is done similarly to the flow routing performed by HSPF. Suspended sediments are assumed to be distributed uniformly across the reach and are routed with the equations

$$Q_{ssin(i)}^{(j)} = k_{SS} \left(\frac{SS^{(j-1)}}{V^{(j-1)} \left(\frac{(i-1)+\frac{1}{2}}{2} \right)} \right) Q_{out \left(\frac{(i-1)+\frac{1}{2}}{2} \right)}^{(j-1)} + (1 - k_{SS}) \left(\frac{SS^{(j-1)}}{V^{(j-1)} \left(\frac{(i-1)+\frac{1}{2}}{2} \right)} \right) Q_{out \left(\frac{(i-1)+\frac{1}{2}}{2} \right)}^{(j-1)},$$

(Eq. 65)

$$Q_{ssout(i)}^{(j)} = k_{SS} \left(\frac{SS^{(j)}}{V^{(j)} \left(\frac{i-\frac{1}{2}}{2} \right)} \right) Q_{out \left(\frac{i-\frac{1}{2}}{2} \right)}^{(j)} + (1 - k_{SS}) \left(\frac{SS^{(j)}}{V^{(j)} \left(\frac{i-\frac{1}{2}}{2} \right)} \right) Q_{out \left(\frac{i-\frac{1}{2}}{2} \right)}^{(j)},$$

(Eq. 66)

By substitution:

$$SS_{\left(i+\frac{1}{2}\right)}^{(j)} = \frac{SS_{\left(i-\frac{1}{2}\right)}^{(j)} + \sum_{k=1}^N E_{(i)(k)}^{(j)} - D_{(i)}^{(j)} + Q_{s \sin(i)}^{(j)} \Delta t - k_{ss} \left(\frac{SS_{\left(i-\frac{1}{2}\right)}^{(j)}}{V_{\left(i-\frac{1}{2}\right)}^{(j)}} \right) Q_{out\left(i-\frac{1}{2}\right)}^{(j)} \Delta t}{1 + (1 - k_{ss}) \left(\frac{Q_{out\left(i+\frac{1}{2}\right)}^{(j)}}{V_{\left(i+\frac{1}{2}\right)}^{(j)}} \right) \Delta t},$$

(Eq. 67)

The routing coefficient, k_{ss} , describes the influence sediment flow rates at the beginning and end of the time step have on the average sediment flow rate for the time step over the stream-reach. Higher values put more emphasis on the sediment flow rates at the start of the time step, and lower values put more emphasis on the flow rates at the end of the time step.

Chapter 4: Study Watershed

The South Elkhorn Watershed (61.8 km²) located within the South Elkhorn basin (478.5 km²) in the Bluegrass Physiographic Region of Central Kentucky, which can be seen in Figure 10. Figure 11 shows the watershed and its mixed land-use. The watershed was chosen for application of the new sediment model formulation primarily due to (i) the dominance of in-stream sediment transport processes in the watershed, (ii) the history of urbanization and deposition of legacy sediments in-stream, and (iii) the performance of past studies including sediment fingerprinting by Davis (2008) and aggregate analysis by Sliter (2007) and the on-going collection of data being performed in the watershed.

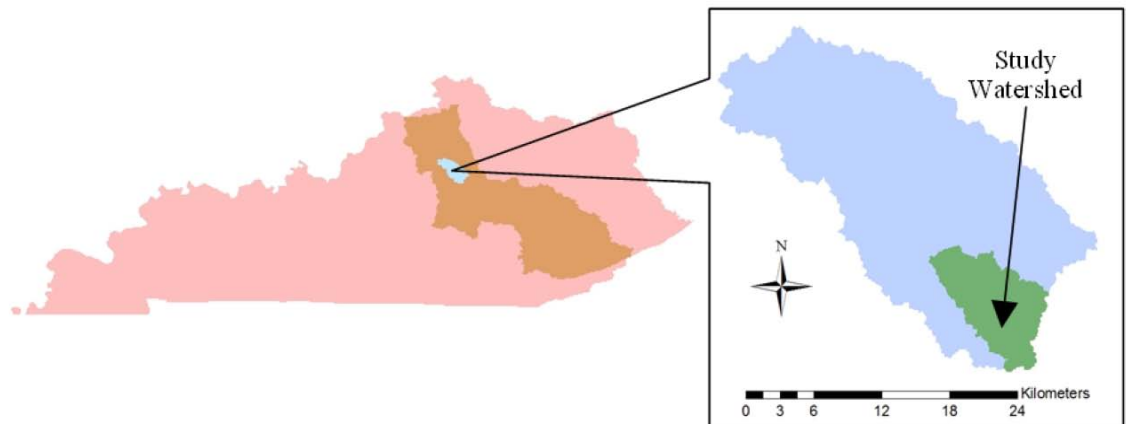


Figure 10: *Location map for the study watershed.*

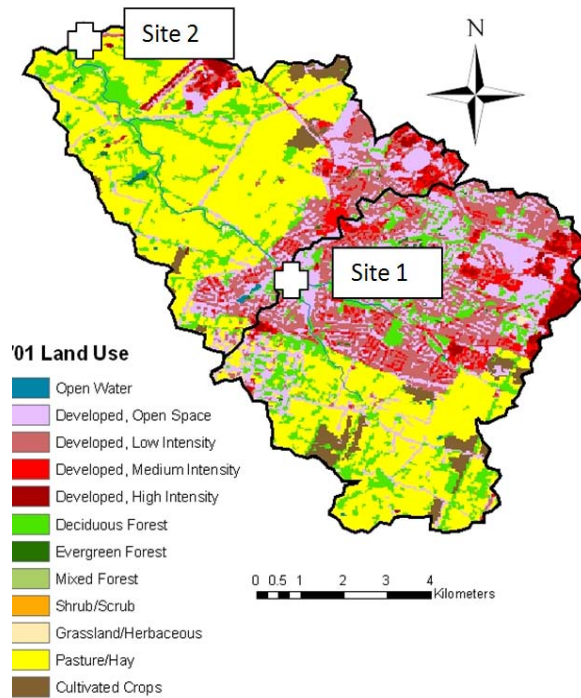


Figure 11: *Map of the South Elkhorn Watershed, Lexington Ky.*

In-stream sediment transport processes in the watershed include sediment transport within the stream corridor and includes streambank erosion, streambed erosion and storage, and erosion, deposition and development of the SFGL. Erosion of incised and widening streambanks over a bedrock channel is pronounced in the stream system, which is indicative of the mild stream gradients in the Bluegrass Region. The eroding streambanks, which are the prominent source of in-stream sediments, are fairly homogeneous throughout the watershed, and additional soil and environmental variables are generally consistent across the watershed. Streambed sediment storage is also high in the watershed. It has been previously estimated that the volume of sediment within the streambed equals approximately 18,000 Mt, constituting a pool three orders of magnitude higher than the sediment yield during a significant hydrologic event (Davis 2008). The presence of the SFGL is also observed within the stream corridor and has been suggested

to impart control on organic matter signatures and sediment physical structure (Davis 2008, Sliter 2007). While in-stream processes produce a large amount of sediment, upland processes in general do not produce high sediment loads (Coulter et al. 2004). Overland erosion processes such as rill and inter-rill erosion are only a small contribution to sediment loads in the South Elkhorn watershed, thus model development can be achieved under fairly controlled conditions.

Urbanization has been pronounced in the upper half of the watershed and is believed to have increased streambank erosion, in-stream storage, and the presence of legacy sediments . The urbanization rate for the South Elkhorn was estimated using the 1992 and 2001 National Land Cover Datasets, which can be seen in Figure 12. All cells containing values for an urban land cover code in the South Elkhorn were summed to obtain an estimate of urban land cover for the years 1992 and 2001. It was found that there was approximately 11.6 km² of urban area in 1992 and 27.7 km² in 2001. This analysis determined the urbanization rate as being 1.6 km² per year between the years 1992 and 2001. The NLCD data used to derive this urbanization rate occurred during a period of pronounced urban development during the late 1990's. For the urbanization rates used for this thesis, four urbanization rates were chosen being 0 km² per year, 0.4 km² per year, 0.8 km² per year , and 1.6 km² per year.

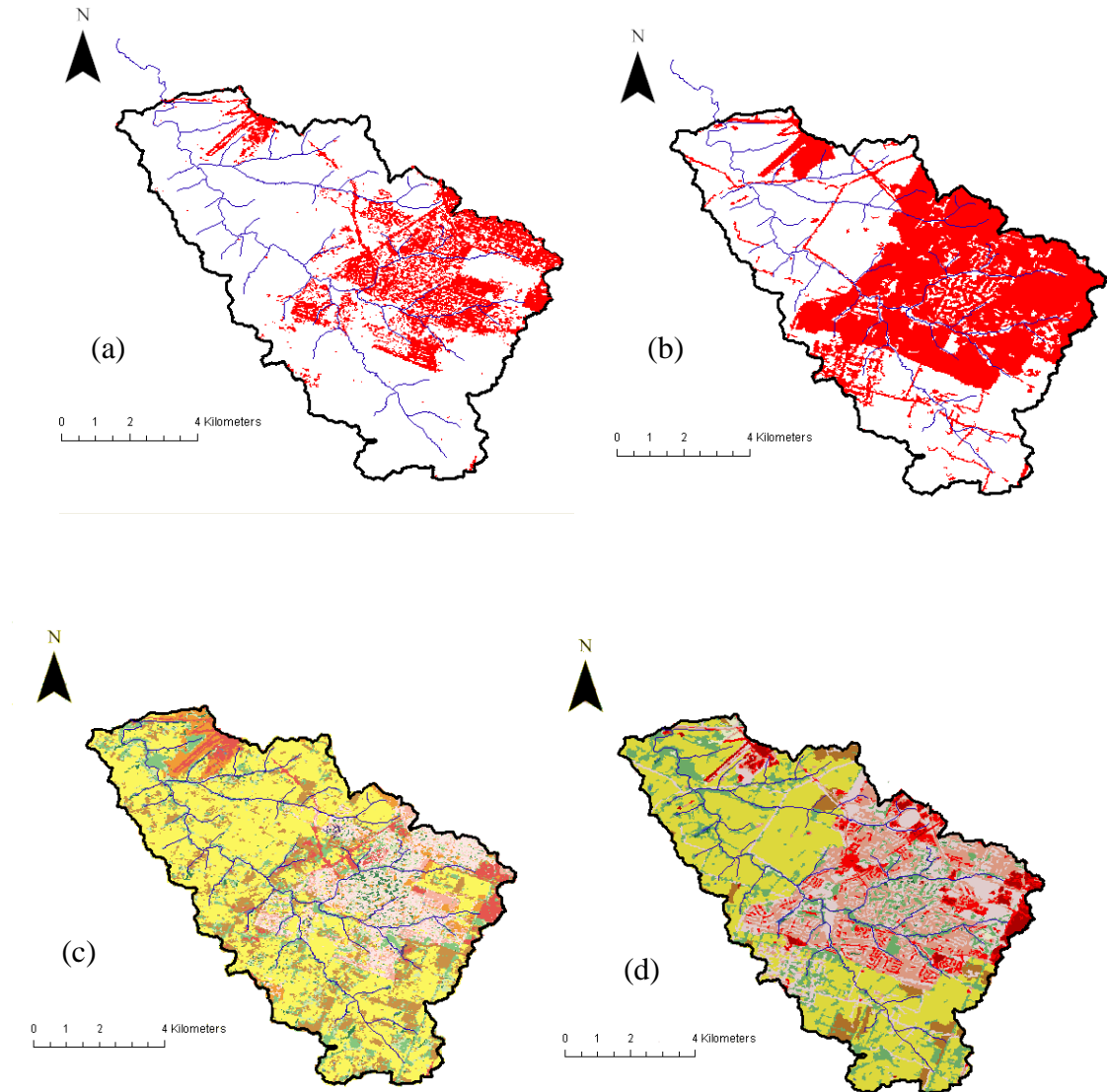


Figure 12: (a) 1992 urban area, (b) 2001 urban area, (c) 1992 NLCD, and (d) 2001 NLCD.

The South Elkhorn is a multi land use lowland watershed with urban and non-urban land cover, and is representative of other small scale basins in the bluegrass region of Kentucky. At this time, the region has pronounced sedimentation problems in its streams primarily as the result of bank erosion processes, thus making the model development a regional environmental need. In addition, the lowland watershed contains

pronounced storage of sediment which has been cited as an unknown source of carbon to regional and global carbon budgets (Cole et al. 2007). Due to the above sediment issues, the watershed has been designated as a testbed for sediment transport model and method development in order to work towards gaining knowledge regarding sediment pollution and carbon dioxide degassing from streambeds. The South Elkhorn has been an experimental watershed where tracer development and sediment fingerprinting methodologies have been improved over the past four years. Stream flow and precipitation data is available for the watershed. Weather data is readily available from NOAA. The Lexington Airport is located inside the study watershed and hourly precipitation, temperature, and wind speed data are easily accessible. Flow and water depth data is also easily accessible from USGS gage 03289000 located at the outlet of the watershed.

Chapter 5: HSPF Watershed Model Calibration, Validation, and Sensitivity

Analysis

5.1 Model Set Up

HSPF was set up using Better Assessment Science Integrating Point and Non-Point Sources (BASINS) software package available via free download from the EPA website. BASINS uses an easy to use Graphical Information Systems (GIS) interface to integrate spatial and temporal data together with EPA hydrologic and water quality models. Input data for the hydrologic component of HSPF includes land cover, topology, and climatology data. Land cover data is available from the National Land Cover Dataset (NLCD) available from the USGS. Topology data is also available from USGS as a digital elevation model (DEM) with 10 meter resolution. Climatology data includes air temperature, percent sun, and precipitation and are available from the National Oceanic and Atmospheric Administration (NOAA). A NOAA weather observatory is available at the Bluegrass Airport located within the study area near the outlet which collects precipitation and air temperature data hourly. Percent sun data was collected from NOAA as a dataset containing the average monthly percent sun values for the Louisville Kentucky area, the closest observatory to the study area. This percent sun data was disaggregated into average daily values. The hydrologic model was calibrated with flow data available at the outlet of the watershed from USGS Gage 03289000. This flow data is collected every five minutes, and was aggregated into an hourly time series for calibration of the hydrologic model HSPF. Table 1 shows the input and calibration data and for HSPF and its origin.

Table 1: *Table of Input and Calibration Data for HSPF and origin.*

HSPF Data	Source	Link	Parameters Estimated
Hourly Precipitation	NOAA	http://www.ncdc.noaa.gov/oa/ncdc.html	Precipitation during time step
Maximum Hourly Temperature	NOAA	http://www.ncdc.noaa.gov/oa/ncdc.html	Potential Evapotranspiration
Minimum Hourly Temperature	NOAA	http://www.ncdc.noaa.gov/oa/ncdc.html	Potential Evapotranspiration
Dewpoint Temperature	NOAA	http://www.ncdc.noaa.gov/oa/ncdc.html	Potential Evapotranspiration
Percent Sun	NOAA	http://www.ncdc.noaa.gov/oa/ncdc.html	Potential Evapotranspiration
Land Use	USGS	http://nationalmap.gov/viewers.html	Surface Area for each HRU, Subcatchment Delineation, Mannings n for overland flow plane.
Topology	USGS	http://nationalmap.gov/viewers.html	Subcatchment Delineation, stream length, channel slope, upland slope, Length of overland flow plane
Streamflow	USGS	http://waterdata.usgs.gov/nwis/rt	Calibration data at watershed outlet

HSPF is a lumped parameter model which combines areas of similar spatial properties and calculates hydrologic processes across these areas. Several factors influenced the delineation of sub-basins for HSPF, including soil cover, land cover,

topography, and stream length (Abed and Whitely, 2002). Soil cover was found to be homogenous for the majority of the South Elkhorn so topography, land cover, and stream length were used to define the delineation. The hydrologic routing algorithms used in the HSPF model are accurate when the flow time through individual reached approximates the simulation time step (Donigian, 1984). HSPF assumes that the volume of water that flows out of the sub-basin/reach during a time step exits to the downstream sub-basin/reach during the next time step. Stream length was therefore one of the most influential factors for sub-basins. Based on this criterion, the stream length must be equivalent to the product of the mean stream velocity of the reach and the time step. For this watershed, it was found that reach lengths be between 756 and 4184 meters corresponding to a low 0.14 cms flow and a high 28 cms flow with a nominal value of 2220 meters for a normal 2.8 cms event.

A large- and small-subcatchment delineations were created to determine the hydrologic model sensitivity to size of the delineation. For the delineations the stream length was within the range of the reach length needed for maintaining the time step-spatial domain assumption of the model, i.e., 756 and 4184 m for the hourly time step. The small delineation tended to underpredict high flow events while the large delineation performed better. The larger sub-basin delineation was chosen and determined to be optimal because high flows transport the majority of the annual water volume out of the watershed. A larger delineation captures these larger flow events while smaller delineations do not have the resolution needed to capture these events.

5.2 Model Calibration

Hydrologic simulation combines the physical characteristics and properties of the watershed such with the observed meteorological data via a series of interacting equations to produce a simulated hydrologic response. The hydrologic response of any watershed can be broken down into a few key processes, thus all watersheds have similar hydrologic components but the dominant processes vary and different hydrologic responses occur on different watersheds. Actual runoff is simulated in HSPF after accounting for all hydrologic losses which include evapotranspiration, deep percolation, and soil moisture storage. HSPF simulates the hydrologic response of the actual runoff from four components including surface runoff from impervious areas, surface runoff from pervious areas, interflow from pervious areas, and groundwater flow. Observed data from the watershed is not discretized into these components, and thus their relative weights must be inferred from hydrologic calibration.

Model calibration and validation are a critical step required for any model. Calibration for HSPF is an iterative process involving parameter estimation, running the model, comparison of observed data to simulated data, refinement of parameter, and running the model again until all parameters have been calibrated and the model is at its best solution. HSPF is a highly parameterized model, and components that cannot be measured must be estimated and adjusted through calibration. BASINS Technical Note 6 provides initial estimates and logical ranges for the many hydrologic parameters that control the HSPF model. HSPF was calibrated in accordance with the procedure outlined in Donigian (2002) which recommended yearly volume be calibrated first, then seasonal, monthly, base flow, and individual storm events.

The watershed Model Hydrologic Simulations Program Fortran (HSPF) was calibrated using the flowrate data collected between the dates January 1, 2006 to December 31, 2008. Donigian (2002) recommends at least three years of data be available for calibration/verification, and many studies have used this calibration period or less (Brun and Band, 2000; Bergman et al., 2002; Tzoraki and Nikolaidis, 2007; Mishra et al., 2007; Jeon et al, 2007; Diaz-Ramirez, et al. 2008). To compare simulated flows to observed flows, the percent difference (%Diff) between the observed and simulated values as for yearly, seasonal, monthly, and daily volumes was used as the test as well as the coefficient of determination (R^2), and the Nash-Sutcliff coefficient (NS).

$$R^2 = \left[\frac{\sum_{i=1}^n (O_i - O_{avg})(S_i - S_{avg})}{[\sum_{i=1}^n (O_i - O_{avg})]^{1/2} [\sum_{i=1}^n (S_i - S_{avg})]^{1/2}} \right]^2 \quad (\text{Eq. 68})$$

$$NS = 1 - \frac{\sum_{i=1}^n (O_i - S_i)^2}{\sum_{i=1}^n (O_i - O_{avg})^2} \quad (\text{Eq. 69})$$

$$\%Diff = \frac{(O_i - S_i)}{O_i} * 100 \quad (\text{Eq. 70})$$

where O_j is the observed value at time period i , O_{avg} is the average observed value for the time period, S_i is the simulated value for the time period, and S_{avg} is the average simulated value for the time period. The hydrologic model was calibrated with flow data available at the outlet of the watershed from USGS Gage 03289000. This flow data is collected every five minutes, and was aggregated into an hourly time series for calibration of the hydrologic model HSPF.

What is considered a “good” calibration is subjective, by the most researchers agree on a few key truths about numerical models. These truths include the recognition

that models are approximations of reality and cannot be expected to simulate reality perfectly, there is no single test statistic that will validate a model, both graphical comparison and statistical tests are needed to calibrate and validate a numerical model, and models cannot be expected to be more accurate than their input datum. Table 2 shows the most commonly accepted values for the test statistics R^2 and percent difference for the comparison of observed stream flows with simulated stream flows (Donnigian, 2002).

Table 2: *Table of commonly accepted hydrologic model calibration statistics.*

Statistic	poor	fair	good	very good
R^2 (daily)	<0.61	0.62-0.72	0.73-0.81	>0.81
R^2 (monthly)	<0.64	0.65-0.76	0.77-0.85	0.86-1.0
% Diff (monthly/annual)	>25	15-25	10-15	<10

For this study, the model was considered calibrated when the percent difference for monthly flow volumes were at or less than 20% of their observed values. To calibrate the model, parameters which could not be directly measured or indirectly estimated with GIS were calibrated to the observed data.

Table 3 displays the hydrological parameters for HSPF and their range of values (Donigian, 1984),

Table 4 shows the bulk parameters and their calibrated values, Table 5 shows the upper zone nominal storage monthly calibrated values, Table 6 shows the maximum interception storage monthly values, and Table 7 displays lower zone evapotranspiration parameter monthly values.

Table 3: *Table of HSPF parameters and their range of values.*

HSPF Hydrology Parameters and their range of values			
LZSN	Lower zone nominal soil moisture storage	50.8-381.0	(mm)
SLSUR	Slope of overland flow plane in pervious area	0.001-0.30	
NSUR	Manning's n for overland flow plane of pervious areas	0.05-0.5	
LSUR	Length of overland flow plane in pervious areas	30.48-213.36	(m)
INFILT	Index to infiltration capacity	0.025-12.7	(mm/hr)
KVARY	Variable groundwater recession	0.0-127.0	(1/mm)
AGWRC	Base groundwater recession	0.92-0.999	
DEEPPFR	Fraction of groundwater inflow to deep watertable (lost)	0.0-0.5	
BASETP	Fraction of remaining evapotranspiration from baseflow	0.0-0.2	
AGWET P	Fraction of remaining evapotranspiration from active GW	0.0-0.2	
CEPSC	Interception storage capacity	0.0-10.2	(mm)
UZSN	Upper zone nominal soil moisture	12.7-50.8	(mm)
INTFW	Interflow inflow parameter	1.0-10.0	
IRC	Interflow recession parameter	0.3-0.85	
LZETP	Lower zone evapotranspiration parameter	0.0-0.9	
ILS			
SLSUR	Slope of overland flow plane in impervious area	0.001-0.15	
ILS			
LSUR	Length of overland flow plane in impervious area	15.24-76.2	(m)
ILS			
NSUR	Manning's n for overland flow in impervious areas	0.01-0.15	
ILS			
RETSC	Retention storage capacity in impervious areas	0.254-7.62	(mm)

Table 4: Table of HSPF parameters and their calibrated values for a large delineation.

	wetland	urban	forest	upland shrub	cropland	grassland	pasture
LZSN	0.254	0.254	0.254	0.254	0.254	0.254	0.254
SLSUR	0.0099	0.0099	0.0099	0.0099	0.0099	0.0099	0.0099
NSUR	0.01	0.1	0.4	0.4	0.3	0.2	0.2
LSUR	121.92	121.92	121.92	121.92	121.92	121.92	121.92
INFILT	12.7	12.7	12.7	12.7	12.7	12.7	12.7
KVARY	0	0	0	0	0	0	0
AGWRC	0.88	0.78	0.88	0.88	0.88	0.88	0.88
DEEPPFR	0	0	0	0	0	0	0
BASETP	0	0	0	0	0	0	0
AGWETP	0	0	0	0	0	0	0
INTFW	1	1	1	1	1	1	1
IRC	0.85	0.85	0.85	0.85	0.85	0.85	0.85
ILS							
SLSUR	N/A	0.0099	N/A	N/A	N/A	N/A	N/A
ILS LSUR	N/A	121.92	N/A	N/A	N/A	N/A	N/A
ILS NSUR	N/A	0.05	N/A	N/A	N/A	N/A	N/A
ILS							
RETSC	N/A	0	N/A	N/A	N/A	N/A	N/A

Table 5: Table of the upper zone nominal storage monthly calibrated values for a large delineation.

	UZSN Monthly Values (cm)						
	wetland	urban	forest	upland shrub	cropland	grassland	pasture
Jan	5.08	5.08	5.08	5.08	5.08	5.08	5.08
Feb	5.08	5.08	5.08	5.08	5.08	5.08	5.08
Mar	5.08	5.08	5.08	5.08	5.08	5.08	5.08
Apr	5.08	5.08	5.08	5.08	5.08	5.08	5.08
May	5.08	5.08	5.08	5.08	5.08	5.08	5.08
Jun	7.63	7.63	7.63	7.63	7.63	7.63	7.63
Jul	7.63	7.63	7.63	7.63	7.63	7.63	7.63
Aug	7.63	7.63	7.63	7.63	7.63	7.63	7.63
Sep	7.63	7.63	7.63	7.63	7.63	7.63	7.63
Oct	5.08	5.08	5.08	5.08	5.08	5.08	5.08
Nov	5.08	5.08	5.08	5.08	5.08	5.08	5.08
Dec	5.08	5.08	5.08	5.08	5.08	5.08	5.08

Table 6: *Table of the interception monthly calibrated values for a large delineation.*

CEPSC Monthly Values (cm)							
	wetland	urban	forest	upland shrub	cropland	grassland	pasture
Jan	0	0	0	0	0	0	0
Feb	0	0	0	0	0	0	0
Mar	0	0	0	0	0	0	0
Apr	0.508	0.508	0.508	0.508	0.508	0.508	0.508
May	0.508	0.508	0.508	0.508	0.508	0.508	0.508
Jun	2.54	2.54	2.54	2.54	2.54	2.54	2.54
Jul	2.54	2.54	2.54	2.54	2.54	2.54	2.54
Aug	2.54	2.54	2.54	2.54	2.54	2.54	2.54
Sep	2.54	2.54	2.54	2.54	2.54	2.54	2.54
Oct	2.54	2.54	2.54	2.54	2.54	2.54	2.54
Nov	0	0	0	0	0	0	0
Dec	0	0	0	0	0	0	0

Table 7: *Table of the lower zone evapotranspiration parameters and their monthly calibrated values for a large delineation.*

LZETP Monthly Values							
	wetland	urban	forest	upland shrub	cropland	grassland	pasture
Jan	0	0	0	0	0	0	0
Feb	0	0	0	0	0	0	0
Mar	0	0	0	0	0	0	0
Apr	0.05	0.05	0.05	0.05	0.05	0.05	0.05
May	0.2	0.2	0.2	0.2	0.2	0.2	0.2
Jun	0.05	0.05	0.05	0.05	0.05	0.05	0.05
Jul	0.05	0.05	0.05	0.05	0.05	0.05	0.05
Aug	0.05	0.05	0.05	0.05	0.05	0.05	0.05
Sep	0.05	0.05	0.05	0.05	0.05	0.05	0.05
Oct	0.05	0.05	0.05	0.05	0.05	0.05	0.05
Nov	0	0	0	0	0	0	0
Dec	0	0	0	0	0	0	0

Basins Technical Note 6 was used extensively for the estimation of parameters and as a guide for calibration. Some parameter values, including impervious land retention storage (ILS RETSC), impervious land overland slope length (ILS LSUR), and

base groundwater recession (AGWRC), are not within their recommended range of values. The base groundwater recession constant was fit to the groundwater recession of the data, values within the range recommended did not simulate base flow well. Impervious retention storage was calibrated to the observed data, as alterations to this value decreased the accuracy of the model. Impervious retention storage in the study watershed can be assumed to be close to zero since the majority of urban areas route water off of the buildings, parking lots, and driveways and into drainage ditches without retaining any significant depth of precipitation. Values for the length of the overland flow plane were left as the BASINS derived value as this parameter was found to be insensitive to the overall water budget and hydrograph timing. Other values such as infiltration (INFILT) and the interflow recession constant (IRC) were set to their maximum and minimum values respectively. Although these values were calibrated to the observed data, this is assumed to be a reasonable average value for infiltration and interflow recession. During the winter months, simulated storm peaks are lower than observed storm peaks. This implies that infiltration values need to be decreased to that more moisture is available to runoff. However, during the winter months simulated storm peaks are well above observed storm peaks, implying that infiltration values need to be higher. In reality, infiltration values are probably much lower than those assumed for this model, but because of the extremely dry drought/near drought conditions the study watershed experiences during the summer months the soil becomes less homogeneous. The top soils during this season usually crack open because of the lack of moisture, so for the summer months the upper zone moisture storage should increase substantially, which can be simulated with monthly values, and the infiltration rate should

increase greatly, which cannot be simulated with monthly values, because of the quasi-conduit flow from the cracks in the top-soils.

5.3 Model Sensitivity

Previous studies performing sensitivity analysis on HSPF have concluded that the groundwater recession parameter, infiltration, interflow recession and inflow parameters, upper zone and lower zone storages, and lower zone evapotranspiration are the most sensitive parameters controlling streamflow (Diaz Ramirez et al., 2008; Abed and Whitely, 2002). A sensitivity analysis was performed on the calibration parameters. The sensitivity analysis consisted of varying a single parameter through its lowest, one quarter, midpoint, three quarter and maximum values while maintaining all other parameters constant. Figure 13 displays the results of the sensitivity analysis. The horizontal axis is the relative value of the parameter, and the vertical axis is the relative change in the output, stream flow, from the midpoint value. The output value compared for this analysis was the sum of flow for the years 2007 and 2008.

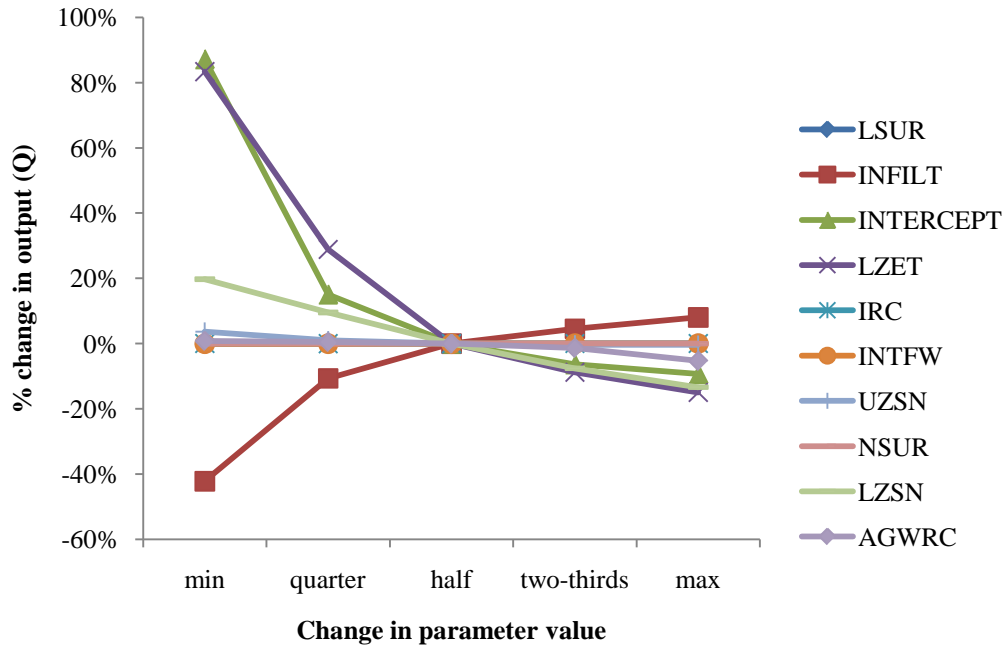


Figure 13: Chart of HSPF parameters and their sensitivity to a large delineation.

Length of the overland flow plane, interflow recession constant, the interflow outflow parameter, and overland surface roughness were insensitive to changes in values, although the test statistic for this analysis was flow volume and these parameters would affect the timing of the hydrograph more than the outflow volume. The upper zone nominal storage slightly controls of flow volumes at lower values. Increasing upper zone nominal storage from its minimum value increases the storage and thus exposure of stored moisture to evapotranspiration processes, but larger values would be ineffective at lowering the annual water balance because the maximum evapotranspiration is not controlled by the supply of moisture but by the potential evapotranspiration time series which is an input to HSPF. Similarly, the base flow recession constant have a slight sensitivity toward controlling flow volumes at higher values, because higher values keep more moisture in groundwater storage available to evapotranspiration processes. Low values for the lower zone evapotranspiration, interception, and lower zone nominal

storage increase the outflow volume drastically while larger values decrease outflow values pronouncedly, but not drastically. Lower values for interception and lower zone nominal storage directly control the availability of moisture for evapotranspiration processes and also delay moisture from entering the stream reach. Higher values will delay water from entering the system, but the maximum loss from the system is controlled by the potential evapotranspiration time series so increasing these values will only increase the delay the water out of the system and not increase the losses. Infiltration decreases stream flow volumes pronouncedly at lower values and increase volumes at higher values. Infiltration controls the division between surface and subsurface processes, or how much of the moisture supply runs off into the stream channel and how much infiltrated and is put in lower and upper zone storage. High infiltration values will produce more water in the lower zone and groundwater, and result in more base flow to the stream, while lower value will produce more direct runoff. As infiltration rates increase, total volume of streamflow increases because the rate of evaporation from the lower zone soil storage is lower than the rate of evaporation from the upper zone and surface soil storage.

5.4 Model Validation

The first year of data, 2006, was used as a warm up period for HSPF and its values were not considered in calibration or validation. The calendar year 2007 was used for calibration and the calendar year 2008 was used for validation. A daily time step was used for all calibration and validation calculations. Table 8 shows the correlation, percent difference, and Nash-Sutcliff coefficient for the 2007 and 2008 annual volumes. Table 9 shows the seasonal percent difference for 2007 and 2008. The correlation is

“fair” and the annual percent different is “very good.” Seasonal percent differences show a trend of over estimating flows during the summer months. The relative percent difference is high, but because summer flows are so low this may not be a representative statistic, as the difference between the observed and the simulated summer flows are close. Figure 14 and Figure 15 show a timeseries of the simulated and the observed flows at a daily time step for the 2007 and 2008 calendar year.

Table 8: *Table of observed and simulated flow statistics for the year 2007 and 2008.*

Year	Observed Volume (Mcf)	Simulated Volume (Mcf)	Percent Difference	Correlation	Nash- Sutcliff
2007	1008	975.22	-3.28%	0.68	0.33
2008	1328	1280.26	-3.58%	0.68	0.78
2007-08	2336	2255.48	-3.45%	0.68	0.56

Table 9: *Table of observed and simulated flow statistics for calendar seasons.*

Year	Winter Percent Difference	Spring Percent Difference	Summer Percent Difference	Fall Percent Difference
2007	-9.05%	5.16%	56.60%	-15.09%
2008	-18.59%	9.37%	71.01%	-1.83%

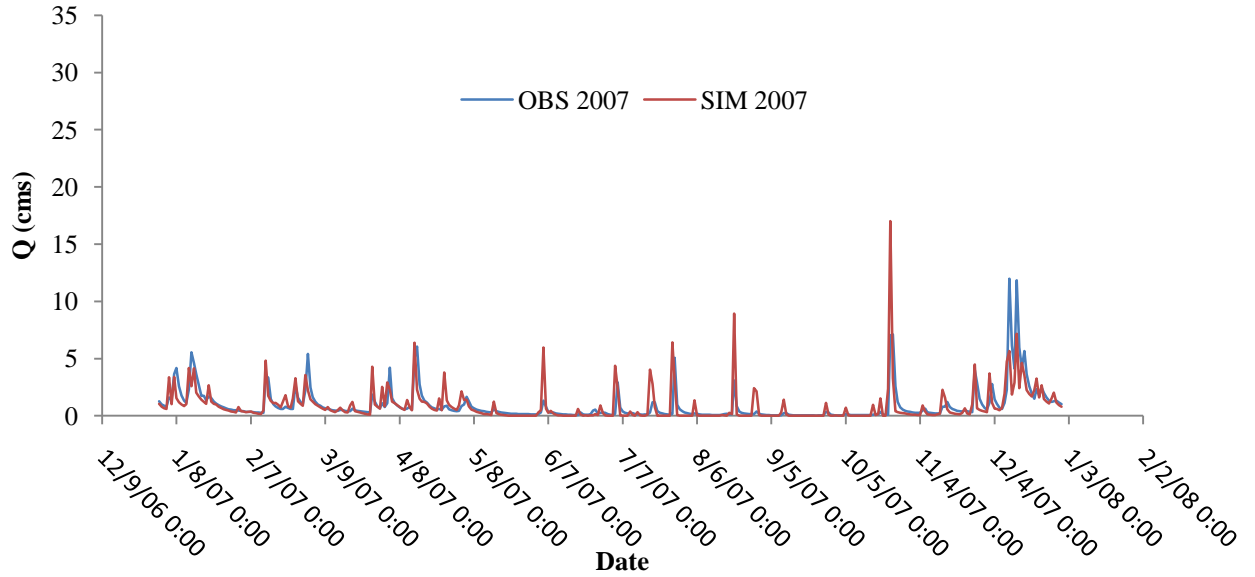


Figure 14: Observed and simulated flows for 2007.

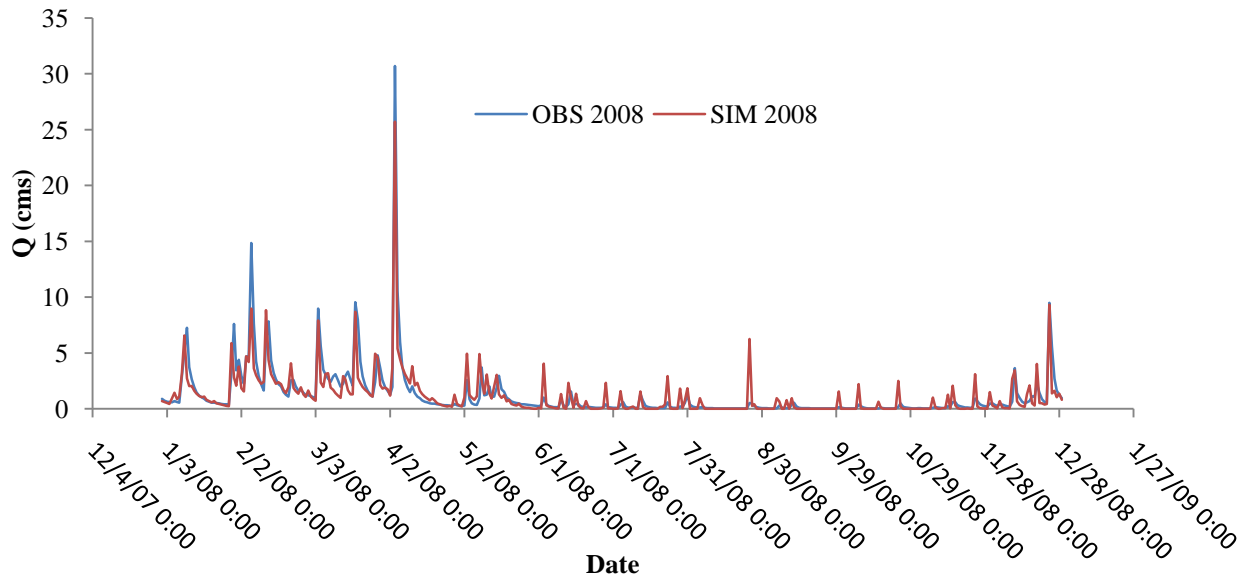


Figure 15: Observed and simulated flows for 2008.

To aid in validation of HSPF a frequency distribution of the daily observed flows to the daily simulated flows was performed. Table 10 and Table 11 show the results of this analysis. The number of daily low flows and high flows appear to be representative

of the study watershed. To further test this assumption, a two tailed paired t-test assuming unequal variances was used with the observed and simulated flow timeseries. Table 12 and Table 13 show the results of this analysis for the years 2007 and 2008 respectively. The null hypothesis was that the mean difference between both samples (the simulated and observed daily flow values for 2007 and 2008) is zero. The t statistics for both years were lower than the critical t value of 1.97 assuming a 95% confidence, and the null hypothesis was not rejected. It was assumed that the simulated values from the model are an appropriate representation of the study watershed.

Table 10: *Table of observed and simulated flow frequencies for the year 2007.*

2007 Observed Flow		2007 Simulated Flow	
Event (cms)	Frequency	Event (cms)	Frequency
0.28	141	0.28	172
0.71	241	0.71	232
1.42	305	1.42	301
2.83	339	2.83	337
4.25	352	4.25	352
5.66	357	5.66	359
14.16	365	14.16	364
28.32	365	28.32	365

Table 11: *Table of observed and simulated flow frequencies for the year 2008.*

2008 Observed Flow		2008 Simulated Flow	
Event (cms)	Frequency	Event (cms)	Frequency
0.28	156	0.28	171
0.71	239	0.71	210
1.42	281	1.42	266
2.83	325	2.83	327
4.25	345	4.25	349
5.66	354	5.66	356
14.16	365	14.16	366
28.32	366	28.32	367

Table 12: *Table of observed and simulated daily flow t-test for 2007.*

	2007 Observed Flows	2007 Simulated Flows
Mean	31.94	30.91
Variance	2633.87	2895.80
Observations	364.00	364.00
t Statistic	0.47	
t Critical	1.97	

Table 13: *Table of observed and simulated daily flows t-test for 2008.*

	2008 Observed Flows	2008 Simulated Flows
Mean	42.07	39.53
Variance	7185.05	4781.68
Observations	363.00	363.00
t Statistic	1.22	
t Critical	1.97	

Chapter 6: In-Stream Model Calibration

The in-stream sediment processes model was applied to the South Elkhorn lowland watershed. Input data to the sediment model included flow output from HSPF for each subcatchment and time step as well as measured stream bathymetry. Parameterization of the model was performed based on parameter values reported in the literature, the prevailing streambank, streambed and SFGL processes occurring within the study site, and adjustment during calibration.

6.1 Model Set Up, Input Data and Parameterization

The sediment transport model was set up with the same resolution as the hydrologic model. Input data for the sediment transport model included flow data from the hydrological model as well as channel slopes, side slopes, bankfull height, channel widths, channel lengths, time step, routing coefficients, Manning's n for the channel, sediment transport coefficients, boundary flow between high and low flows, maximum allowable supply of SFGL sediments, initial bed storage for the SFGL and the streambed, bulk density of bank sediments, sediment generation rates for the biologically active and inactive fractions of the SFGL, and erosivity coefficients. Sediment sources for each subcatchment included SFGL, bed, and bank sources. Flows from each stream reach in HSPF were used to drive the sediment transport model for that stream reach. The model was set up for simulation on an hourly time step for two subcatchments. Table 14 shows a chart of all the input data and parameter values for the sediment transport model that was used in the calibration and validation runs and later used for predicting urbanization scenarios.

Table 14: Table of input data and parameter values for the sediment transport model.

S	Channel slope.	0.00044	m/m
H_{bank}	Bankfull depth.	2	m
W_{reach}	Channel bottom width.	6.25	m
W_{flood}	Floodplain width on one side of channel	30	m
L_{reach}	Channel length.	10525	m
m	Side slope.	3.3	m/m
n	Mannings coefficient for channel.	0.02	
SA_B	Surface area of the banks.	21050	m ²
k_p	Settling depth coefficient.	calculated	unitless
k_{ss}	Sediment routing coefficient.	0.01	unitless
$Q_{boundary}$	Boundary between low and high flows.	2.50	m ³ /s
$S_{sfgl(max)}$	Maximum allowable supply of SFGL in the channel.	243400	kg
$S_{sfgl(sed)}$	Initial supply of SFGL sediment in the channel.	0	kg
$S_{sfgl(bio)}$	Initial supply of SFGL biofilm in the channel.	0	kg
$S_{(bed)}$	Initial supply of bed sediments in the channel.	5400000	kg
$\rho_{B(banks)}$	Bulk density of bank sediments.	1500	kg/m ³
$\rho_{B(sfgl)}$	Bulk density of SFGL sediments.	1000	kg/m ³
$G_{sfgl(bio)}$	Generation rate of SFGL biofilm.	9.07E-08	kg/m ² .s
$G_{sfgl(sed)}$	Generation rate of SFGL sediments.	1.84E-06	kg/m ² .s
t_d	SFGL development time	30	days
ω_s	Mean settling velocity of suspended material.	4.50E-05	m/s
$C_{tc(low)}$	Transport capacity coefficient for low flows.	1.20E-05	m ^{1/2} .s ² /kg ^{1/2}
$C_{tc(high)}$	Transport capacity coefficient for high flows.	1.50E-05	m ^{1/2} .s ² /kg ^{1/3}
$C_{\tau(l)}$	Shear stress coefficient adjusting bed/bank shear.	calculated	unitless
$C_{\tau(l)}$	Shear stress coefficient for unsteady flow.	30	unitless
$\tau_{cr(sfgl)}$	Critical shear of the SFGL source.	0.05	Pa
$\tau_{cr(bed)}$	Critical shear of the bed source.	2	Pa
$\tau_{cr(bank)}$	Critical shear of the bank source.	2	Pa
$a_{(sfgl)}$	Erodibility of the SFGL source. (Calculated)	8.94E-04	kg/Pa.m ² .s
$a_{(bed)}$	Erodibility of the bed source. (Calculated)	2.12E-04	kg/Pa.m ² .s
$a_{(bank)}$	Erodibility of bank source. (Calculated)	2.12E-04	kg/Pa.m ² .s

For the fluvial properties described by Equations (24) through (29), stream channels were considered to be trapezoidal based on data from numerous cross-sections. Average side slopes, bankfull depths, and channel widths were found with 12 channel cross sections measured near Sites 1 and 2. Manning's n values for the reaches were considered to be constant 0.02 and were estimated from a depth discharge curve at the outlet of the watershed. The channel slope of the South Elkhorn Creek was 0.00044, which was estimated with a combination of field measurements from a longitudinal profile and GIS analysis. Stream lengths were estimated using topography and land-use maps in the GIS ArcMap. Floodplain width was used to estimate channel depths and shear stresses under flooding conditions. Floodplain width was considered to be 30 meters on each side of the channel based on observations. Bankfull depth was estimated with the cross sectional data for each channel.

The deposition coefficient, k_p , used in Equation (59), was determined through the empirical function described in Equation (64), and the sediment routing, k_{ss} , coefficient was determined through calibration. The separation between the high and low flow transport functions, defined as $Q_{boundary}$, was found to be approximately 2.50 cms. This flow rate corresponds to the point when pronounced sediment transport begins and was chosen as the boundary between low flow and high flow events. Figure 16 shows relationship between storm yield, peak storm flow rate, and the high/low flow boundary 2.50 cms.

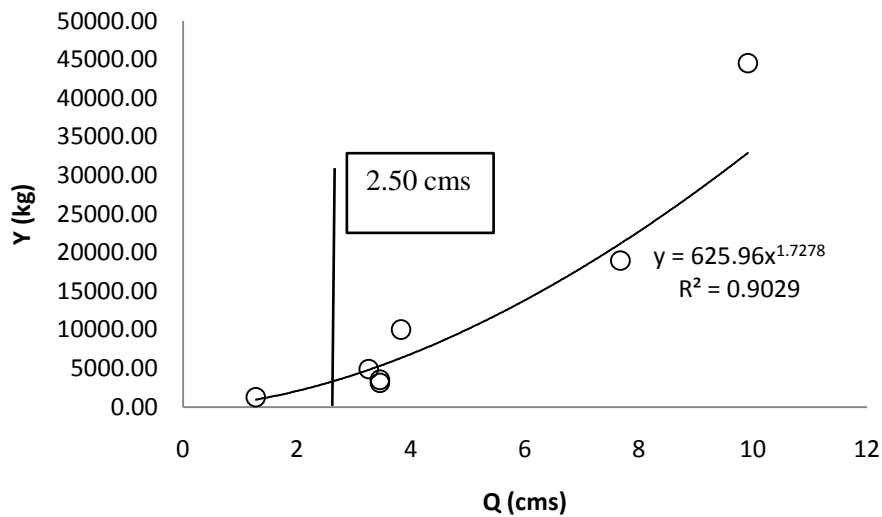


Figure 16: Graph of peak storm flow and sediment yield showing 2.50 cms as the boundary between high and low flows.

Initial sediment supply in Equations (36), (43), (49), and (55) were assumed infinite for the streambanks, and estimated for the SFGL and streambed initial conditions. Surface area, $SA_{(k)}$, of the erosion sources in Equations (36), (43), (49), and (55) were computed uniquely for each source. The SFGL was measured to cover 74% of the streambed, with the remaining 26% being scoured zones of the bedrock channel, and thus $SA_{(sfgl)}$ was calculated as the streambed area upstream of the sampling site times the percent cover. It is well known that the distribution of deposited fine sediments can vary across the streambed due to stream heterogeneity and flow complexity in bends, depression zones, e.g., potholes in bedrock streams, and pools. However, in staying consistent with the one dimensional average nature of the conceptual model, an average streambed sediment depth was used for the SFGL and bed sources in terms of supply.

In order to estimate the depth of stored sediment in the streambed, 57 measurements were collected on a three lateral by 19 longitudinal grid with 6 meter streamwise spacing from a reach within the South Elkhorn on January 9, 2009. An average streambed sediment depth of 7.4 cm was calculated. Initial channel widths were estimated with the cross sectional data and along with channel lengths. An assumed bed sediment bulk density of 1500 kg/m^3 was used, and the measured sediment bed depths were used to estimate the initial bed supply, $S_{(bed)}$. Channel widths were updated using Equation (48) based on the occurrence of bank erosion, which in turn updated the current surface area of the bed and the SFGL. Further data collection of streambed sediment depth across seasons and before and after large hydrologic events will be useful in future modeling. The streambank surface area of erosion was modeled using Equation (44). The bulk density of bank sediments was assumed to be 1500 kg/m^3 .

The maximum supply of the SFGL was estimated by assuming the neutrally buoyant mixture has a bulk density of 1000 kg/m^3 , and that the SFGL can only grow/deposit to a maximum depth of 0.5 cm (Droppo and Stone 1994; Droppo et al. 2001). Using the initial cross section data for the channel width and the GIS data for the channel length the maximum supply of SFGL in each subcatchment was predicted. Of this estimated maximum SFGL supply, the biofilm accounted for 4.7% of the mass of the SFGL with 95.3% of the mass being due to the inorganic sediment, as seen in Equations (50) and (52). Initial values of the sediment supply in the SFGL and the initial biofilm supply in the SFGL were assumed to be zero.

Based on study of the literature, biofilms tend to reach development and biofilm thickness becomes constant after approximately 4 to 7 days (Liu et al., 1993; Lau and Liu

et al., 1993; Garny et al., 2008; Garny et al., 2009). Further, a 5 day biofilm establishment time has been used for one of the few SFGL experiments that exist (Droppo et al., 2001) to reach biostabilization. Rates of biofilm development will vary based on a number of controls including nutrient levels within the flow, sunlight, and dissolved oxygen (Thornton, 2002; Sponza, 2002). It should be pointed out that the past biofilm studies were in flumes where the biofilm development was monitored on the surface of a smooth bed. In the SFGL, the biofilm will develop within the interstices of the sediment grains, and it is expected that full biofilm development will be on the order of one week during pronounced growth to months. During this time, biostabilization occurs within the SFGL. In addition to stabilization of the streambed, biofilm development within the SFGL will add mass in the form of biomass to the SFGL. Data was collected from the South Elkhorn Watershed study site in order to approximate the increase in biomass within the SFGL due to biofilm development. Streambank soil was used as the initial media for assessing increased biomass in the streambed since streambank soil is the dominant origin of the sediment matrix within the bed. 50 streambank sediment samples and 50 samples of the SFGL from streambed sediments with a developed biofilm were used to approximate the increase in biomass due to biofilm development in the SFGL. Total organic carbon (TOC) analysis was performed on the samples using an elemental analyzer and it was found the streambank samples were 1.6 g C per 100 g sediment and the streambed samples were 4.3 g C per 100 g sediment. Thus, the increase in carbon associated with the biomass from the biofilm development was 2.7 g C per 100 g sediment matrix. Using the work of Nelson and Sommers (1982), it was assumed that 58% of the organic matter is made up of organic

carbon. Thus, the increase in mass due to the biofilm growth and accumulation of other organic matter (e.g. Fine-Grained organic matter, leaf material, and accumulated dissolved organic matter) for this system is 4.7 g per 100 g sediment or approximately a 5% increase in the mass of the SFGL when the biofilm is fully developed. Using this data, the biofilm generation rate in the SFGL, as seen in Equation (52), was estimated as $9.07 \times 10^{-8} \text{ kg/m}^2 \cdot \text{s}$. The rate of sediment addition to the SFGL through bioturbation, as seen in Equation (50), of the bed sediments was estimated by assuming that the SFGL becomes completely developed in 30 days, and a generation time of the SFGL sediment is then given as $1.84 \times 10^{-6} \text{ kg/m}^2 \cdot \text{s}$. The generation rates will be impacted by the choice of the development time and SFGL maximum depth; both of these parameters were investigated in the sensitivity analysis and a range of values was considered including 5 to 90 days for the development time and 1 mm to 10 mm for the SFGL maximum depth. This gives the maximum values for the SFGL biofilm and sediment generation rates as $5.44 \times 10^{-6} \text{ kg/m}^2 \cdot \text{s}$ and $1.10 \times 10^{-4} \text{ kg/m}^2 \cdot \text{s}$ respectively, and the minimum values for the SFGL biofilm and sediment generation rates as $6.04 \times 10^{-9} \text{ kg/m}^2 \cdot \text{s}$ and $1.23 \times 10^{-7} \text{ kg/m}^2 \cdot \text{s}$ respectively. The following equations show how the generation rate for the SFGL sediments and biofilm were estimated

$$G_{sfgl (sed)} = \frac{0.953 D_{sfgl \max} \rho_{sfgl}}{t_d}, \quad (\text{Eq. 71})$$

$$G_{sfgl (bio)} = \frac{0.047 D_{sfgl \max} \rho_{sfgl}}{t_d}, \quad (\text{Eq. 72})$$

Where $G_{sfgl (sed)}$ is the sediment generation rate for the SFGL [$\text{kg/m}^2 \cdot \text{s}$], $G_{sfgl (bio)}$ is the biofilm generation rate for the SFGL [$\text{kg/m}^2 \cdot \text{s}$], D_{sfgl} is the maximum SFGL depth [m],

ρ_{sfgl} is the bulk density of the SFGL [kg/m³], and t_d is the development time of the SFGL [s].

Only one sediment size class, fine sediments less than 53 μm , is modeled. It is assumed that the sediment yield of the watershed is consisted mainly of this size class. Mean grain diameter was estimated through the use of microscopic analysis of suspended sediment samples, and a mean diameter of approximately 15 μm was found (Sliter 2007). Using experimental data from Rouse (1937), which is available in Figure 4.4 of Chang (1988), and an empirical equation for the settling velocity of non-spherical particles from Dietrich (1982) the settling velocity for this size fraction was estimated to be between 0.01 and 0.15 cm/s.

Equations for the transport capacity of fluvial system are usually empirically based on flume studies (Dou, 1974; Yan et al., 2008; Ahmandi et al., 2006; Guy et al., 2009; Madej et al., 2009). Transport capacity is synonymous with the critical sediment discharge or the maximum allowable sediment discharge of the flow regime under equilibrium conditions and that this value is not unique but dependent upon the bathymetry of the reach, the current flow regime, and whether the reach is currently experiencing deposition or erosion (Hessel and Jetten, 2007; Yan et al., 2008; Madej et al., 2009). Transport capacity equations, and thus their coefficients, are unique to each study area. Because of this uncertainty, transport capacity was treated as a calibration parameter and parameterization of the transport capacity coefficient in Equation (31) was accomplished by calibrating the transport coefficient to the sediment yield data at the outlet.

The shear stress coefficient, C_τ , is used to estimate applied shear stress to the SFGL, bed, and banks in Equation (40). C_τ is determined using a boundary shear stress distribution for a trapezoidal channel outlined in Chang (1988). The coefficient is a function of the side slope and the bottom width to depth ratio. An equation was fitted based on the relationship presented in Chang (1988) and the coefficient for bed shear is given by the equation

$$\begin{aligned}
C_{\tau(\text{bed})} = & \\
& 0.00000405 \left(\frac{W_{\text{reac } h(i)}^{(j)}}{H(i)^{(j)}} \right)^6 + 0.00021201 \left(\frac{W_{\text{reac } h(i)}^{(j)}}{H(i)^{(j)}} \right)^5 - 0.00437492 \left(\frac{W_{\text{reac } h(i)}^{(j)}}{H(i)^{(j)}} \right)^4 + \\
& 0.04505583 \left(\frac{W_{\text{reac } h(i)}^{(j)}}{H(i)^{(j)}} \right)^3 - 0.241185 \left(\frac{W_{\text{reac } h(i)}^{(j)}}{H(i)^{(j)}} \right)^2 + 0.58925899 \left(\frac{W_{\text{reac } h(i)}^{(j)}}{H(i)^{(j)}} \right) + \\
& 1.00975426,
\end{aligned}$$

(Eq. 73)

and the shear stress coefficient for the banks is given as

$$C_{\tau(\text{bank})} = 0.0024825 \left(\frac{W_{\text{reac } h(i)}^{(j)}}{H(i)^{(j)}} \right)^2 - 0.0773109 \left(\frac{W_{\text{reac } h(i)}^{(j)}}{H(i)^{(j)}} \right) + 1.6.$$

(Eq. 74)

Figure 17 shows a graph of the shear stress coefficients.

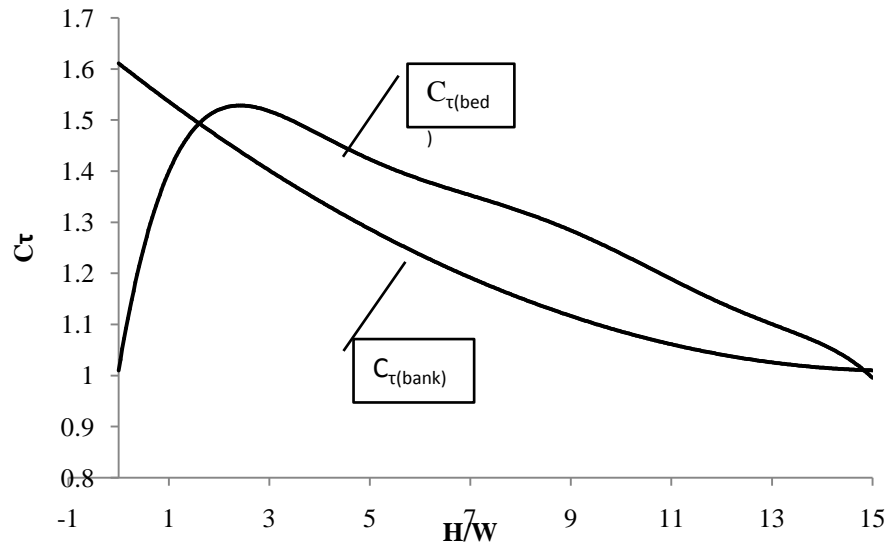


Figure 17: Graph of C_{τ} . Where the horizontal axis represents the depth to width ratio and the vertical axis is the shear stress coefficient.

In order to model fluvial erosion with Equations (36), (43), (49), and (55), $b_{(k)}$ was assumed to be 1 for all fluvial erosion sources, which agrees with the concept of erosion being a shear driven process and agrees with the assumption of a number of other studies (Hanson and Simon, 2001; Sanford and Maa, 2001; Wynn et al., 2008; Simon et al., 2009). Erodibility and critical shear stress for these equations, $a_{(k)}$ and τ_{cr} , were parameterized uniquely for each erosion source based on literature reported values and equations. Sanford and Maa (2001) values for erodibility were based on in-situ tests of harbor sediments (Baltimore Harbor, MD) and tend to overlap with the relationship for the erodibility coefficient presented by Hanson and Simon (2001), which was based on analyses of in-situ erodibility tests of streambeds in loess areas of the Midwestern United States, for the low range of τ_{cr} approximately less than 0.3 Pa. Thus, these values for $a_{(k)}$ and τ_{cr} work well for the SFGL. The SFGL is realized to stabilize overtime due to

biofilm development, i.e. biostabilization. Droppo et al. (2001) showed that initially deposited material had a critical shear of 0.024 Pa and increased to 0.325 Pa after a five day biofilm development period. Corresponding erodibility values can be realized to be about 0.002 [s/m] for a critical shear of 0.02 Pa and 0.0006 [s/m] for a critical shear of 0.3 Pa. The critical shear stress for the bed sediments was assumed to be approximately 0.3 to 2 Pa, and an erodibility coefficient was calculated to range between 0.0006 and 0.0002 [s/m] (Hanson and Simon, 2001; Simon and Thomas, 2002). The critical shear stress for bank sediments were assumed to be approximately 2 to 20 Pa with a calculated erodibility coefficient of 0.0002 to 0.00007 [s/m] (Hanson and Simon, 2001; Simon and Thomas, 2002). In summary, due to the agreement found in multiple studies the relationship between the erodibility coefficient and critical shear stress reported in Hanson and Simon (2001) and Simon and Thomas (2002) was used here as

$$a_{(k)} = 2.0 \times 10^{-7} \tau_{cr(k)}^{-0.5} \quad (\text{Eq. 75})$$

Several tributaries are present in the study watershed, and to model the contribution of sediment from these sources a point source was included at the inlet of the downstream catchment. This point source represents the contribution of sediment from these tributaries which drain the mixed urban/agricultural uplands. Data from 135 suspended sediment samples taken at the halfway point of the watershed over two years were used to calibrate an empirical model for these tributaries. It was assumed that the suspended sediment data collected at this halfway point is representative of the sediment contribution from the tributaries and the uplands of the study watershed. The upland and tributary sediment contribution model is given by the equation

$$C_{tribs(i)}^{(j)} = 600 \left(1 - e^{-0.03Q_{(i)}^{(j)}} \right), \quad (\text{Eq. 76})$$

where $C_{tribs(i)}^{(j)}$ is the concentration contribution from the tributaries and the uplands [mg/l], and $Q_{(i)}^{(j)}$ is the flow rate for the watershed [m³/s]. For the urbanization runs, the effect of the urbanizing uplands on the upland and tributary sediment contribution model was predicted using data from Coulter et al. (2004). Coulter et al. (2004) studied the sediment loadings from several small watersheds with mixed urban and agricultural land covers in the Bluegrass region of Kentucky near the South Elkhorn study watershed. Table 15 shows the mean annual sediment concentration from different land use watersheds.

Table 15: *Table of mean Total Suspended Solids loading (Coulter et al. 2004).*

Average Upland and Tributary Contribution to Sediment Loading	
Agricultural	13.3 mg/l
Urban	23.1 mg/l
Mixed	20.8 mg/l

The cumulative sediment concentration from the uplands and tributaries is given by the equation

$$TSS_{uplands} = 0.45(TSS_{urban}) + 0.55(TSS_{agricultural}), \quad (\text{Eq. 77})$$

where TSS_{urban} is the sediment concentration contribution from the urban area, $TSS_{agricultural}$ is the sediment concentration contribution from the agricultural area, 0.45 is the area fraction of urban land in the study watershed, and 0.55 is the area fraction of agricultural land in the study watershed. The ratio between the mean sediment

concentration from agricultural and urban watersheds as given by Coulter et al. (2004) is given by the equation

$$\frac{TSS_{agricultural}}{TSS_{urban}} = \frac{13.3}{23.1}, \quad (\text{Eq. 78})$$

By substituting Equation (78) into Equation (77) the contribution from agricultural and urban areas of the study watershed is given by the equations

$$TSS_{agricultural} = 0.75(TSS_{uplands}), \quad (\text{Eq. 79})$$

$$TSS_{urban} = 1.30(TSS_{uplands}), \quad (\text{Eq. 80})$$

and the contribution from the uplands and tributaries for the entire watershed are given by the equation

$$TSS_{watershed} = f_{urban} (TSS_{urban}) + f_{agricultural} (TSS_{agricultural}), \quad (\text{Eq. 81})$$

Where f_{urban} and $f_{agricultural}$ are the land area fraction for urban and agricultural areas respectively. By substituting Equations (76), (79), and (80) into Equation (81).

$$TSS_{watershed} = C_{int} (f_{urban} (1.30) + f_{agricultural} (0.75)) C_{tribs(i)}^{(j)}, \quad (\text{Eq. 82})$$

To account for the difference between an integrated concentration profile and simply multiplying concentration by flow rate, Equation (82) was multiplied by the coefficient C_{int} . This coefficient was determined by comparing the mean difference between sediment yields determined through concentration profile integration and through multiplication of the flow rate by the sediment concentration for selected

observations. The coefficient was determined to be 1.7. The coefficient was determined to be 1.7. The term ($f_{urban}(1.23) + f_{agricultural}(0.71)$) is called the urban area coefficient.

6.2 Calibration Data Collection and Calculations

Special data collection routines were employed to gather the necessary temporal resolution needed for this research. Emphasis was placed on the temporal variability of suspended sediment concentration across storm events and under base flow conditions. This resolution was needed in order to study how sediment flux changes as the flow rate and shear stress change across the storm event. The following will describe the sampling, collection, analysis and synthesis of the data.

6.2.1 Suspended Sediment Samples

Distributed samples of suspended sediment were collected throughout entire storm events using a Teledyne ISCO water sampler that was installed at the outlet of the study watershed. The automated sampler was programmed to collect 500 ml samples at the onset of a storm event at either one or two hour intervals. The inlet for the sampler was placed near the streambed but sufficiently above the bed so as not to collect bed load sediments. Samples were returned to the University of Kentucky Hydrosystems Laboratory for total suspended solids analysis. Whatman GF/C 1.2 μm glassfiber filters were rinsed with 100 ml of de-ionized organic free water to remove any residual fine solids and dried in a 103°C oven to remove all water prior to sample analysis. Filters were placed in a desiccator after removal from the oven to allow the samples to acclimate to room temperature without absorbing ambient water vapor and weighed to obtain a pre-sample weight. Suspended solids samples were then measured for their volume and run through a prepared Whatman filter using a vacuum manifold. The filters were then dried

again in a 103°C oven for 24 hours to remove all moisture. Filters were then placed in a dissector and thereafter weighed. The concentration of sediment in stream at the depth of the inlet at the time when the sample was taken is given as

$$TSS = \frac{W_{filter+sed} - W_{filter}}{V_{sample}}, \quad (\text{Eq. 83})$$

where W_{filter} is the weight of the rinsed and dried filter [mg], $W_{filter+sed}$ is the weight of the filter after the sample has been passed through the filter [mg], and V_{sample} is the volume of the sample [L], and TSS is the concentration of sediment [mg/L]. A total of 144 samples over seven storm events were used for calibration of the in stream model. Figure 18 shows the concentration and flow rate curves for the seven events.

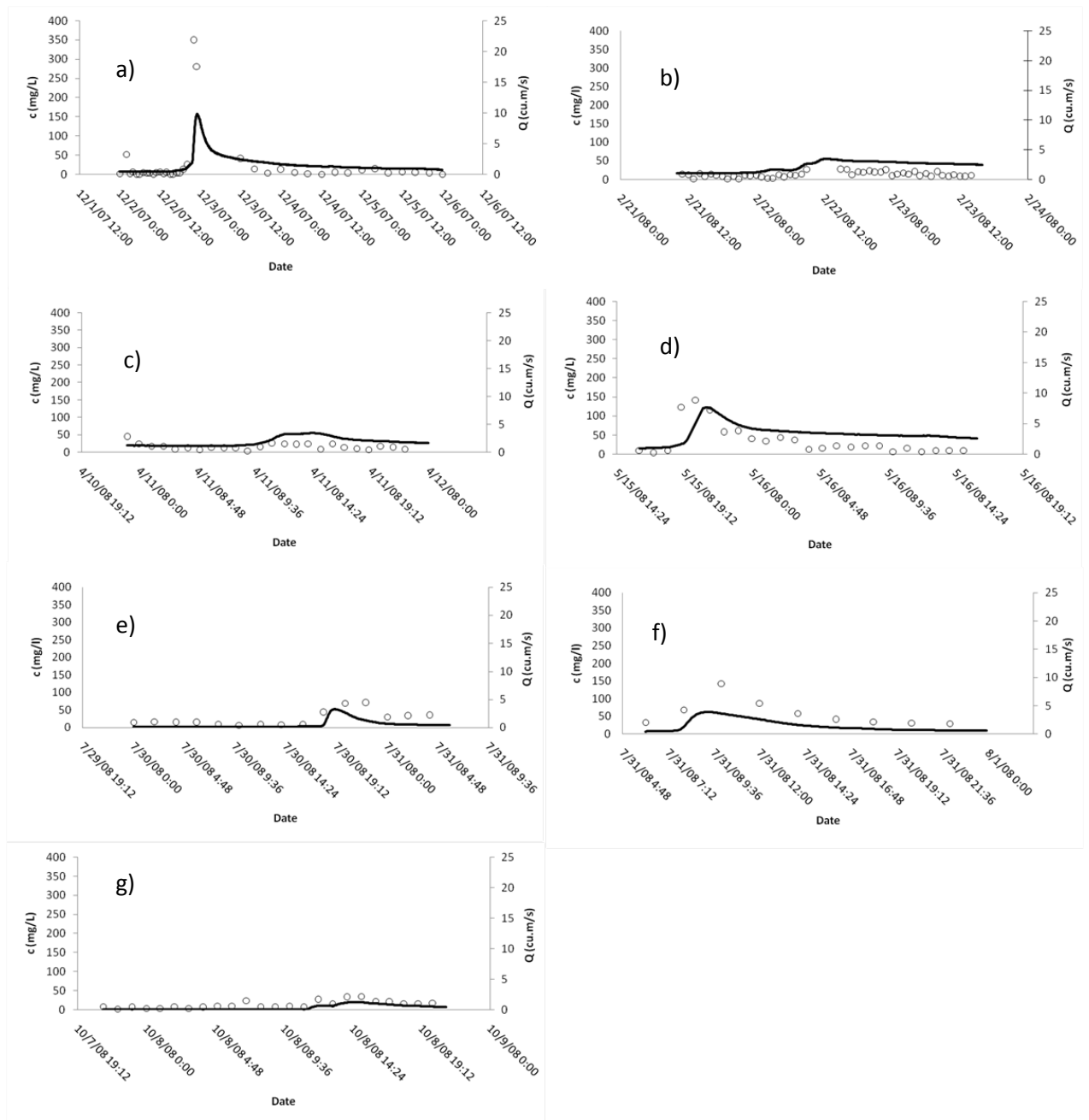


Figure 18: TSS concentration (points) and flow rate (solid black) data for a) December 2, 2007, b) February 21, 2008, c) April 10, 2008, d) May 15, 2008, e) July 30, 2008, and f) July 31, 2008, and g) October 7, 2008.

6.2.2 Sediment Yield Data Analysis

In order to provide data for calculation of suspended sediment yield in the watershed, suspended sediment was collected and thereafter the Einstein approach was used to estimate sediment yield. A total of seven storm events were used for estimation of sediment yield. The yield for the storm events were evaluated using Einstein's approach (1950) which is described in (Chang, 1988). The suspended sediment discharge was obtained by integrating

$$q_{ss} = \int_a^D Cudz \quad (\text{Eq. 84})$$

where q_{ss} is the discharge of suspended sediment per unit channel width, a is the lower limit where suspension begins, C is the sediment concentration, and D is the depth. The Einstein integration yields the equation

$$q_{ss} = 11.6C_a U_*' \left[2.303 \log \left(\frac{30.2D}{\Delta} \right) I_1 + I_2 \right] \quad (\text{Eq. 85})$$

where

$$I_1 = 0.216 \frac{A^{z_*-1}}{(1-A)^{z_*}} \int_A^1 \left(\frac{1-\eta}{\eta} \right)^{z_*} d\eta \quad (\text{Eq. 86})$$

$$I_2 = 0.216 \frac{A^{z_*-1}}{(1-A)^{z_*}} \int_A^1 \left(\frac{1-\eta}{\eta} \right)^{z_*} \ln(\eta) d\eta \quad (\text{Eq. 87})$$

I_1 and I_2 are function of A and z^* and were integrated numerically using (Nakato, 1984). The sediment concentration, C , can be calculated at any time instant with Equation (60), (61), and (62).

C_a will be calculated using concentration at the ISCO sampler inlet depth, C_Y , which can be used in Equation (60) and rearranged as

$$C_a = \frac{C_Y}{\left[\left(\frac{H-Y}{Y} \right) \left(\frac{a}{H-a} \right) \right]^{z^*}} \quad (\text{Eq. 88})$$

where Y is the depth of the depth at the inlet as defined before.

The yields for an individual storm event were determined by integrating the sediment rate function over the entire storm hydrograph as

$$S_y = \int_0^T Q_s dt \quad (\text{Eq. 89})$$

where 0 is the onset of the storm event, T is the end of the event, and Q_s [kg/s] is the sediment flow rate (q_{ss}) integrated over the width of the channel.

A storm hydrograph is defined as the flow period between the onset of the hydrograph until the point in time when pronounced flow acceleration ceases and the flow regime returns to base flow conditions. This base flow separation method was taken from (Chow, 1988). The onset of acceleration of the flow over time was defined as the point when flow acceleration begins, and the end of the flow acceleration was determined as a function of the peak flow (Q_p)

$$N = 4.094e^{0.004Q_p} \quad (\text{Eq. 90})$$

where N is the length of time from the time of peak flow to the time when storm acceleration ends and the flow regime returns to base flow conditions.

Figure 19 shows the results of application of the Einstein equation using flow and sediment concentration data in the watershed. Table 16 provides sediment yield results for the events sampled.

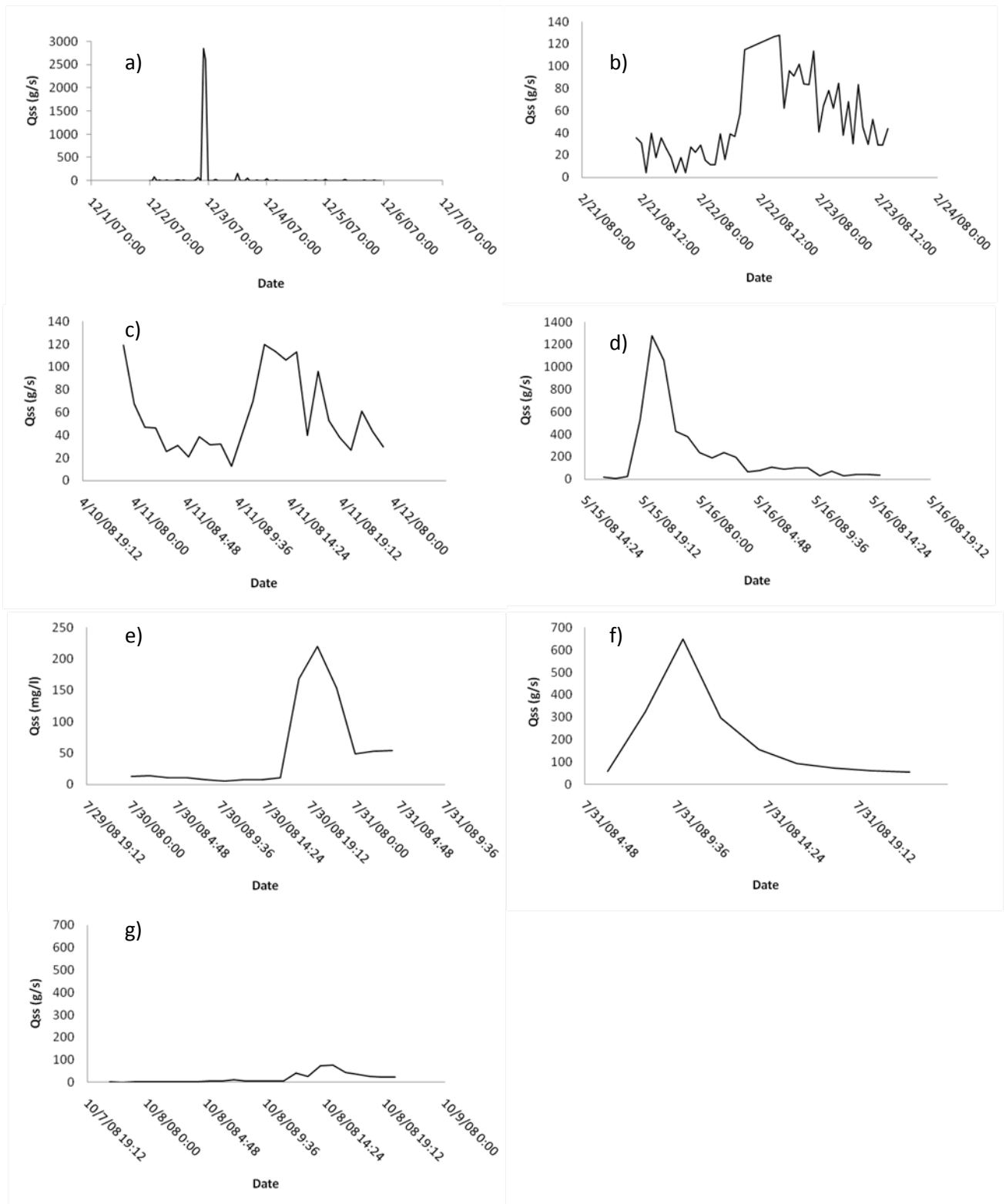


Figure 19: Figure of sediment flow over time for the storm events a) December 2, 2007,

b) February 21, 2008, c) April 10, 2008, d) May 15, 2008, e) July 30, 2008, and f) July 31, 2008, and g) October 7, 2008.

Table 16: Table of sediment yield for each storm event.

DATE	Q (cms)	Y (kg)
12/2/2007	9.91	44543
2/21/2008	3.45	3527
4/10/2008	3.45	3115
5/15/2008	7.67	18974
7/30/2008	3.26	4925
7/31/2008	3.82	10031
10/7/2008	1.27	1254

6.3 Model Calibration

The parameters that could not be measured or estimated, were calibrated to fit the sediment yield data at the outlet of the watershed. Calibration parameters for this model included the transport capacity coefficients, the shear stress coefficient, sediment routing coefficient, and the critical shear stress for each sediment source, which directly affected the erodibility parameter of the sediment source. The in-stream sediment transport model was calibrated using the sediment yield data from the Einstein integration. A time integrated approach was used to calibrate modeled sediment yield data to the observed sediment yield data. Total yields for each storm event, including base flow events, were compared with total model yields for the same time period. The storm events of December 2, 2007; February 21, 2008; April 10, 2008; and May 14 2008 were used for model calibration and the storm events of July 30, 2008; July 31, 2008, and October 7, 2008 were used for model validation. Visual comparison of the observed and modeled sedigraph was used to match the shape of the modeled sedigraph to the observed sedigraph. Donigian (2002) recommended a general guideline for the calibration of the

sediment transport component for HSPF. Table 17 shows these recommended guidelines.

Table 17: *Table of general guidelines for sediment component evaluation (Donigian, 2002).*

Statistic	poor	fair	good	very good
%Diff (monthly/annual)	>45	30-45	20-30	<20

Calibration of total sediment yield was accomplished by adjusting the transport capacity coefficients for high and low flows, the shear stress coefficient, and the sediment routing coefficient. Two separate transport capacity functions for high and low flows were used for this model. It was found in the initiation calibration stage that the transport of sediment varied between low flows and high flows. Both functions take the same shape as Equation (31), but the coefficients differ and were adjusted through calibration with observed data. The shear stress coefficient was used to match the observed sedigraph peak to the simulated sedigraph peak, and the sediment routing coefficient was adjusted to match the timing of the modeled sedigraph with the observed sedigraph. Table 18 shows the observed and simulated yield for the calibration and validation events, the percent difference between the modeled and the observed yields, the correlation and the Nash-Sutcliff efficiency. These statistics are based on the total yields for the individual storm events and not point to point comparison of the observed and simulated hourly yields. Figure 20 shows the graphs of the observed sedigraph and the modeled sedigraph.

Table 18: *Table of observed and simulated sediment yield statistics.*

Event Dates	Observed Yield (kg)	Simulated Yield (kg)	Mean Relative Error	Correlation	Nash-Sutcliff
Calibration: Dec 2 2007, Feb 21 2008, April 10 2008, and May 14 2008.	70,161	55,387	19.70%	0.73	0.57
Validation: July 30 2008, July 31 2008, and Oct 7 2008.	19,030	14,200	-24.30%	0.89	0.67

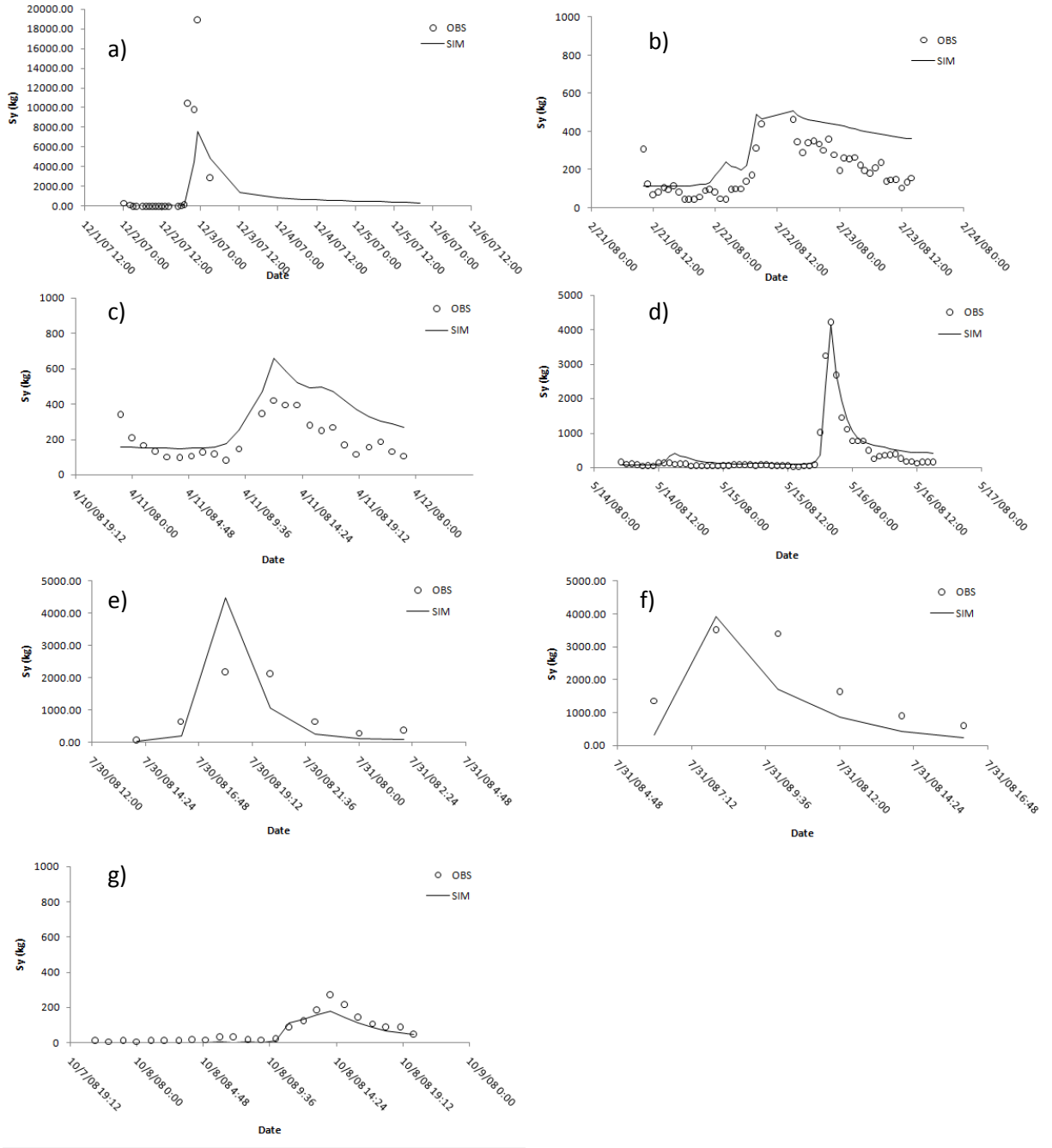


Figure 20: Graphs of observed and modeled sediment yield for the storm events on a) December 2, 2007, b) February 21, 2008, c) April 10, 2008, d) May 15, 2008, e) July 30, 2008, and f) July 31, 2008, and g) October 7, 2008.

6.4 Model Sensitivity

Calibration parameters as well as estimated parameters were varied through their range of values so as to assess how sensitive the model outputs were to these estimated/calibrated parameters. These parameters included the settling depth coefficient, transport capacity coefficients for high and low flows, mean particle settling velocity, generation rates for the SFGL biofilm and sediment component, critical shear stress for the sediment sources, erodibility coefficients, shear stress coefficient for unsteady flow, and the sediment routing coefficient. The impact of all of the above parameters upon the sediment yield was analyzed, and thereafter the impact of the settling depth coefficient and the settling velocity upon deposition were analyzed as were the impact of the development time, maximum depth of the SFGL, and critical shear stress of the bed, bank and SFGL upon the fractions of sediment from different sources.

Table 19 shows the range of values for the calibration coefficients. These values were varied through their range given in

Table 19 and the results can be seen in Figure 21 for sediment yield at the outlet of the watershed.

Table 19: *Table of sensitivity parameters and range of values.*

Calibration Parameters and Values				
		min	max	
k_p	Settling depth coefficient.	0.0001	0.5	unitless
$C_{tc(low)}$	Transport capacity coefficient for low flows.	6.00E-06	1.20E-04	$m^{1/2}.s^2/kg^{1/2}$
$C_{tc(high)}$	Transport capacity coefficient for high flows.	6.00E-06	1.20E-04	$m^{1/2}.s^2/kg^{1/3}$
ω_s	Mean settling velocity of suspended material.	1.00E-05	5.00E-04	m/s
$\tau_{cr(sfgl)}$	Critical shear of the SFGL source.	0.024	0.8	Pa
$\tau_{cr(bed)}$	Critical shear of the bed source.	0.3	20	Pa
$\tau_{cr(bank)}$	Critical shear of the bank source.	0.3	20	Pa
$a_{(sfgl)}$	Erodibility of the SFGL source.	1.29E-03	2.24E-04	$kg/Pa.m^2.s$
$a_{(bed)}$	Erodibility of the bed source.	3.65E-04	4.47E-05	$kg/Pa.m^2.s$
$a_{(bank)}$	Erodibility of bank source.	3.65E-04	4.47E-05	$kg/Pa.m^2.s$
$C_{\tau(2)}$	Shear stress coefficient for unsteady flow.	1	100	unitless
k_{ss}	Sediment routing coefficient	0.01	0.99	unitless
t_d	SFGL Development time	1	90	days
D_{sfgl} max	Maximum SFGL depth	0.1	1	cm

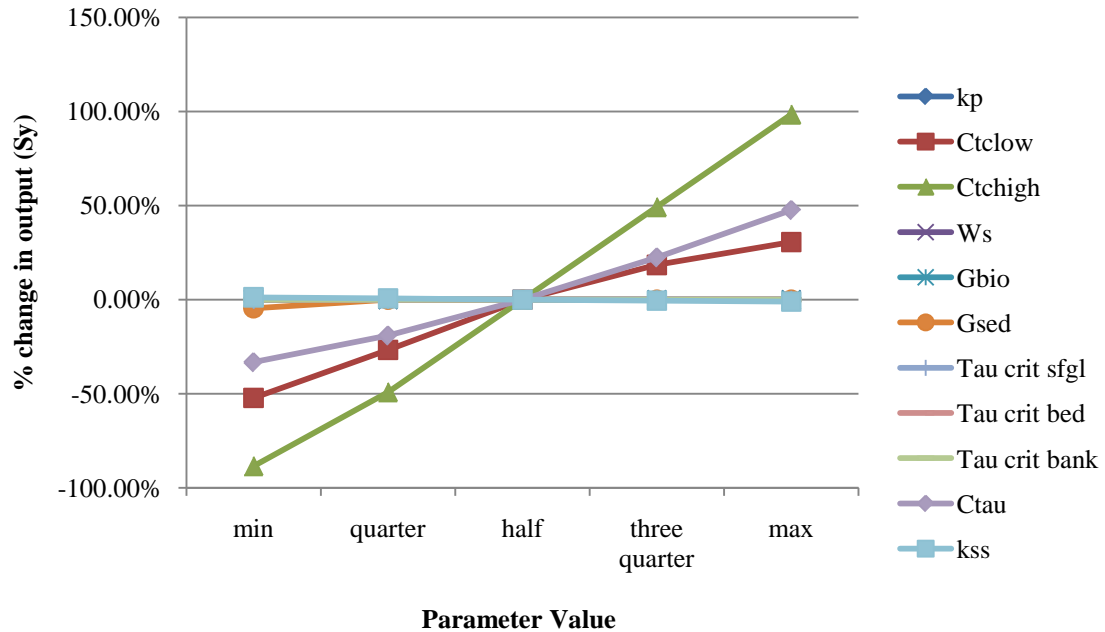


Figure 21: Chart of in-stream sediment model parameters and their sensitivity.

Results from the sensitivity analysis in Figure 21 indicate that the parameters that are most sensitive to sediment yield are the transport capacity coefficient for high flows, transport capacity coefficient for low flows, and the unsteady flow coefficient. A lowland watershed such as the South Elkhorn does not have high fluid shear stresses in the channel unless the channel is experiencing a hydrograph, so the majority of sediment transport would occur during large storm events and thus the transport capacity coefficient for large flows and unsteady shear stress coefficient are very dominant parameters. The critical shear stresses and erodibility for the sediment sources do not affect the yield at the outlet. This indicates that the study site is transport limited and not shear stress or supply limited. The reason for this transport limitation is because of the gentle lowland watershed slopes. Increased streamflow into the channel corridor increases the magnitude of transport capacity, shear stress, and erosion, but does not

increase the transport capacity so much that the system becomes shear stress or supply limited. Instead, the increasing flow erodes the available sediment from the banks and the bed. This is logical, because the South Elkhorn is a 3rd order stream in a lowland watershed.

With regards to deposition in the model (see Figure 22), it was found that the deposition coefficient, which was a new model parameter, is not overly sensitive to deposition. The deposition coefficient is representative of the mean depth that the sediment particle has to fall in order to deposit. The deposition coefficient inversely affects the mass of sediment that deposits to streambed sources, so it is expected that as the deposition coefficient decreases the streambed deposition should increase. While the parameter was not sensitive for the low flow depths of the stream, perhaps it would be important in deeper flows. The settling velocity was found to be a sensitive parameter with regards to deposition, and deposition to the bed increases as the settling velocity increases. Settling velocity had a direct relationship to the shape of the falling limb of the sedigraph. As settling velocity increases, the falling limb of the sedigraph decreased, decreasing total storm yield and increasing deposition. This effect is from the increasing settling velocity which removes suspended sediments before the streamflow can flush them out of the watershed. The sediment routing coefficient does not affect the yield at the outlet, because this coefficient is used to affect the timing of the modeled sedigraph and does not affect any sediment transport processes.

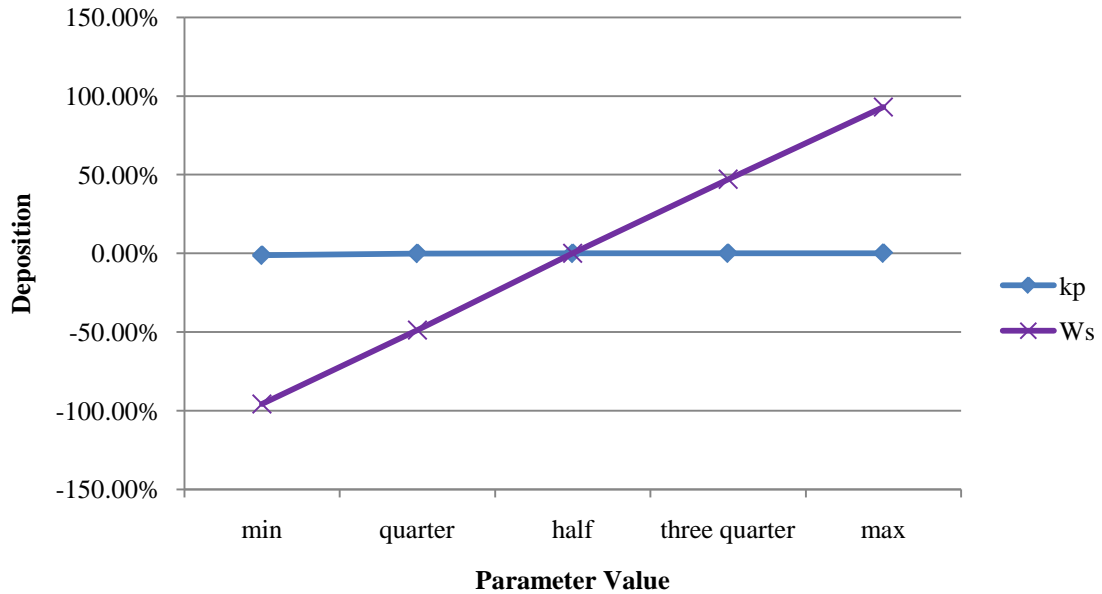


Figure 22: *Chart of deposition coefficient and settling velocity sensitivity.*

The SFGL development time and maximum SFGL depth parameter affect the supply of sediment in the SFGL and the fraction of eroded material from the sediment sources, but do not affect the yield at the outlet because under equilibrium conditions the stream is always transport limited. Figure 23 and Figure 24 respectively show the effect of varying the SFGL development time and maximum depth under tributary loading (Figure 23a and Figure 24a) and no tributary loading conditions (Figure 23b and Figure 24b).

Under tributary loading, the development time does not pronouncedly affect the source fractions of eroded material because the supply of sediments from the tributary/upland source is enough to satisfy the transport capacity under all but high flow events, which gives the SFGL ample time to develop even with a very slow 90 day development time. However, the maximum SFGL supply affects the fraction of eroded

material from the sediment sources at low values. The maximum SFGL supply directly affects the maximum contribution of the SFGL to the sediment yield during a storm event. At low SFGL maximum supply's, there is not enough SFGL to satisfy the transport capacity and other sources begin to erode.

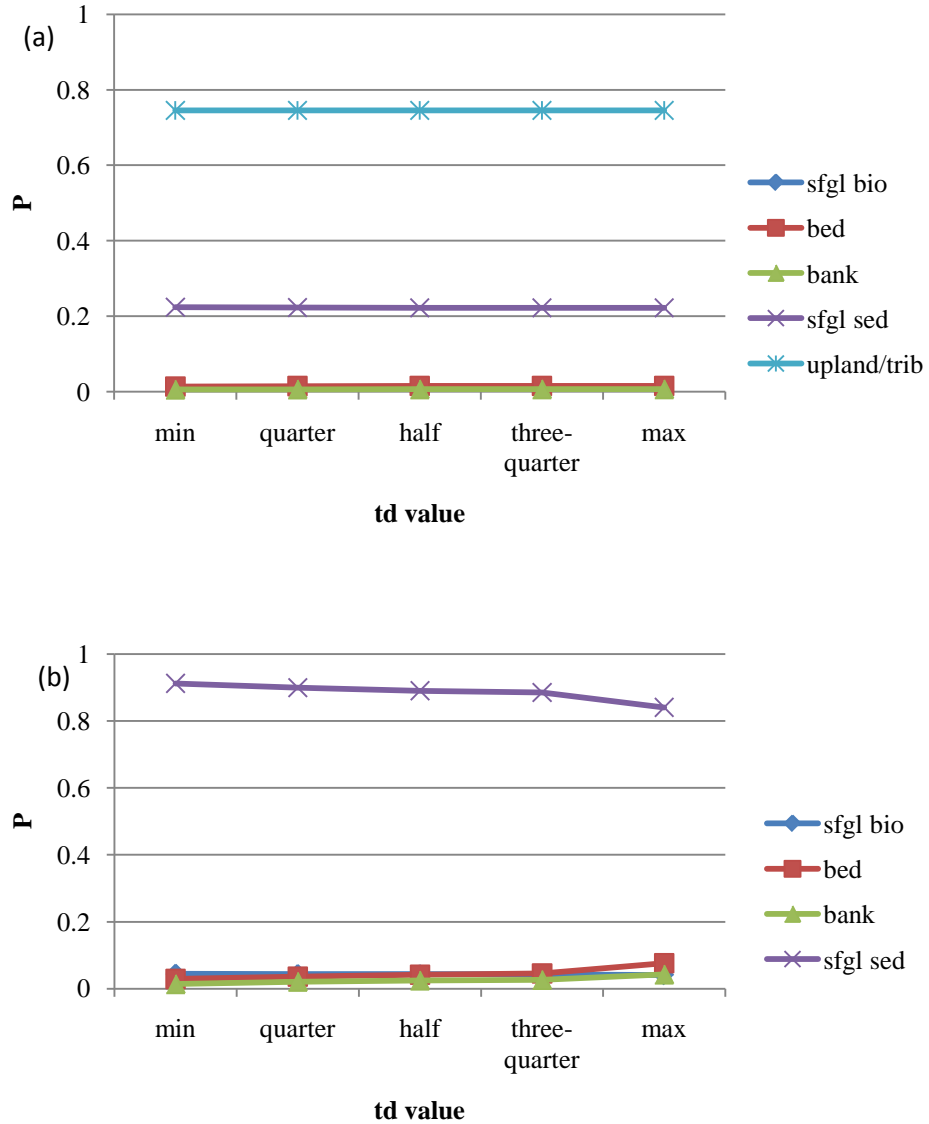


Figure 23: Chart of eroding sediment fractions with changes in t_d parameter with (a) tributary loading and (b) no tributary loading.

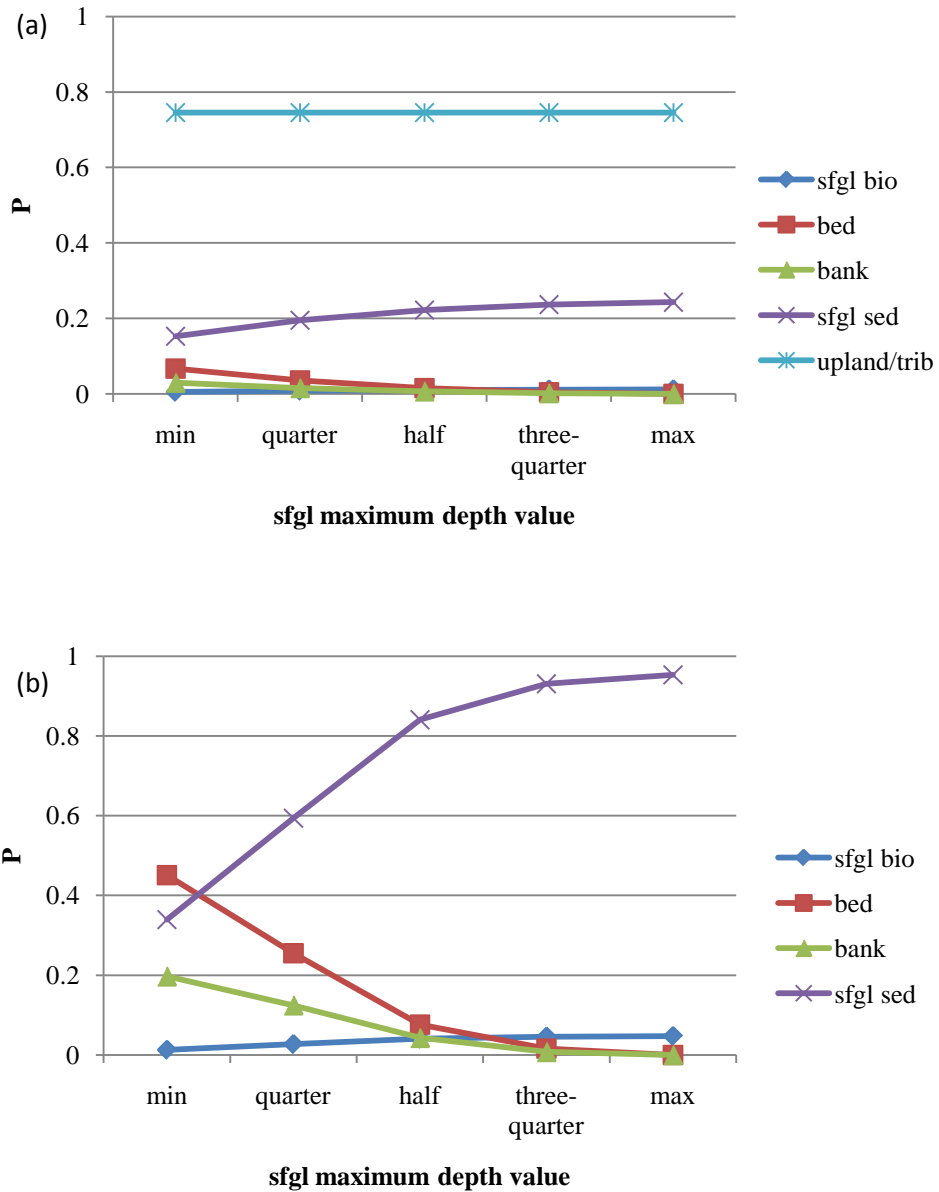


Figure 24: Chart of eroding sediment fractions with changes in D_{sfgl} max parameter with (a) tributary loading and (b) no tributary loading.

Under the conditions when no tributary loading is simulated (Figure 23b and Figure 24b), bed and bank erosion become more dominant when the SFGL development

time is high because the supply of SFGL sediments is reduced, while under faster generation rates the SFGL fraction dominates the sediment yield. Similar, reducing the SFGL maximum depth reduces the supply of the SFGL sediments and bed and bank sediment sources become more dominant, while increasing the SFGL maximum depth increases the supply of SFGL sediments and bed and bank sources become less dominant.

The critical shear stresses for SFGL, bed, and bank sources slightly affect the source fractions at low values, but not greatly. Figure 25, Figure 26, and Figure 27 show the effect of varying critical shear stresses for SFGL, bed, and bank sources respectively on the source fractions. Lower values of the critical shear stress increase the erodibility of the source and decrease the threshold for the onset of erosion and increase the total eroded mass for that source while reducing all subsequent sources. Because the stream is transport limited and the contribution from the tributary/upland source is enough to satisfy the transport capacity under all but high flows, the SFGL, bed, and banks do not erode pronouncedly unless the channel is under high flow conditions. Under high flow conditions, there is ample shear to exceed the critical shear stress and prevent an erosion limit, so the critical shear for the SFGL, bed, and bank sources do not greatly affect the erosion fractions.

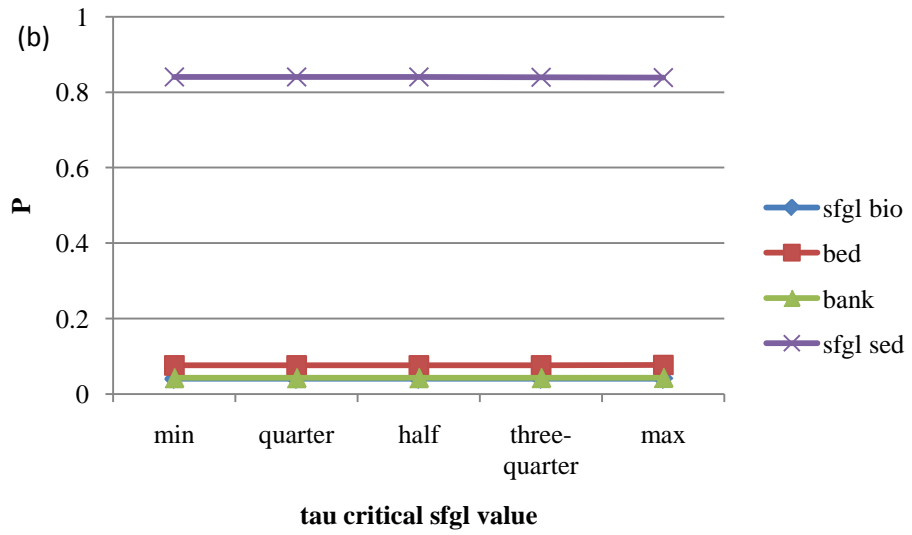
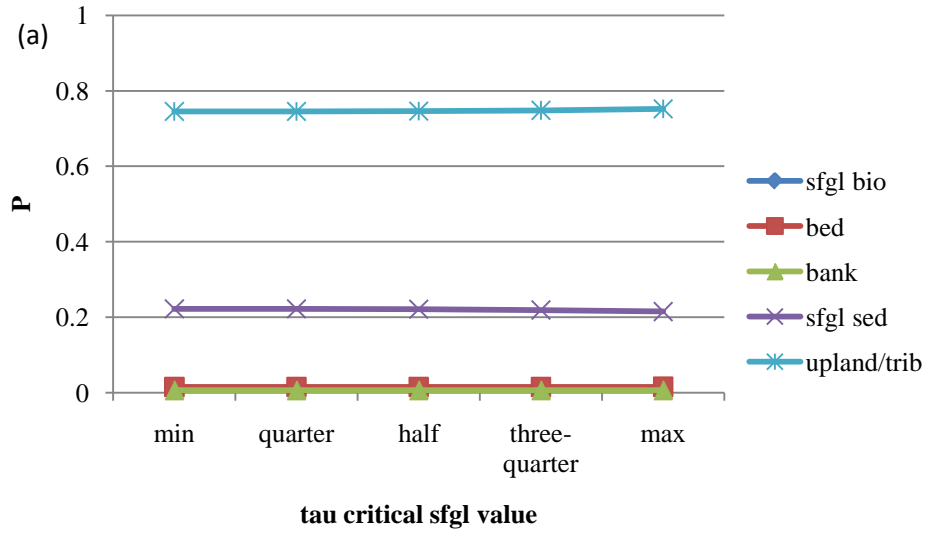


Figure 25: Chart of eroding sediment fractions with changes in $\tau_{cr (sfgl)}$ parameter.

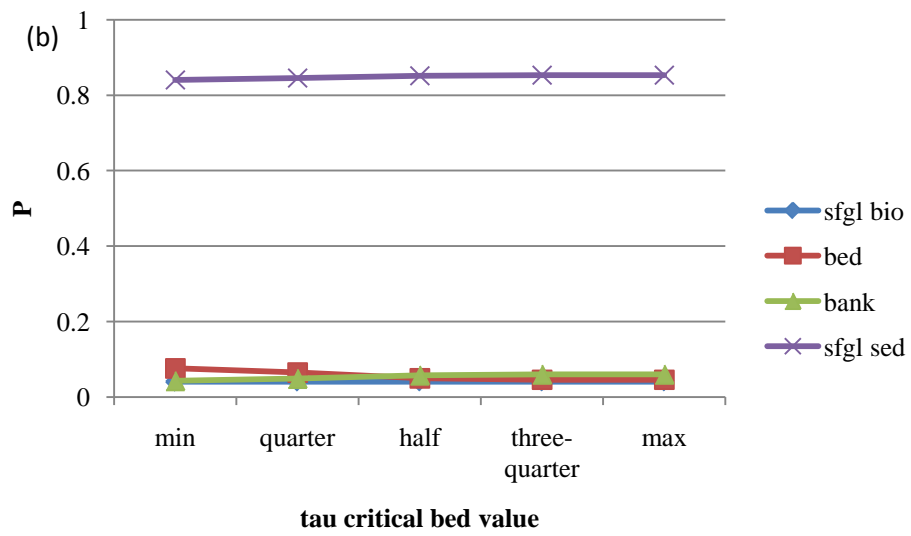
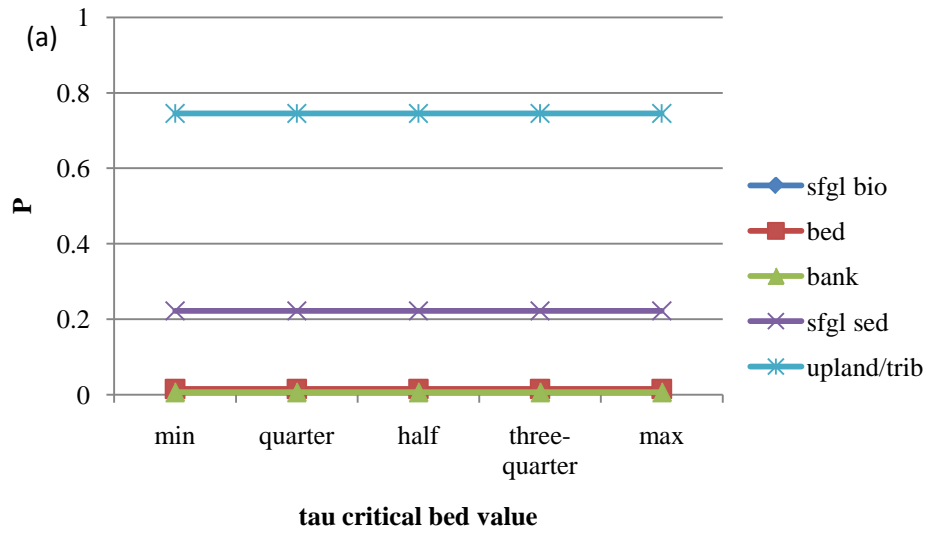


Figure 26: Chart of eroding sediment fractions with changes in $\tau_{cr}(bed)$ parameter.

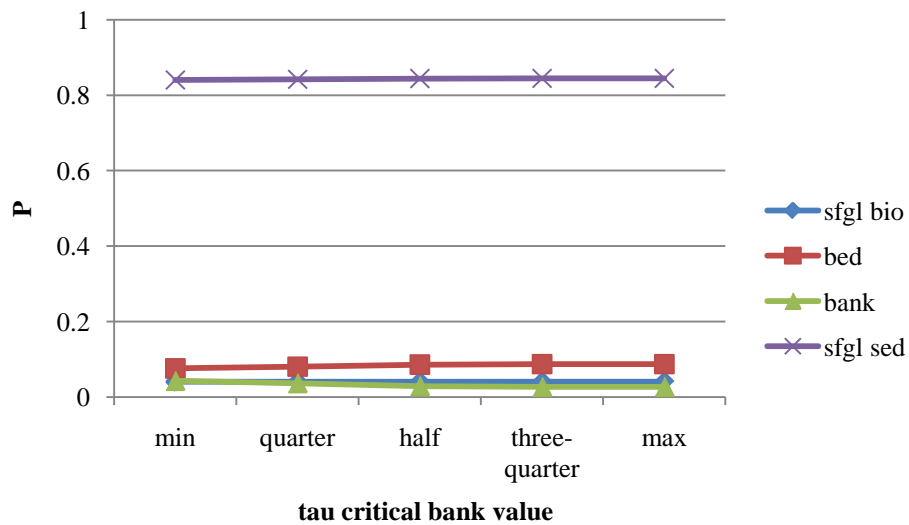
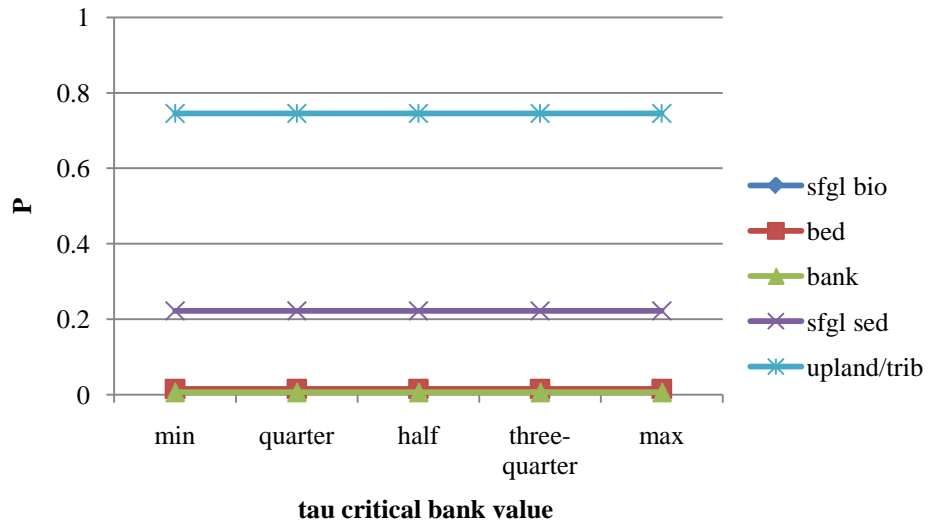


Figure 27: Chart of eroding sediment fractions with changes in $\tau_{cr (bank)}$ parameter.

6.5 Model Validation

The storm events of December 2, 2007; February 21, 2008; April 10, 2008; and May 14 2008 were used for model calibration and the storm events of July 30, 2008; July 31, 2008, and October 7, 2008 were used for model validation. Table 16 shows the correlation, percent difference, and Nash-Sutcliff coefficient for the calibration and

validation period. The percent difference for both periods is “good.” Nash-Sutcliffe efficiencies and Correlation Coefficients for the two periods are above 0.55 and 0.73 respectively. The in-stream sediment transport model is assumed to be representative of the South Elkhorn watershed.

6.6 Discussion

Variations of the modeled sediment yield data to the observed data can be described as either coming from modeling limitations or calibration data limitations. Peaks for the modeled data tend to either under or over estimated the peak yield for a storm event and this can be ascribed to a limitation of the supply function. Sediment supply for each source is an estimate, and predicting when a source will deplete is inherently difficult. Stream reaches are modeled as linear open channels with homogenously distributed sources across the reach. In reality, the reaches contain areas of stable and unstable banks, slump banks appear intermittently when incised banks are present, bed sources are located in depositional areas along the reach where stream velocities and bed shear stress are reduced, and the surface fine grained lamina only deposits in pools along the stream reach and not in the riffle or runs. This modeled idealization of the stream/reach explains most of the errors associated with the sediment yield results.

Chapter 7: Sediment Transport Model Results

7.1 Results of Current Conditions

The sediment transport model was calibrated and validated for the time period between January 1, 2006 and December 31, 2008. Sediment input from the uplands/tributaries, mean particle settling velocity, transport capacity coefficients for high and low flows, shear stress acceleration coefficient, sediment routing coefficient, development time for the SFGL, maximum SFGL depth, and the critical shear stresses and erodibilities for the sediment sources were calibrated within a range of values found from other studies to match the available sediment yield, bed storage, and erosion data from the study watershed. Under the calibrated conditions, deposition and erosion processes within the channel work in concert so that the bed is in a state of equilibrium where the bed is neither eroding or growing annually. For this analysis, the sediment model is run using flowrate measurements at the outlet of the watershed. The flowrate at the start of the channel was found by scaling the flowrates at the outlet by area (using the Army Corp areal discharge method) and then transposed back by three hours to account for the travel time.

7.1.1 Sediment Yield

The sediment yield for the three year calibration and validation period is 11,959 metric tons. This is 3,986 metric tons per year. The events which transported the most sediment out of the watershed correspond with the high flow rate events for the watershed. These sediment flux and stream flow trends can be seen in Figure 28 and Figure 29 respectively.

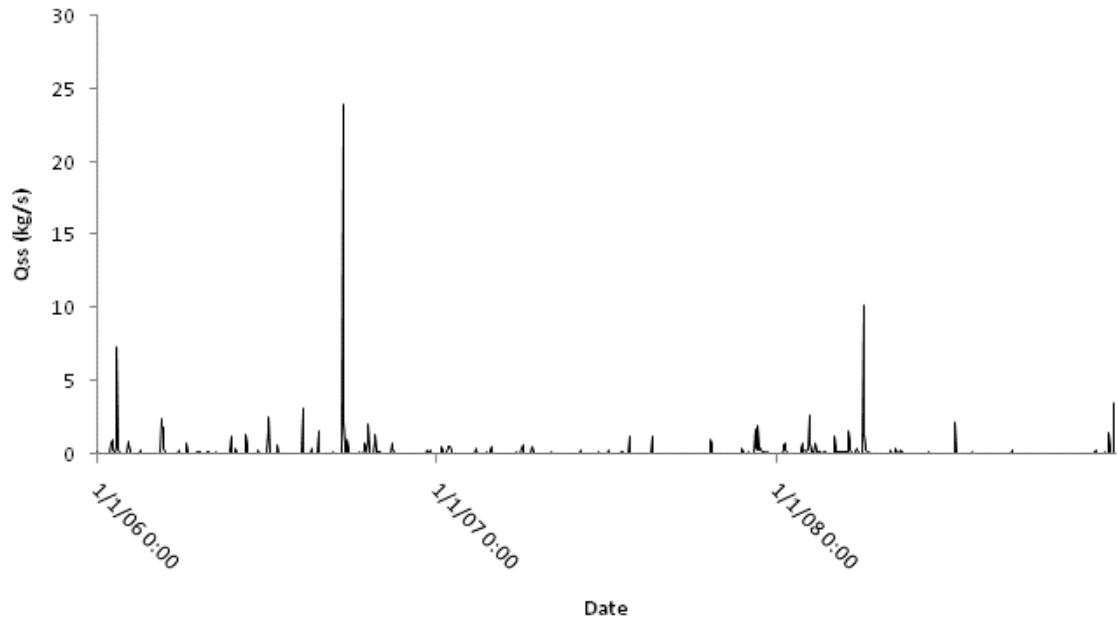


Figure 28: Figure of Sediment Flux (kg/s) for the three year calibration and validation period.

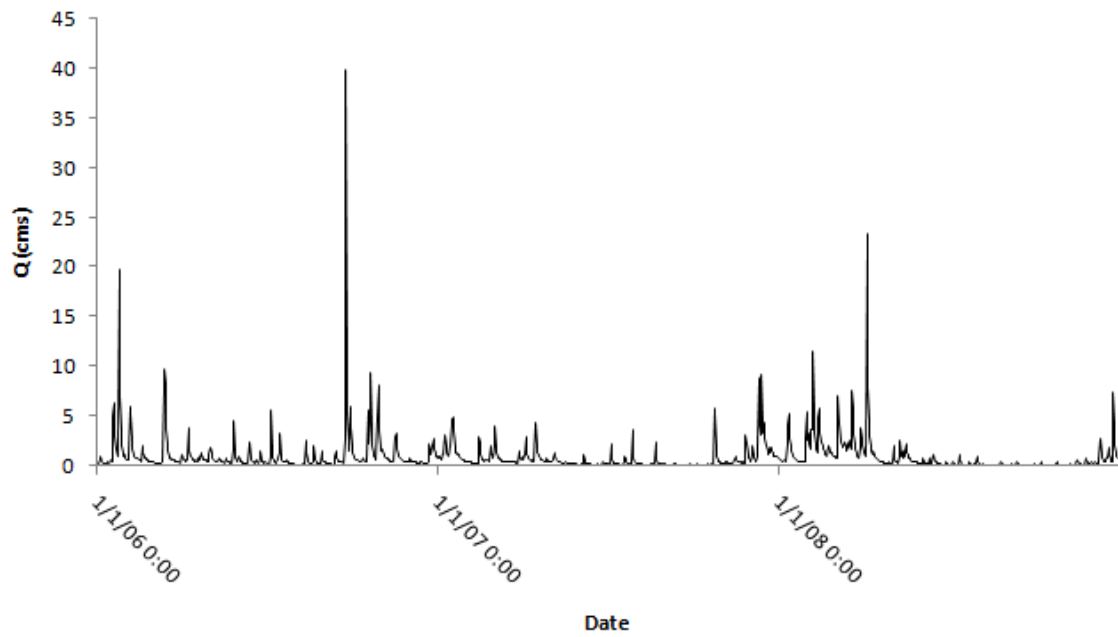


Figure 29: Figure of stream flow (cms) for the three year calibration and validation period.

The distribution of sediment yield versus storm return period was assessed for the results as shown in Table 20. The one day return interval for stream flow will yield approximately 8.64 kg of sediment. The flow rate for the one day return interval is 0.02 cms and is a very low baseflow flow rate for the South Elkhorn watershed. The seven day return interval for stream flow will yield approximately 9 metric tons of sediment. This weekly storm event is 1.6 cms and is a high baseflow event for the South Elkhorn watershed. The boundary between low and high flows was chosen as 2.5 cms for the sediment transport model. The return interval for this boundary is approximately 12 days and the yield for this event is 21 metric tons. The thirty day return interval for stream flow will yield approximately 64 metric tons of sediment. The monthly flow event is approximately 4.75 cms and is a storm of pronounced sediment transport for the South Elkhorn watershed. The high flow events greater than 20 cms have a return interval of one year. These were found to be the most pronounced sediment transport events and transported 734 metric tons of sediment. Tabular results for this frequency analysis in Table 20 also present data for 60 and 120 day return intervals.

Table 20: *Table of return interval (days), stream flow (cms), sediment flux (kg/s), and total daily yield (kg).*

<i>RI</i> (days)	<i>Q</i> (cms)	<i>Q_{ss}</i> (kg/s)	<i>S_y</i> (t/day)
1	0.02	0.0001	0.00864
7	1.65	0.10	9
15	2.85	0.33	29
30	4.75	0.74	64
60	6.30	1.45	125
120	8.80	2.20	190
365	21.80	8.50	734

7.1.2 Sediment Yield Source Fractions

The sediment yield at the outlet of the watershed was discretized into five sediment sources: 1) SFGL biofilm, 2) SFGL sediments, 3) Streambed, 4) Streambanks, and 5) Tributaries/Uplands. Sediment erosion was modeled individually for each source depending on each source's critical shear stress, erodibility, fluvial shear stress at the source, and fluvial transport capacity. The average fraction of eroded material that came from each source was determined by multiplying the sediment yield for each hourly interval by the fraction of each sediment source currently in suspension [Equation (42)]. These values were then summed for the three year calibration and validation period and divided by the total yield for the three year calibration and validation period. The sediment budget for the three year calibration and validation period can be seen in Figure 30.

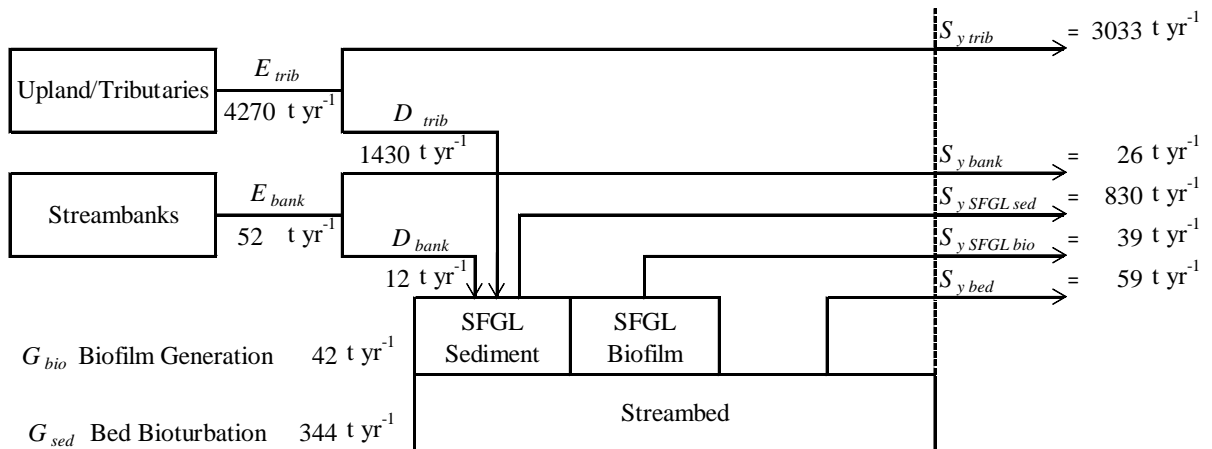


Figure 30: Sediment budget (metric tons per year) in the South Elkhorn watershed for the three year calibration and validation period.

Sediment eroded from the tributaries/upland sources and streambanks will either deposit to the streambed or SFGL or be transported out the watershed. Sediment eroded

from the SFGL sources and streambed sources will either deposit back to the SFGL or streambed or be transported out the watershed. The fraction of material each source contributes to the total sediment yield and the annual sediment yield for each sediment source can be seen in Table 21.

Table 21: *Table of source fractions and annual yields for the three year calibration and validation period.*

	P_s	E_s (t yr ⁻¹)	D_s (t yr ⁻¹)	S_y (t yr ⁻¹)
Upland/Tributary	0.761	4270	1430	3033
SFGL sediment	0.208	1358	391	830
SFGL biofilm	0.010	64	18	39
Streambed	0.015	124	28	59
Strambank	0.006	52	12	26

7.1.3 Temporal Change in the Streambed

Figure 31 shows a graph of bed supply and bed depth. The change in the bed storage is related to the frequency of low and high flow events, which are the most erosive events. Under this equilibrium bed condition, deposition to the bed and erosion from the bed are approximately equal and the total mass of stored material in the streambed does not change annually. It is seen in Figure 31 that a number of flow and sediment erosion and deposition periods exist for the streambed including the following:

- i. Low Flow SFGL Flushing Events: These events are for low and moderate hydrologic events in the watershed that erode, or flush, SFGL sediments. In turn, SFGL generation further develops sediment within the streambed *via* bioturbation and relatively low sediment deposition. Thus the net change is bed degradation during Low Flow SFGL Flushing Events.

- ii. High Flow Deposition Events: These events are characterized by high tributary erosion, SFGL erosion, and sometimes bank and bed erosion. The high flow events result in pronounced deposition to the SFGL and the streambed. Thus the next change is streambed aggradation and loss of sediment from bank and tributary sources during High Flow Deposition Events.

In between periods of streambed degradation and aggradation, short-term equilibrium of the streambed is seen where change in elevation of the streambed is not pronounced. In the long-term, relative equilibrium is also seen.

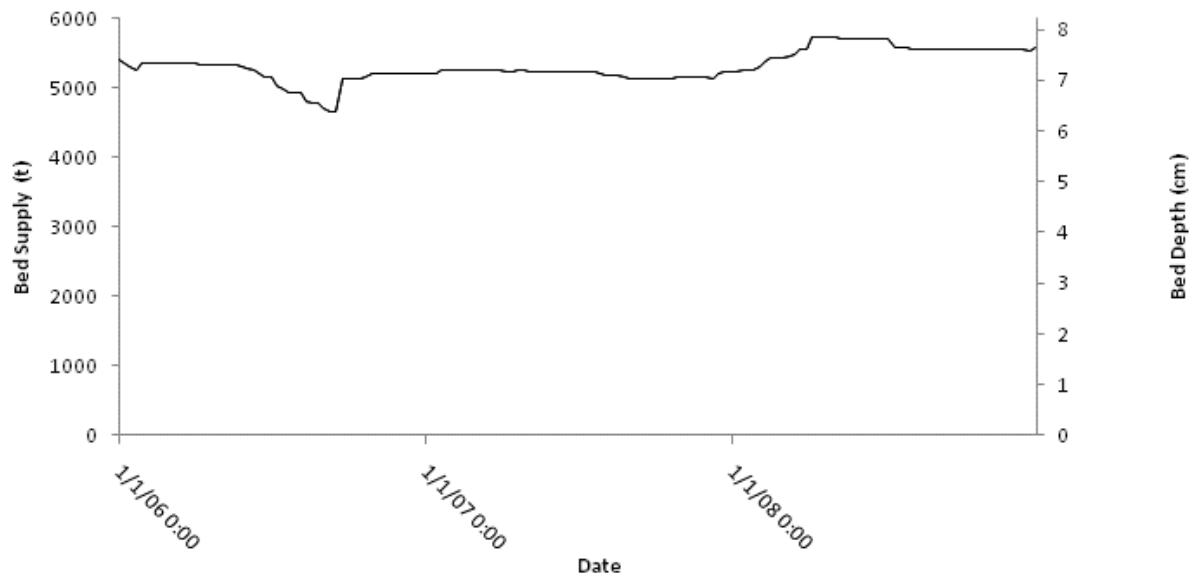


Figure 31: *Graph of bed supply (kg) and bed depth (cm) for the three year calibration and validation period.*

7.1.4 Temporal Change in the SFGL

Figure 32 shows a graph of SFGL supply and depth. The temporal change in the SFGL supply is dependent upon the flow in the channel. During the onset of a large storm event the SFGL begins to erode. If a hydrologic event is large enough, at the peak of the event the SFGL becomes depleted (see Figure 32) and the flow begins to erode the bed and bank sediment sources. During the recession limb of a large storm event, the sediments currently in suspension in the water column begin to settle into the SFGL and bed storages. These processes can be seen during the larger flow events. Smaller flow events do not have the power necessary to fully erode all SFGL sediments and instigate the erosion of streambed and streambank sources. The SFGL supply regeneration is from the bioturbation of bed sediments, biofilm development, and deposition from the stream column.

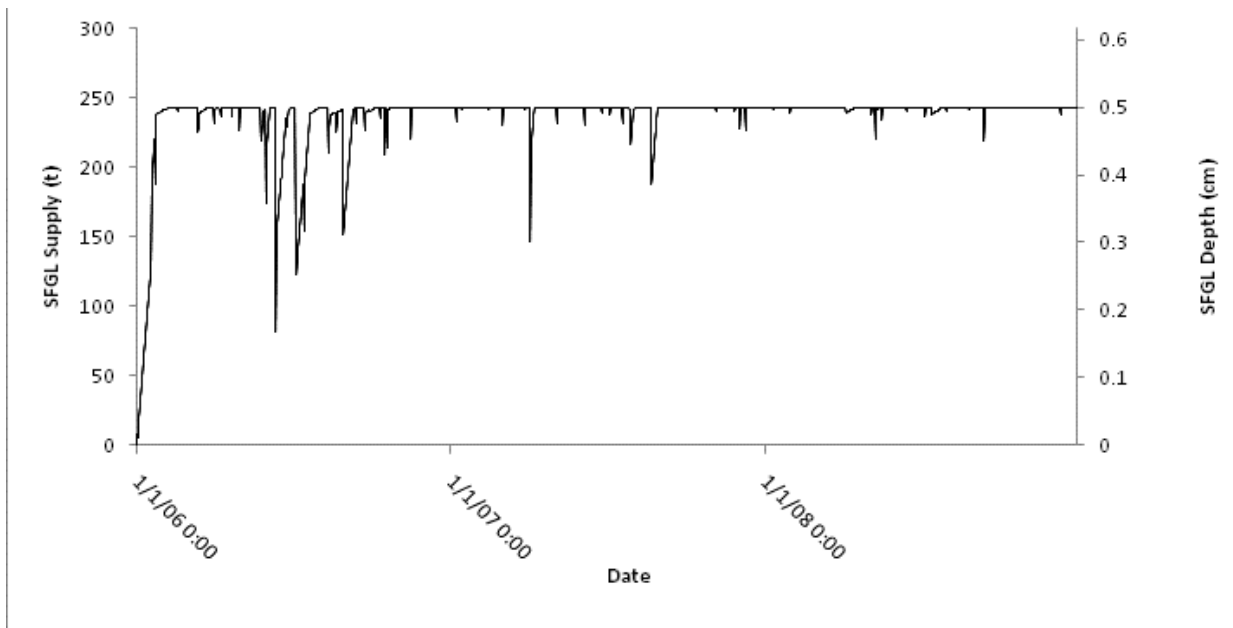


Figure 32: *Graph of SFGL supply (kg) and bed depth (cm) for the three year calibration and validation period.*

SFGL sediments in the SFGL sediment storage, streambank storage, streambed storage, and from the tributary/upstream source are assumed to be passive and not contain any active biological material. Total generation of new biological material is estimated from the sediment transport model using Equation (52) as 42 metric tons per year. Biological material does not die and decay in this model, and inclusion of equations for decomposition of biological material in the SFGL will be important in future improved models.

7.1.5 Bank Erosion

Figure 33 shows a graph of total bank material eroded and the depth of bank erosion. Bank erosion only occurs when the SFGL has been fully eroded, sufficient shear at the bank source, and sufficient transport capacity exists during very high flow events (see a comparison of Figure 32 and Figure 33). Total annual erosion from the banks is approximately 42 metric tons. Bank erosion occurs only during high magnitude flow events with a return period of approximately one year, equal to approximately 20 cms. Total bank erosion for the three year calibration and validation period is approximately 4.9 mm, or 1.6 mm per year. The sediment transport model assumes that erosion occurs uniformly across the entire cell, but in reality the majority of bank erosion occurs near the outlet of the watershed. Assuming approximately 0.5 kilometers of banks are eroding near the outlet, then the channel near the outlet widens by approximately 3.2 cm per year. Qualitative observations of the channel near the outlet confirm that these bank erosion and widening rates seem appropriate.

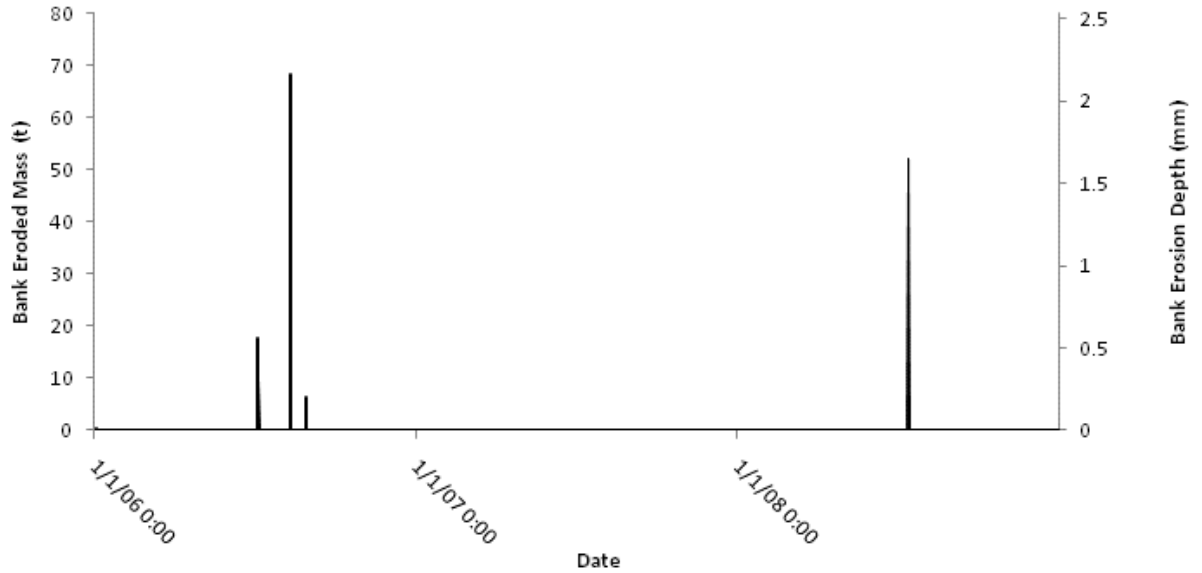


Figure 33: Figure of bank erosion mass (kg) and bank depth eroded (m) for the three year calibration and validation period.

7.2 No Loading from Uplands/Tributaries

Based on the initial run for the calibrated condition, it was seen that the SFGL has high importance in controlling streambank and streambed erosion as well as generation of biological material in the streambed. For these reasons, a number of cases were run to assess the behavior of the SFGL and sediment budget under different sediment loading conditions. The sediment transport model was rerun with no loading from the upland/tributary source. This change causes the bed to be in a non-equilibrium state. Without the addition of sediments from the tributary/upland source, the stream begins to erode the bed and banks more readily to satisfy the transport capacity deficit.

7.2.1 Sediment Yield

Figure 34 shows the sediment flux for the calibration and validation period with no upland/tributary input. Without the loading from the tributaries, total sediment yield from the watershed for the three year calibration and validation period decreases from 11,959 metric tons to 5,880 metric tons, which is 1,960 metric tons per year. Investigation of the sediment transport capacity and sediment concentration in-stream showed that the transport capacity limited condition was modeled predicted from the model during the no tributary loading condition, thus shear limitations is not an explanation of the decreased sediment yield predicted from the results. Rather the decrease is due to the low settling velocity of the mean sediment size fraction. A low settling velocity caused eroded sediments to stay in suspension longer after the transport capacity of the flow decreases during the recession limb of the storm hydrograph and deposition in the channel begins. Sediments stay suspended longer and more are flushed out of the watershed by the flow before the sediments have the ability to deposit. Thus, the no tributary loading results in lower sediment yield. The tributaries provided a high sediment loading to the downstream reach, which increased sediment yield at the outlet and increased deposition to the streambed. Without this additional loading, the bed begins to erode and is not replenished and sediment yield for the watershed decreases.

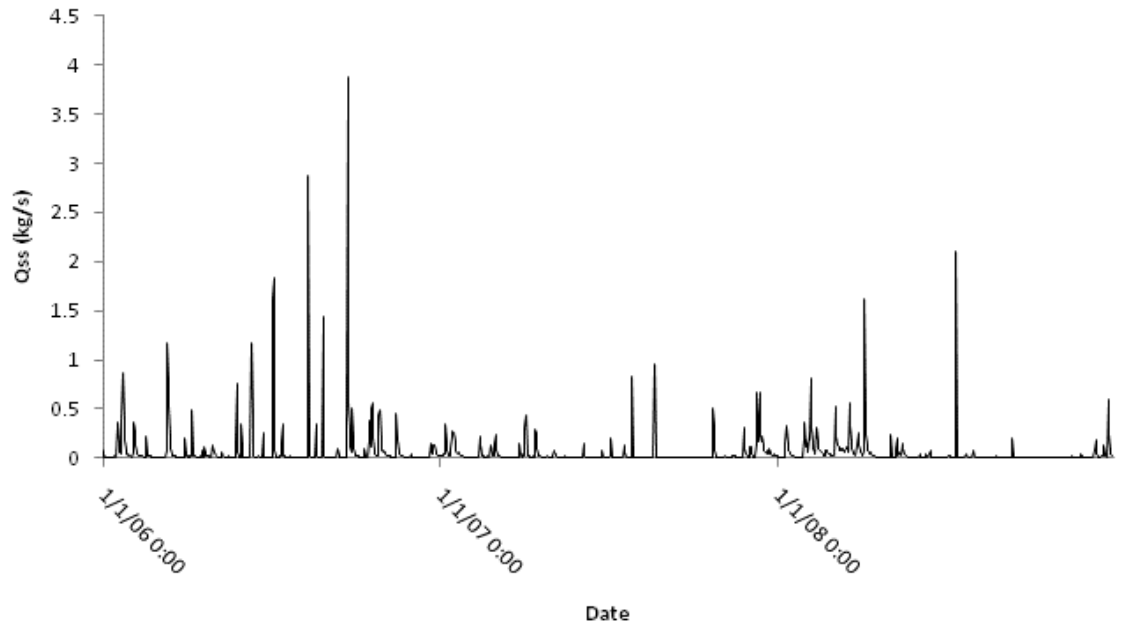


Figure 34: *Sediment flux with no upland/tributary input.*

7.2.2 Sediment Yield Source Fractions

Figure 34 shows the sediment budget for the study watershed with no contribution from the uplands and tributaries. Table 22 shows the annual yield for each source and the fraction of the total yield that each source contributes. By eliminating the sediment contribution from the upland/tributary sources, the total sediment yield for the study watershed decreases, but the sediment contribution from all other sources doubled, which is reflective of the transport capacity limited condition of the lowland watershed. The transport capacity of the stream can no longer be satisfied from the sediment contribution from the uplands/tributaries, so erosion from other sources increases.

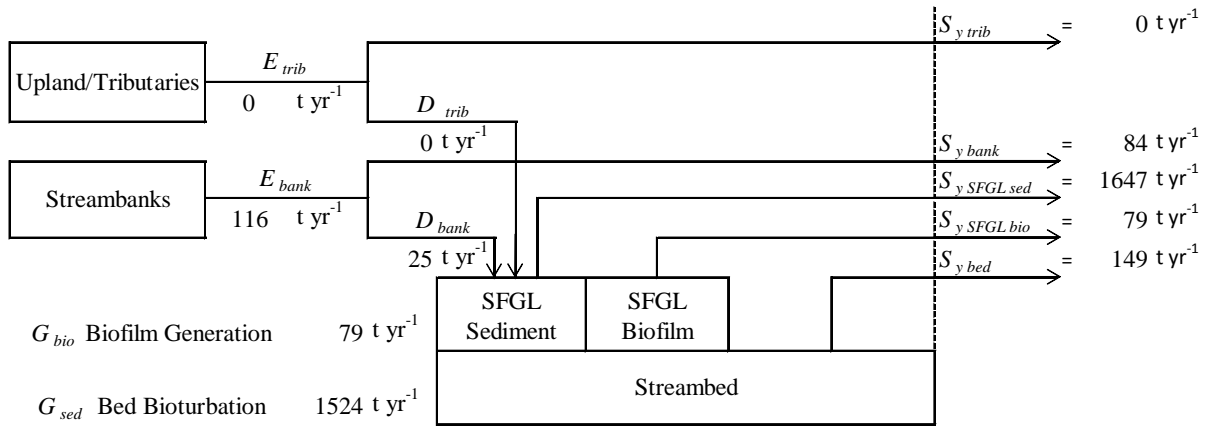


Figure 35: Sediment budget for one year in the South Elkhorn watershed under no upland/tributary loading conditions.

Table 22: Table of source fractions and annual yields for each source.

	P_s	E_s (t yr ⁻¹)	D_s (t yr ⁻¹)	S_y (t yr ⁻¹)
Upland/Tributary	0.000	0	0	0
SFGL sediment	0.841	2102	487	1647
SFGL biofilm	0.040	101	23	79
Streambed	0.076	220	44	149
Strambank	0.043	116	25	84

7.2.3 Temporal Change in the Streambed

Without the contribution of sediments from the tributaries/upland source, SFGL and bed erosion increases to satisfy the transport capacity deficit. Without any deposition from excess tributary/upland source sediments, the bed and the SFGL do not regenerate at the same rate as under bed equilibrium conditions. The SFGL erodes the bed through bioturbation much faster than under bed equilibrium conditions because there is no deposition from the upland/tributary source to build the SFGL storage. The SFGL will continue to degrade the bed until the SFGL reaches its maximum supply limit, and

because erosion of the SFGL increases the SFGL is almost constantly growing and eroding the bed through bioturbation. Figure 36 shows the bed depth and supply for the three year calibration and validation period. Thus, during the no upland/tributary loading scenario Low Flow SFGL Flushing Events cause degradation and High Flow Deposition Events do not carry a large enough sediment load from the tributary upland source to cause deposition.

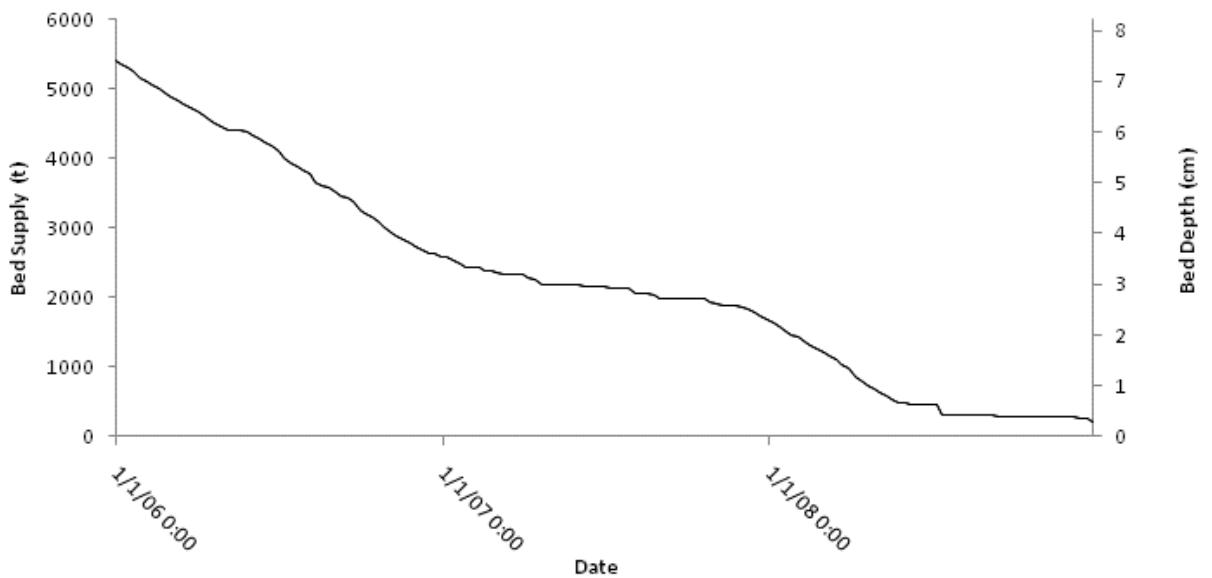


Figure 36: *Graph of bed supply (kg) and bed depth (cm) under no upland/tributary loading conditions.*

7.2.4 Temporal Change in the SFGL

Without the contribution of sediments from the tributaries/upland source, SFGL and bed erosion increases to satisfy the transport capacity deficit. Because of the decrease in deposition from upland/tributary source sediments, the SFGL does not regenerate nearly as fast as under bed equilibrium conditions. Figure 37 shows the SFGL depth and supply for the three year calibration and validation period.

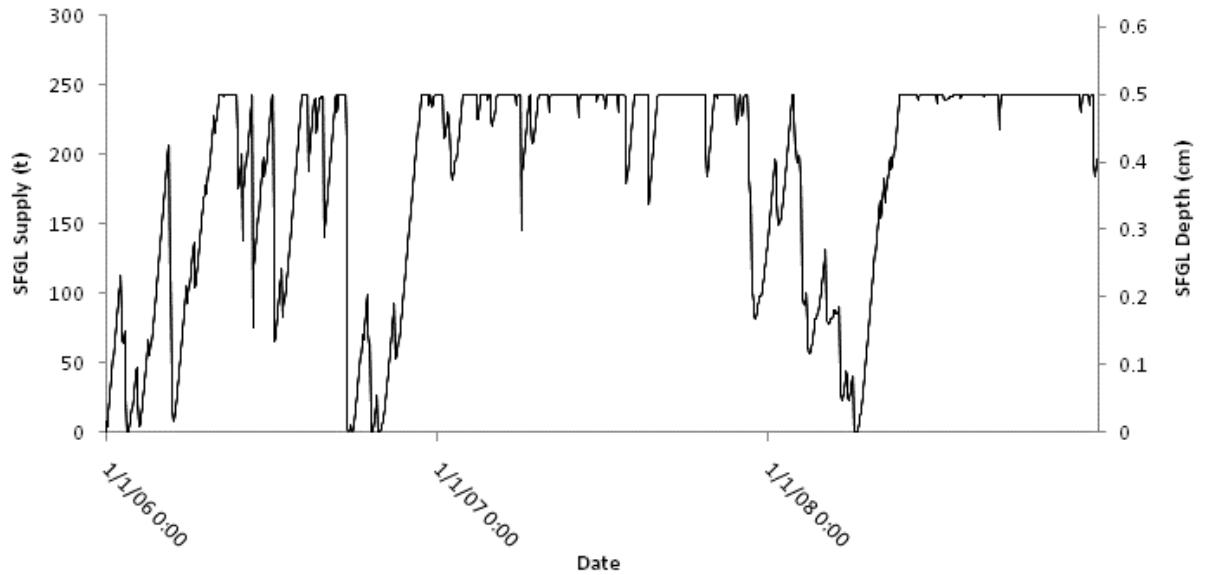


Figure 37: *Graph of SFGL supply (kg) and bed depth (cm) under no upland/tributary loading conditions.*

7.2.5 Bank Erosion

Without the contribution of sediments from the tributaries/upland source, SFGL and bed erosion increases to satisfy the transport capacity deficit. Without the addition of sediment from the upland/tributaries source, deposition to the streambed and SFGL decreases and with the decreased SFGL supply bank erosion occurs more frequently from smaller magnitude events. Figure 38 shows eroded mass from the stream banks and the depth of bank retreat. Total bank erosion increased from 4.9 mm to 11.1 mm of bank erosion for the calibration/validation period, or 3.7mm of bank erosion per year. For a 0.5 kilometer stretch, the channel width increases 7.8 cm per year.

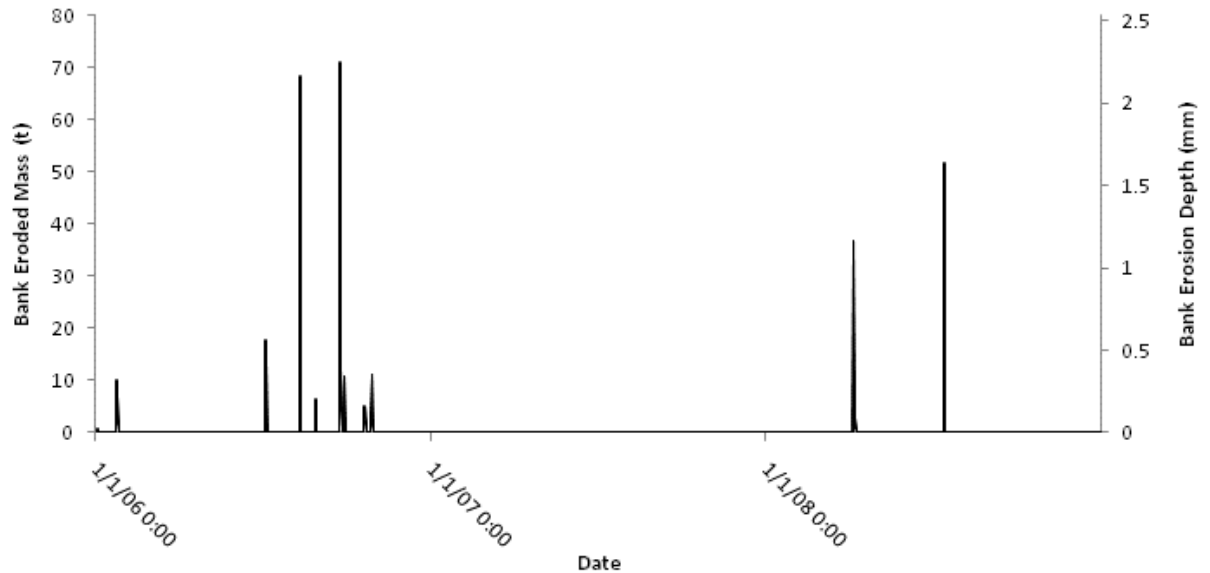


Figure 38: *Figure of bank erosion mass (kg) and bank depth eroded (m) under no upland/tributary loading conditions.*

7.3 Double Loading from Upland/Tributaries

Sediment loading from the tributaries was doubled to simulate a growing streambed condition. This simulation represents additional loading from the upland/tributary source coming from no sediment control structures.

7.3.1 Sediment Yield

Figure 39 shows the sediment flux over the three year calibration and validation period. With the increased loading from the uplands/tributaries, the sediment yield for the three year calibration and validation period increased from 11,959 metric tons to 17,813 metric tons. The increase in sediment yield is due to the increased sediment contribution from the upland/tributary source. Increasing the sediment loading increases the mass of suspended sediments in the downstream cell. If the transport capacity cannot support the sediment loading from the upland/tributary source, then the excess sediment

will deposit to the bed, but because the settling velocity is low the sediments stay suspended longer which allows more time for the streamflow to wash the excess sediments out of the watershed.

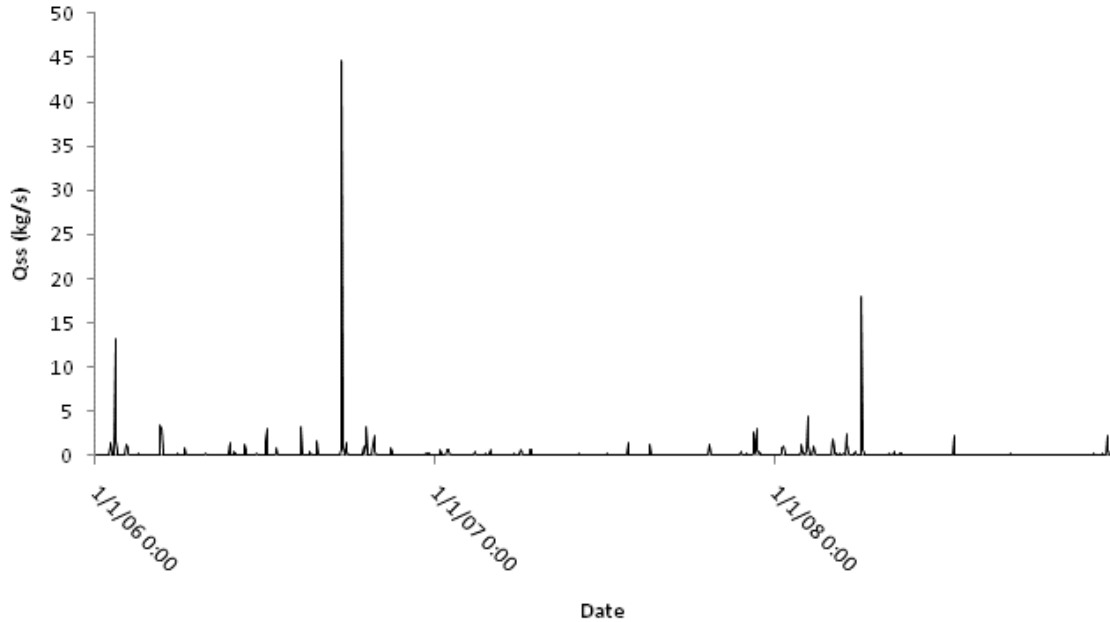


Figure 39: *Sediment flux (kg/s) with increased upland/tributary loading.*

7.3.2 Sediment Yield Source Fractions

Figure 40 shows the sediment budget for the increased upland/tributary sediment source scenario. Table 23 shows the sediment source, fraction each source contributes to the annual sediment yield, and annual sediment yield for each source. By increasing the loading from the upland/tributary source, the sediment yield from the upland/tributary source increases. All the other sources have a marginally decreased sediment yield, but remain ultimately unchanged from equilibrium conditions. The reason there is no great change in the erosion of the bed and bank sources is because only high flow events have the shear and transport capacity capable of eroding these sources, similar to equilibrium

bed conditions. Under all but high flow conditions, the tributary/upland and SFGL sources satisfy the transport capacity and erosion from the other sources is negligible. Deposition increases from all sources because of the increased supply of sediments from the upland/tributary sources. Extra sediments in suspension cause more deposition, and because the stream is assumed to be well mixed excess upland/tributary sediments force a high fraction of SFGL, bed, and bank sediments to deposit when the transport capacity decreases after the storm peak.

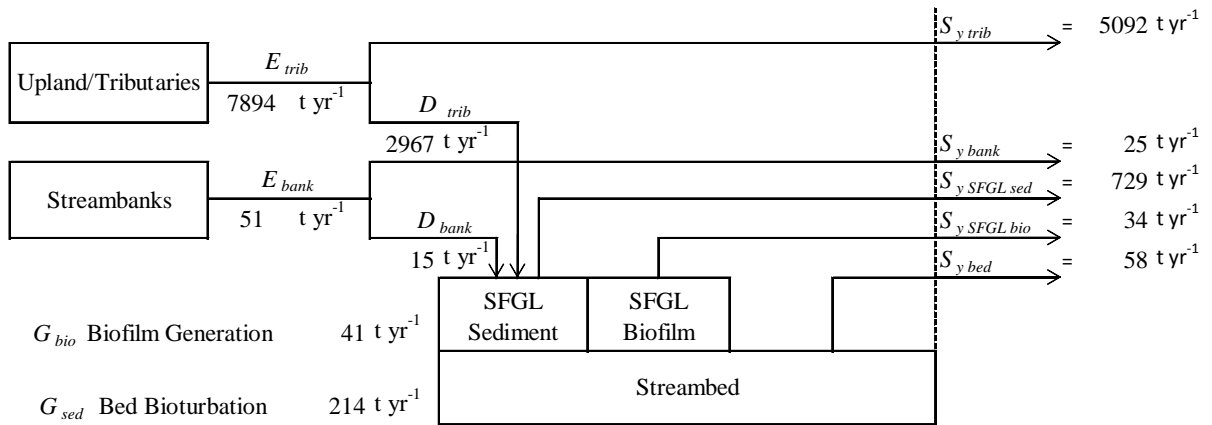


Figure 40: Sediment budget for one year in the South Elkhorn watershed under increased upland/tributary contribution conditions.

Table 23: Table of source fractions and annual yields for each source under increased upland/tributary loading.

	P_s	E_s (t yr ⁻¹)	D_s (t yr ⁻¹)	S_y (t yr ⁻¹)
Upland/Tributary	0.858	7894	2967	5092
SFGL sediment	0.123	1271	424	729
SFGL biofilm	0.006	59	20	34
Streambed	0.010	122	34	58
Strambank	0.004	51	15	25

7.3.3 Temporal Change in the Streambeds

Figure 41 shows the streambed supply and depth, which illustrates the aggrading system from the increased tributary loading. Increasing the contribution of sediments from the upland/tributary source increases the sediments available for deposition in the downstream reach. Increased deposition increases the supply of sediments available in the streambed. Thus, for this scenario Low Flow SFGL Flushing Events are shown to exist and cause degradation however High Flow Deposition Events are more prominent in the long-term due to the increased loading from the tributaries and the net change over the model calibration/validation is bed aggradation.

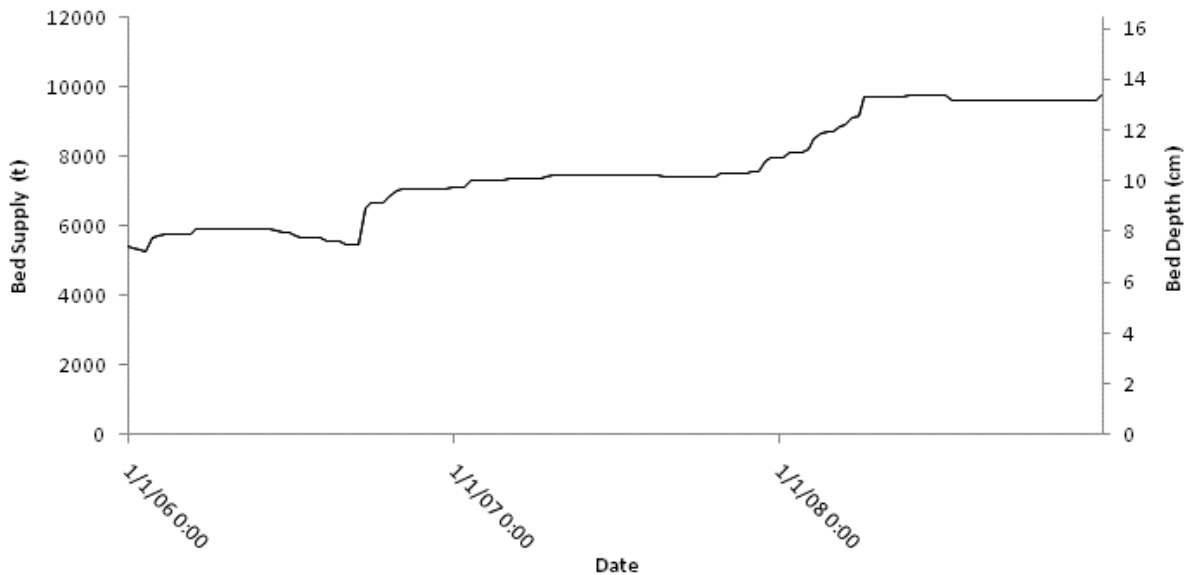


Figure 41: Graph of bed supply (kg) and bed depth (cm) under increased upland/tributary loading conditions.

7.3.4 Temporal Change in the SFGL

Figure 42 shows the mass of the SFGL supply and the depth of the SFGL. Total SFGL erosion decreases from the increased contribution from the upland/tributary source.

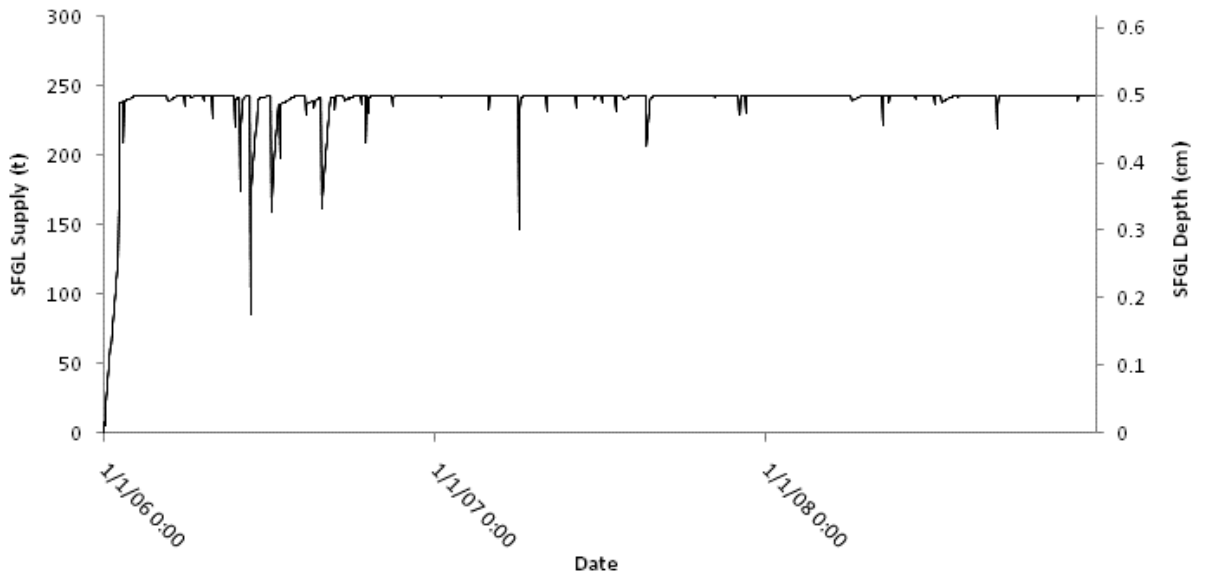


Figure 42: *Graph of SFGL supply (kg) and bed depth (cm) under increased upland/tributary loading conditions.*

7.3.5 Bank Erosion

Figure 43 shows a graph of the mass of eroded bank material and depth of bank erosion. Bank erosion occurs when the SFGL completely erodes and the transport capacity and shear stress of the stream are sufficient to erode the bank material. The streambed is modeled so that only the top 0.5 cm of the streambed is the SFGL, so all excess depositing sediments are routed to streambed storage. Under increased upland/tributary loading the streambed grows, but because the SFGL has a maximum

allowable depth it cannot store excess sediments. The sediment yield from bank erosion decreases slightly, but bank erosion still occurs during high magnitude flow events which have the power necessary to fully erode the SFGL. Bank erosion for this period is approximately 4.8 mm, or 1.6 mm per year. Assuming approximately 0.5 kilometers of banks are eroding near the outlet, then the channel near the outlet widens by approximately 3.4 cm per year.

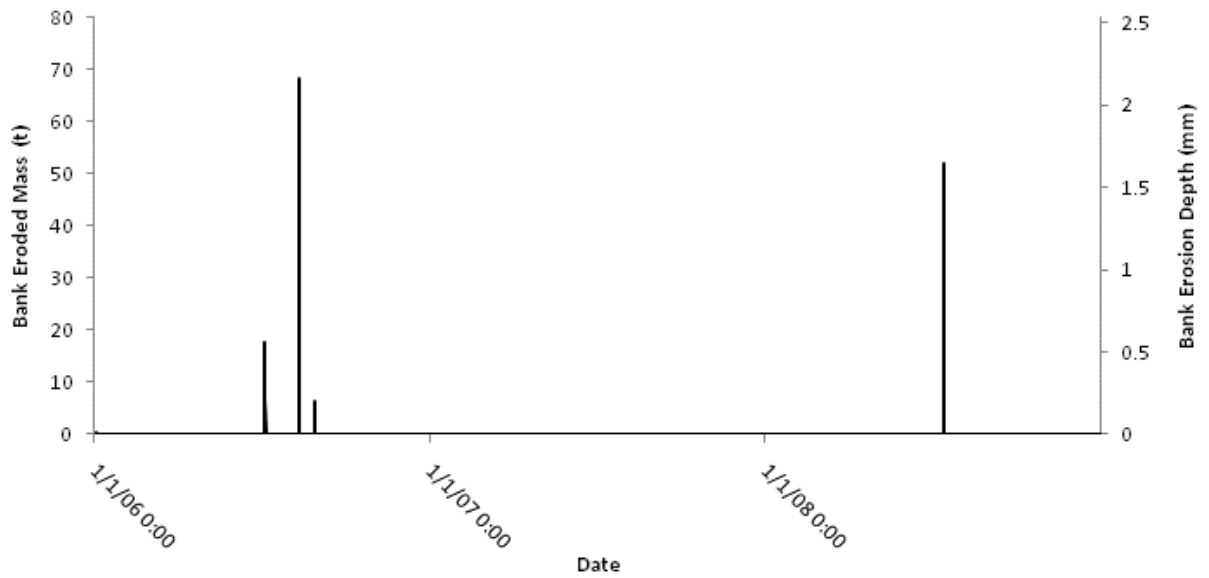


Figure 43: *Figure of bank erosion mass (kg) and bank depth eroded (mm) under increased upland/tributary loading conditions.*

7.4 Discussion of Results for the Three Year Period

For the watershed sediment transport model results, it is shown that the SFGL represents a substantial portion of the sediment budget for the lowland watershed for the present calibrated conditions where the sediment bed was essentially in an equilibrium state as well as for the further model runs where a degrading and aggrading streambed

was investigated. Based on these results, it should be highlighted that the SFGL is an important part of the lowland watershed geomorphology impacting both geomorphologic sediment transport and carbon biological process that are in turn useful for environmental issues, e.g., water quality and total maximum daily load assessments and the export of carbon from watershed systems due to particulate organic carbon flux and carbon dioxide outgassing.

The SFGL is the most erodible sediment in the stream channel and thus it was hypothesized that it first satisfies the transport capacity of the flow. Under this hypothesis, the presence of the SFGL and the streambed keeps the streambanks and streambed from eroding. Further, in the case of a degrading system, it was seen that SFGL erosion acts as an intermediate step in streambed downcutting. Biological activity and bioturbation in the SFGL continue over time to develop eroded bed material. In this manner, biological rates can be seen as important for assessing geomorphologic rates on long time-scales.

The SFGL acts as a temporary storage region for nearly a third of the sediment that enters the 10.5 km stream reach that was focused upon. Deposition and thereafter temporary storage fosters the growth of autotrophic and heterotrophic biologic particulate organic matter in the streambed, which is later transported out of the watershed. In this manner, 42 t yr⁻¹ of organic matter or 24.4 tC yr⁻¹ was produced in the streambed for the calibrated conditions. Of this, 22.6 was transported out of the watershed. The 24.4 tC yr⁻¹ represents a carbon generation term for the watershed most probably from dissolved carbon sources via autotrophic action or existing heterotrophic use of larger plants and soil organic carbon. In terms of carbon flux, this represents 370 gC m² yr⁻¹ from the

streambed surface or $0.4 \text{ gC m}^2 \text{ yr}^{-1}$ from the watershed area. Further assessment of the carbon flux in terms of local and regional carbon budgets may be an important result for future research.

Another item that is important to discuss for the results of this study is the impact of tributary loading to the sediment budget. It is shown that a zero loading from the tributaries, which is representative of a case when watershed conservation measures were drastic to eliminate streambank erosion and transport due to the erosion of sediment from runoff, only decreases sediment yield from the watershed by approximately a 50% decrease. The decrease is due to the starved fluid which erodes the SFGL, streambed and streambank in order to meet the transport limited conditions. It will be expected that full downcutting of the streambed would lead to pronounced erosion of the streambanks (see Chapter 8). While conservation measures might be important at a local scale, it should be seen that the long term benefit may not be seen at the watershed scale due to the fact that sediment is further eroded from a downstream location. In the case of the aggrading streambed, the change in sediment yield of the watershed is also pronounced (i.e., 49% increase in sediment yield), however, it is seen that biological processes are not dampened during this scenario. The degrading bed conditions increase the amount of biological material generated in the watershed. In the model, this is a function of the maximum SFGL depth which limits the growth of biological material. When the SFGL is eroded biological processes can continue of the newly exposed bed material and deposited sediments. Based on these results, it is suggested that the existence of streambed under equilibrium conditions represents the optimal environmental and human condition because biological processes in the streambed can exist but also streambank

erosion and loss of land will not be as pronounced. It is suggested that when performing TMDL assessment and planning to reduce sediment yield from the watershed, assessment of the loading needed to produce an equilibrium streambed condition might be performed prior to watershed conservation measures that would be employed to stabilize streambanks and stop erosion within the uplands of a watershed.

Another important result of this analysis should be that while the zero loading condition is representative of sediment controls in the uplands of the watershed, no controls were in place to reduce the magnitude of the streamflow which is what controls erosion in the stream channel. If retention ponds, water gardens, or other such devices which reduce storm peak and flow acceleration were built then the erosion of the SFGL, bed, and bank sediments would further be reduced. These structures would also reduce the contribution of sediment from the upland/tributary source. A similar result could also be seen if the amount of impervious area in the uplands was decreased. It should also be noted that whether the bed of the study watershed is in equilibrium, growing, or dying is not known. Through qualitative observations, it is theorized that the bed is under equilibrium conditions, but further field measurements need to be performed to verify.

Chapter 8: Urbanization Results

The calibrated and validated HSPF hydrological model coupled with the calibrated and validated sediment transport model was used to quantify the effect urbanization has on the study watershed. HSPF was run with several different impervious area coverages with the intent of simulating the effects of urbanization on the streamflow for the study watershed, and this streamflow output from the HSPF model was used to drive the sediment transport model so as to predict the effect urbanization has on the sediment yield for the watershed, sediment source fractions, SFGL and bed storage, bank erosion, bank retreat, and streamflow.

Figure 44 show a map of the study watershed and the conceptual borders of the impervious areas for the simulation runs. Table 24 shows the tabulated percent impervious area for the entire watershed and the total impervious area for the watershed for each simulation run. The urbanization rates were found by comparing the total impervious area from the 1992 NLCD with the total impervious area from the 2002 NLCD. Impervious area is directly related to urbanization, and the rate of urbanization between the years 1992 and 2002 was predicted as $1.6 \text{ km}^2/\text{yr}$. Because the 1990's was a period of pronounced development, this urbanization rate was assumed to be high and the was further refined. Four simulation runs with the urbanization rates of $0.0 \text{ km}^2/\text{yr}$, $0.4 \text{ km}^2/\text{yr}$, $0.8 \text{ km}^2/\text{yr}$, and $1.6 \text{ km}^2/\text{yr}$ were used for this exercise. HSPF cannot simulate a dynamic land cover so each simulation run used the 20 year landcover that the urbanization rate for that run would return. The landcovers for the $0.0 \text{ km}^2/\text{yr}$, $0.4 \text{ km}^2/\text{yr}$, $0.8 \text{ km}^2/\text{yr}$, and $1.6 \text{ km}^2/\text{yr}$ urbanizations rates were 27.9 km^2 , 36.0 km^2 , 44.0 km^2 , and 60.1 km^2 of impervious area. HSPF and the sediment transport model were

then run under a 20 year simulation period for each simulation run with meteorological data generated from the climate prediction program CLIGEN.

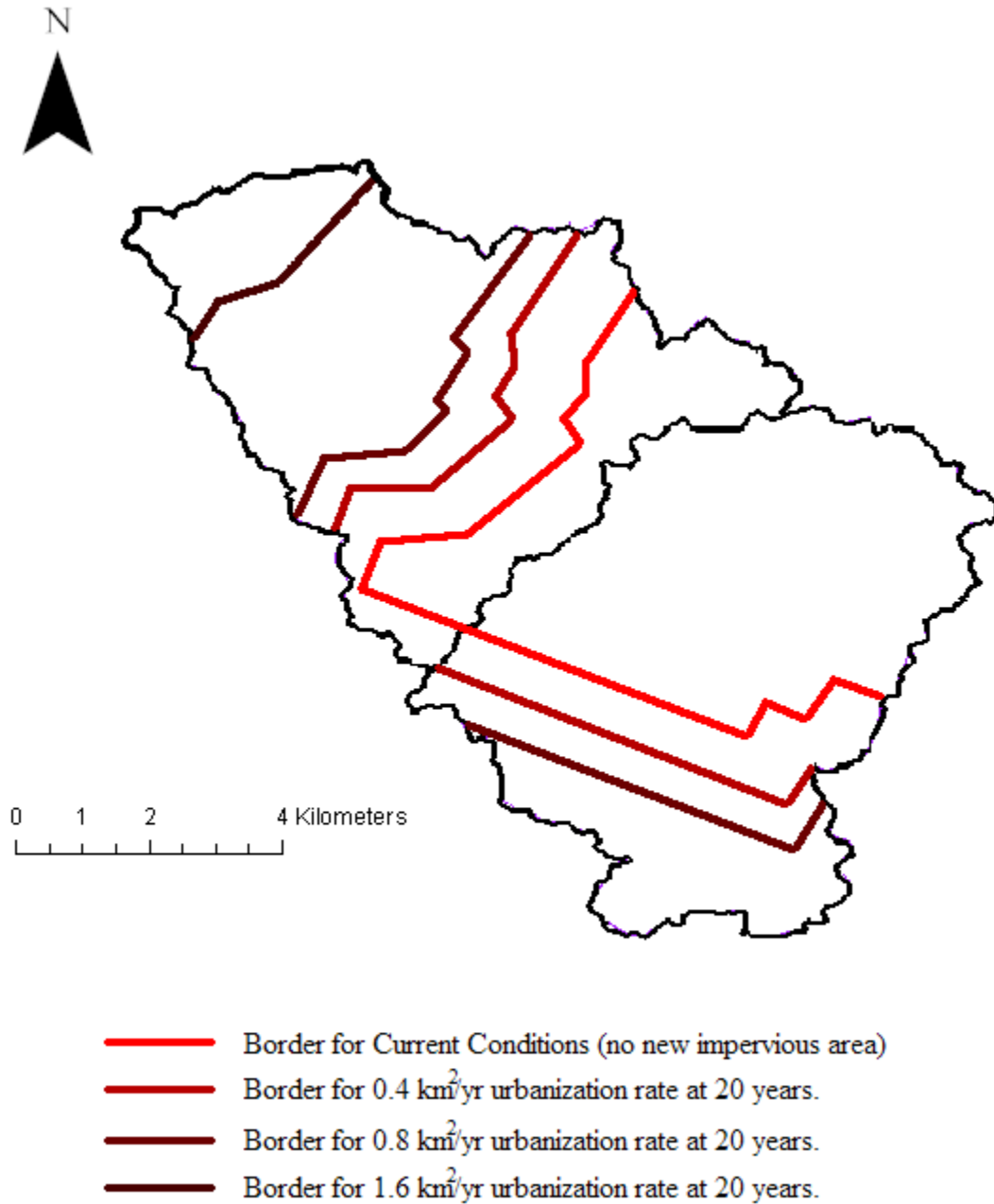


Figure 44: *Map of conceptual Urban/Agricultural borders at 20 years for each estimated urbanization rate.*

Table 24: *Table of impervious areas for each estimated urbanization rate.*

	fraction urban area	Total Impervious Area (km ²)
Current Conditions (no new urbanization)	0.45	27.9
0.4 km ² /yr urbanization rate at 20 years.	0.58	36.0
0.8 km ² /yr urbanization rate at 20 years.	0.71	44.0
1.6 km ² /yr urbanization rate at 20 years.	0.97	60.1

The four different land covers were run with two different upland/tributary input conditions: (1) Sediment contribution from the upland/tributary source was a function of flow rate only (see Equation 76), and (2) Sediment contribution from the upland/tributary source was a function of flow rate and urban area (see Equation 82). This was performed to simulate the effect erosion controls in the uplands would have on in-stream conditions.

The in-stream sediment transport model was re-calibrated with simulated flow data from the upland HSPF model to create a best fit equilibrium bed condition for the calibration/validation period. The new sediment model parameters can be seen in Table 25. In addition, the coefficient in Equation 76 was reduced to -0.01 to create an equilibrium bed condition. For this chapter, the flowrate that drives the sediment was estimated as the average of the flowrate at the outlet of the watershed and the flowrate at

the input of the channel three hours earlier in order to determine the average flood wave the channel is experiencing.

Table 25: Table of input data and parameter values for the re-calibrated sediment transport model.

S	Channel slope.	0.00044	m/m
H_{bank}	Bankfull depth.	2	m
W_{reach}	Channel bottom width.	6.25	m
W_{flood}	Floodplain width on one side of channel	30	m
L_{reach}	Channel length.	10525	m
m	Side slope.	3.3	m/m
n	Mannings coefficient for channel.	0.02	
SA_B	Surface area of the banks.	21050	m ²
k_p	Setting depth coefficient.	calculated	unitless
k_{ss}	Sediment routing coefficient.	0.01	unitless
$Q_{boundary}$	Boundary between low and high flows.	6.05	m ³ /s
$S_{sfgl(max)}$	Maximum allowable supply of SFGL in the channel.	243400	kg
$S_{sfgl(bed)}$	Initial supply of SFGL sediment in the channel.	0	kg
$S_{sfgl(bio)}$	Initial supply of SFGL biofilm in the channel.	0	kg
$S_{(bed)}$	Initial supply of bed sediments in the channel.	5400000	kg
$\rho_{B(bank)}$	Bulk density of bank sediments.	1500	kg/m ³
$\rho_{B(sfgl)}$	Bulk density of SFGL sediments.	1000	kg/m ³
$G_{sfgl(bio)}$	Generation rate of SFGL biofilm.	9.07E-08	kg/m ² .s
$G_{sfgl(bed)}$	Generation rate of SFGL sediments.	1.84E-06	kg/m ² .s
t_d	SFGL development time	30	days
ω_s	Mean settling velocity of suspended material.	4.50E-05	m/s
$C_{\tau(low)}$	Transport capacity coefficient for low flows.	1.00E-06	m ^{1/2} .s ² /kg ^{1/2}
$C_{\tau(high)}$	Transport capacity coefficient for high flows.	4.00E-05	m ^{1/2} .s ² /kg ^{1/3}
$C_{\tau(l)}$	Shear stress coefficient adjusting bed/bank shear.	calculated	unitless
$C_{\tau(l)}$	Shear stress coefficient for unsteady flow.	0.03	unitless
$\tau_{cr(sfgl)}$	Critical shear of the SFGL source.	0.05	Pa
$\tau_{cr(bed)}$	Critical shear of the bed source.	2	Pa
$\tau_{cr(bank)}$	Critical shear of the bank source.	2	Pa
$\alpha_{(sfgl)}$	Erodibility of the SFGL source. (Calculated)	8.94E-04	kg/Pa.m ² .s
$\alpha_{(bed)}$	Erodibility of the bed source. (Calculated)	2.12E-04	kg/Pa.m ² .s
$\alpha_{(bank)}$	Erodibility of bank source. (Calculated)	2.12E-04	kg/Pa.m ² .s

8.1 Frequency analysis Results for the Simulation Periods

The coupled model under simulates the erosion and yield in the channel when compared with the equilibrium bed results of Chapter 7. Table 26 shows a frequency analysis of the observed streamflows and the simulated streamflows. The upland model over-simulates lower streamflows, and under-simulates larger streamflows. The new calibration of the model has a lower transport capacity coefficient for low flows, a higher transport capacity coefficient for high flows, and a lower shear stress coefficient than the calibration used in Chapter 7. These coefficients were used to adjust for the over and under simulation of the streamflows.

Table 26: *Frequency analysis of observed and simulated streamflows.*

<i>RI</i> (days)	OBS <i>Q</i> (cms)	SIM <i>Q</i> (cms)
1	0.02	0.02
7	1.65	1.9
15	2.85	3.2
30	4.75	4.6
60	6.3	6.1
120	8.8	8.0
365	21.8	15.3

Table 27 shows the results of a streamflow and sediment flux frequency analysis. Streamflows and sediment flux rates increase with increasing urban area, and sediment flux rates also increase with the absence of sediment controls in the uplands. With increasing urban area, flow rates increase which increases the transport capacity in the channel and also increase the contribution from the Upland/Tributary source.

Table 27: Table of streamflow and sediment flux frequency analysis for the simulation periods.

Present Conditions			
RI (days)	Q (cms)	Q_{ss} (kg/s)	S_y (t/day)
1	0.02	0.0001	0
7	1.9	0.0175	2
15	3.2	0.205	18
30	4.6	0.415	36
60	6.1	0.68	59
120	8.0	1.05	91
365	15.3	2.15	186

0.4 km ² /yr Urbanization Rate with Upland Sediment Controls				0.4 km ² /yr Urbanization Rate without Upland Sediment Controls			
RI (days)	Q (cms)	Q_{ss} (kg/s)	S_y (t/day)	RI (days)	Q (cms)	Q_{ss} (kg/s)	S_y (t/day)
1	0.02	0.0001	0.00864	1	0.02	0.0001	0.00864
7	2.05	0.02	2	7	2.05	0.02	2
15	3.75	0.34	29	15	3.75	0.34	29
30	5.60	0.60	52	30	5.60	0.61	53
60	7.80	1.00	86	60	7.80	1.05	91
120	10.20	1.40	121	120	10.20	1.45	125
365	19.20	3.40	294	365	19.20	3.60	311

0.8 km ² /yr Urbanization Rate with Upland Sediment Controls				0.8 km ² /yr Urbanization Rate without Upland Sediment Controls			
RI (days)	Q (cms)	Q_{ss} (kg/s)	S_y (t/day)	RI (days)	Q (cms)	Q_{ss} (kg/s)	S_y (t/day)
1	0.02	0.0001	0.00864	1	0.02	0.0001	0.00864
7	2.20	0.03	2	7	2.20	0.03	2
15	4.30	0.41	35	15	4.30	0.42	36
30	6.40	0.75	65	30	6.40	0.80	69
60	9.10	1.20	104	60	9.10	1.30	112
120	11.80	1.65	143	120	11.80	1.85	160
365	22.00	4.20	363	365	22.00	4.80	415

1.6 km ² /yr Urbanization Rate with Upland Sediment Controls				1.6 km ² /yr Urbanization Rate without Upland Sediment Controls			
RI (days)	Q (cms)	Q_{ss} (kg/s)	S_y (t/day)	RI (days)	Q (cms)	Q_{ss} (kg/s)	S_y (t/day)
1	0.001	0.0001	0.00864	1	0.001	0.0001	0.00864
7	2.55	0.08	7	7	2.55	0.09	7
15	5.50	0.59	51	15	5.50	0.64	55
30	8.45	1.10	95	30	8.45	1.25	108
60	12.00	1.60	138	60	12.00	1.95	168
120	15.80	2.40	207	120	15.80	2.95	255
365	28.70	6.80	588	365	28.70	8.60	743

8.2 Sediment Budget Results for the Simulation Periods

Table 28 shows the tabular results for the simulation runs. Figure 45 shows the sediment budgets for the simulation runs. These figures show that the fraction of eroded material, mass of eroded material, deposited mass, and sediment yield for the Upland/Tributary source increases with increasing urban area and increases when erosion controls in the uplands are not implemented. The SFGL sediment and biological fraction of eroded material decrease with increasing urban area and when erosion controls in the uplands are not in place. SFGL sediment and biological eroded mass, deposited material, and sediment yield increase with increasing urban area, but generally decrease without sediment controls in the uplands.

Table 28: Table of annual sediment yields and source fractions for each sediment source for each simulation run.

Present Conditions

	P_s	E_s (t yr ⁻¹)	D_s (t yr ⁻¹)	S_y (t yr ⁻¹)
Upland/Tributary	0.690	1870	543	1284
SFGL sediment	0.296	743	233	551
SFGL biofilm	0.014	36	11	27
Streambed	0.000	0	0	0
Strambank	0.000	0	0	0

0.4 km²/yr Urbanization Rate with Upland Sediment Controls

	P_s	E_s (t yr ⁻¹)	D_s (t yr ⁻¹)	S_y (t yr ⁻¹)
Upland/Tributary	0.715	2789	765	1958
SFGL sediment	0.272	974	291	745
SFGL biofilm	0.013	47	14	36
Streambed	0.000	0	0	0
Strambank	0.000	0	0	0

0.4 km²/yr Urbanization Rate without Upland Sediment Controls

	P_s	E_s (t yr ⁻¹)	D_s (t yr ⁻¹)	S_y (t yr ⁻¹)
Upland/Tributary	0.732	2989	829	2091
SFGL sediment	0.255	952	289	728
SFGL biofilm	0.012	46	14	36
Streambed	0.000	0	0	0
Strambank	0.000	0	0	0

0.8 km²/yr Urbanization Rate with Upland Sediment Controls

	P_s	E_s (t yr ⁻¹)	D_s (t yr ⁻¹)	S_y (t yr ⁻¹)
Upland/Tributary	0.736	3488	943	2470
SFGL sediment	0.252	1097	323	845
SFGL biofilm	0.012	53	16	41
Streambed	0.000	0	0	0
Strambank	0.000	0	0	0

Table 28 continued.

0.8 km²/yr Urbanization Rate without Upland Sediment Controls

	P_s	E_s (t yr ⁻¹)	D_s (t yr ⁻¹)	S_y (t yr ⁻¹)
Upland/Tributary	0.768	3988	1102	2806
SFGL sediment	0.221	1049	317	808
SFGL biofilm	0.011	51	15	39
Streambed	0.000	0	0	0
Strambank	0.000	0	0	0

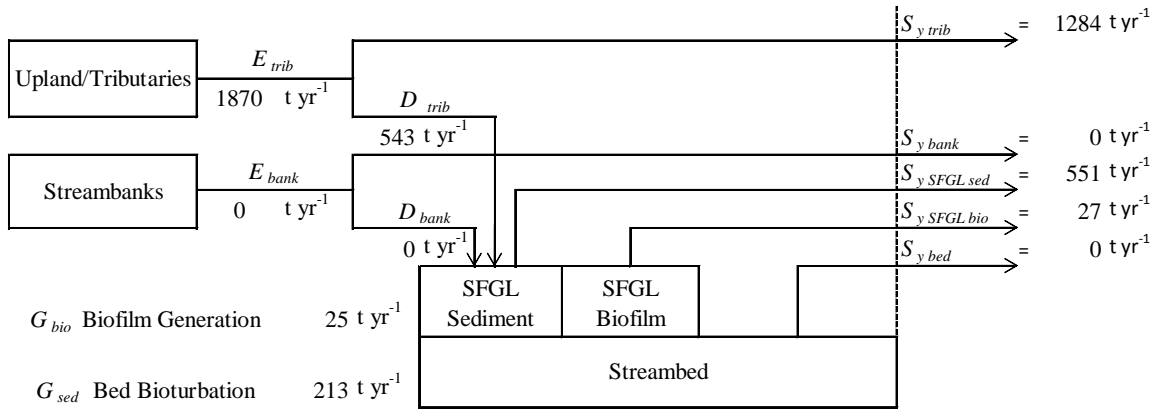
1.6 km²/yr Urbanization Rate with Upland Sediment Controls

	P_s	E_s (t yr ⁻¹)	D_s (t yr ⁻¹)	S_y (t yr ⁻¹)
Upland/Tributary	0.779	5269	1386	3789
SFGL sediment	0.211	1313	376	1027
SFGL biofilm	0.010	63	18	50
Streambed	0.000	0	0	0
Strambank	0.000	0	0	0

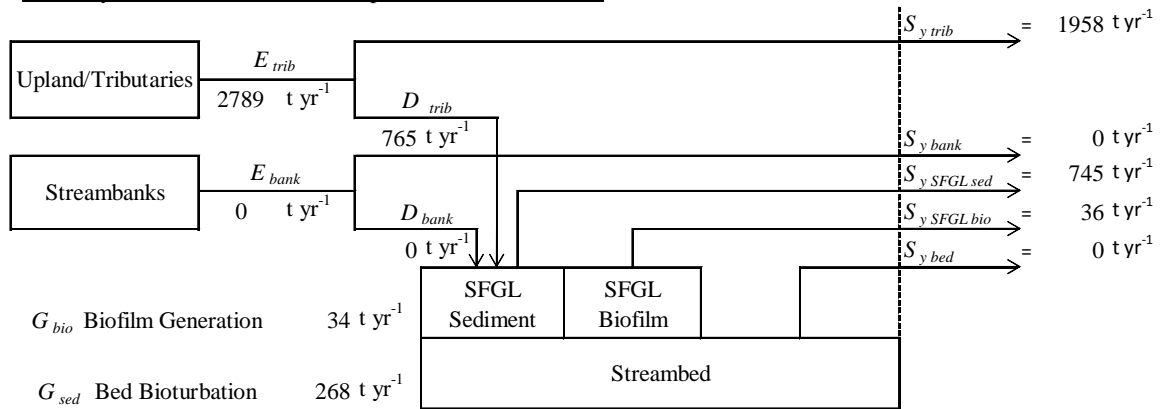
1.6 km²/yr Urbanization Rate without Upland Sediment Controls

	P_s	E_s (t yr ⁻¹)	D_s (t yr ⁻¹)	S_y (t yr ⁻¹)
Upland/Tributary	0.830	6780	1856	4821
SFGL sediment	0.162	1210	364	944
SFGL biofilm	0.008	59	18	46
Streambed	0.000	0	0	0
Strambank	0.000	0	0	0

Present Conditions



0.4 km²/yr Urbanization Rate with Upland Sediment Controls



0.4 km²/yr Urbanization Rate without Upland Sediment Controls

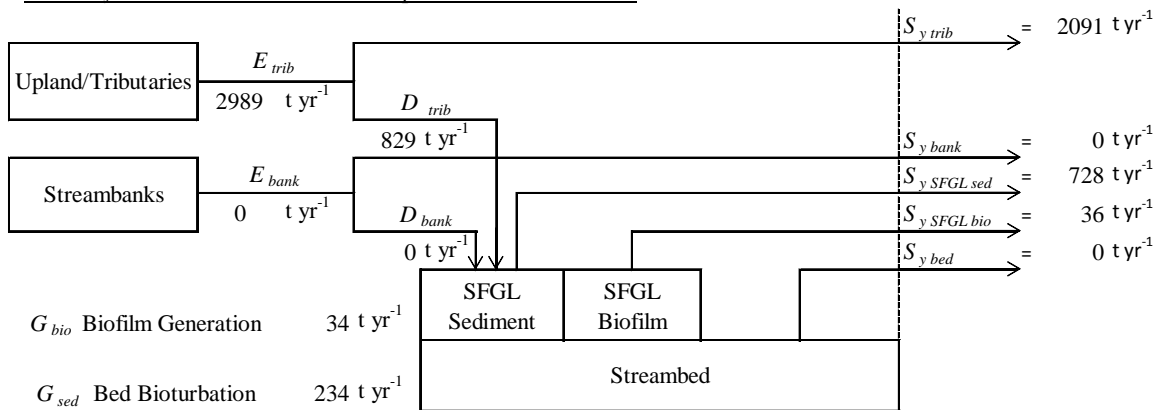
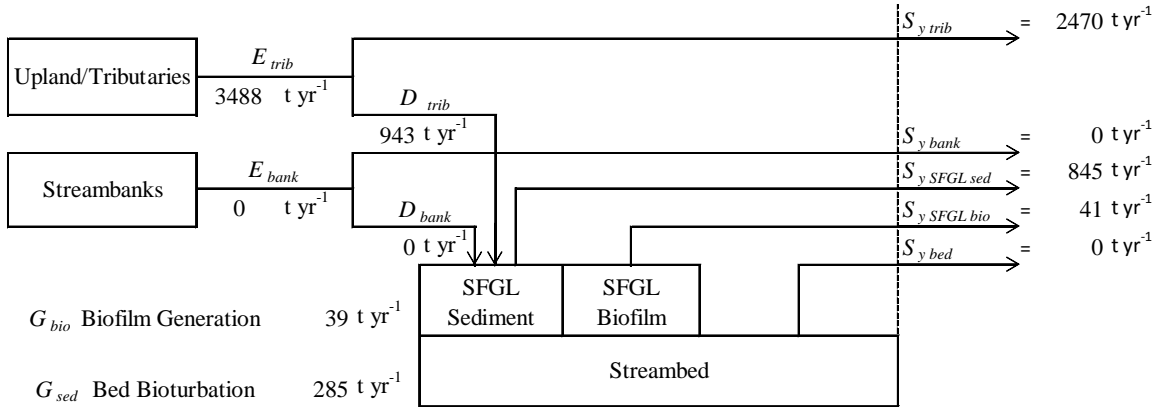
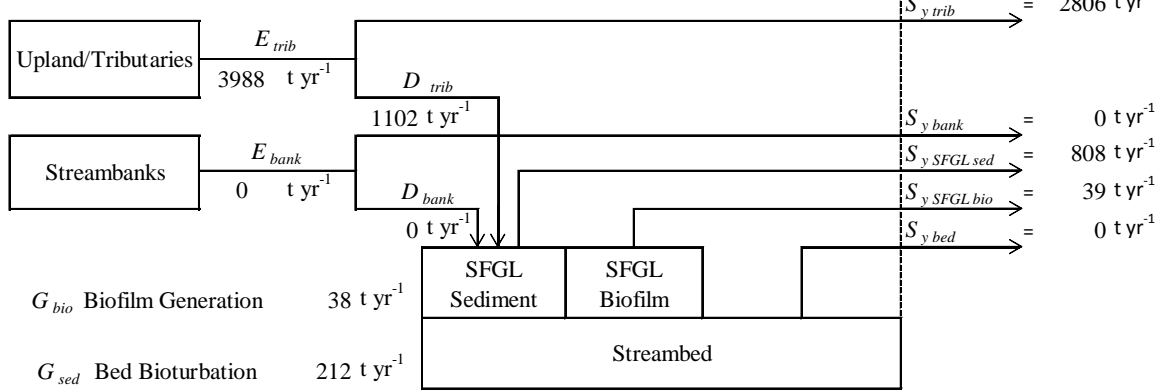


Figure 45 continued.

0.8 km²/yr Urbanization Rate with Upland Sediment Controls



0.8 km²/yr Urbanization Rate without Upland Sediment Controls



1.6 km²/yr Urbanization Rate with Upland Sediment Controls

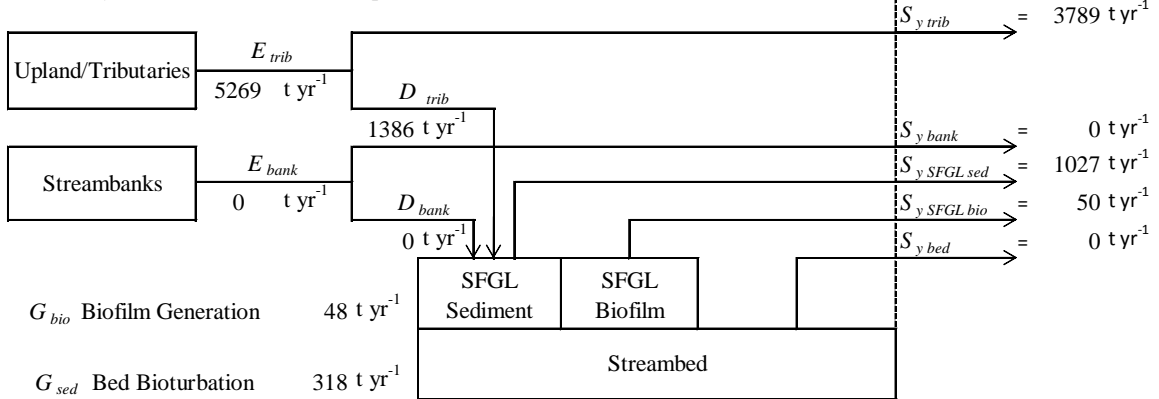


Figure 45 continued.

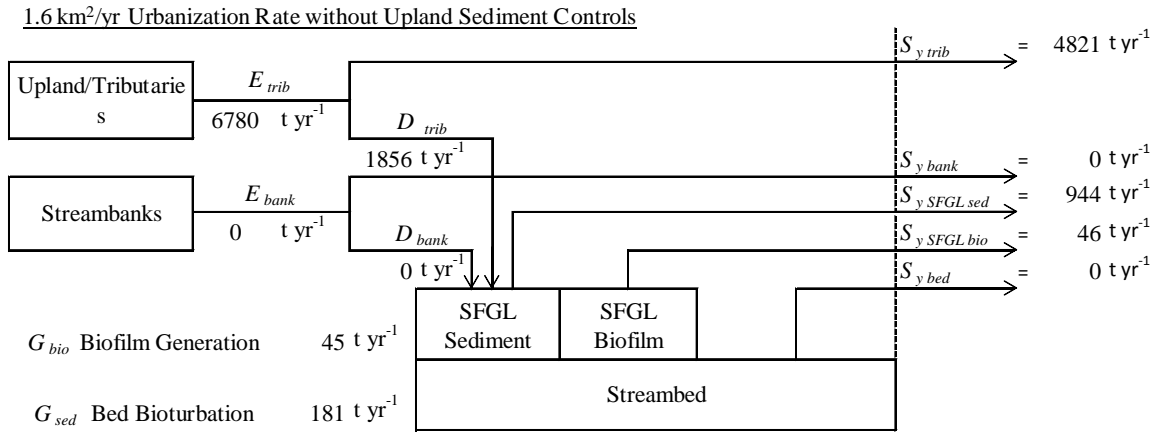


Figure 45: Figure of Sediment Budgets for the simulation periods.

8.3 Bed Supply for the Simulation Period

Figure 46 shows the supply of bed material for the simulation periods. Figure 46 shows the presence of the low flow SFGL flushing events which repeatedly degrade the bed through bioturbation, and the presence of annual High Flow Deposition Events which build the bed supply back up. Bed supply for the simulation periods increased with increasing urbanization rates and increased without the presence of upland erosion controls. At higher urbanization rates, low flow depositional events begin to cease as the transport capacity is almost constantly satisfied from the contribution from the Upland/Tributary source.

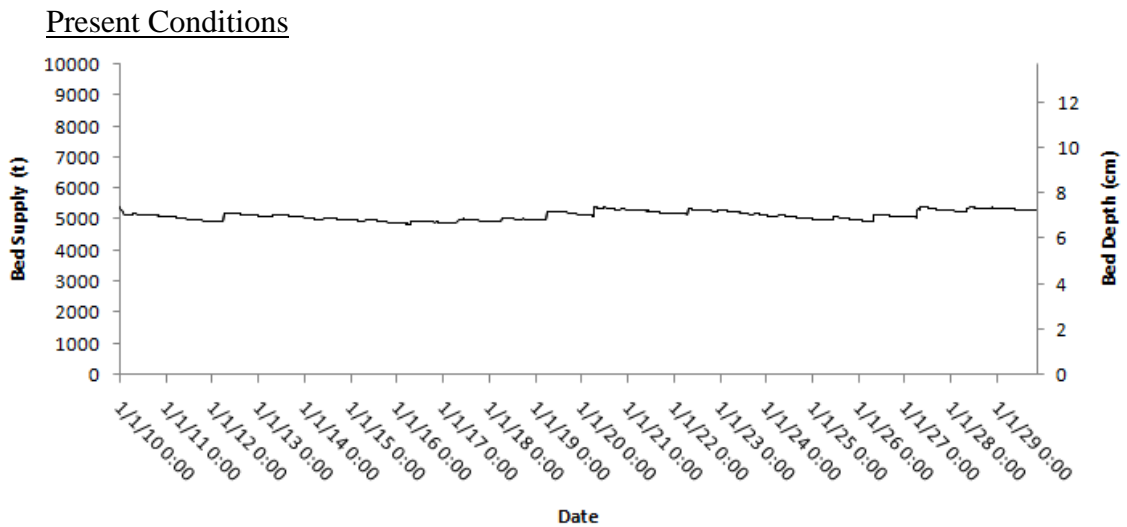
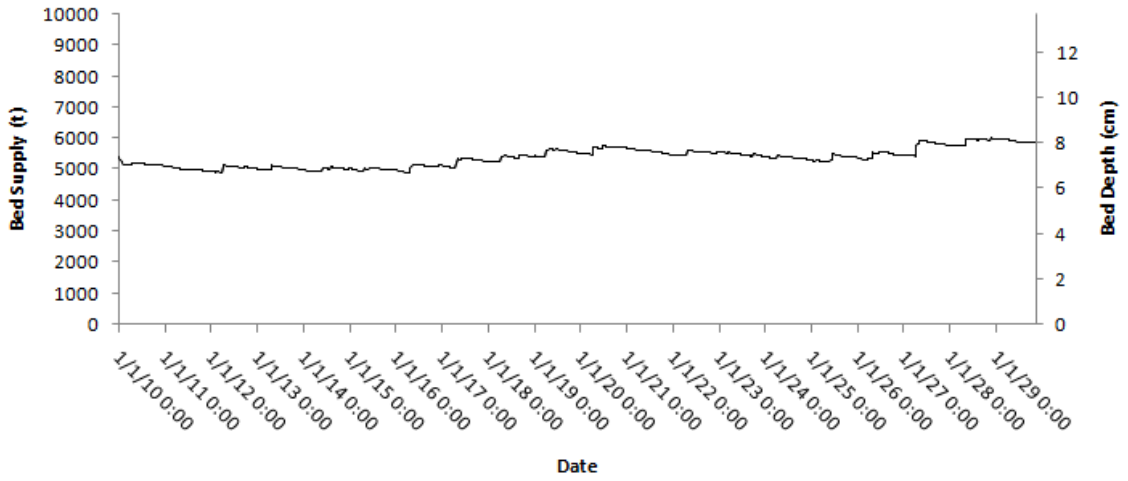
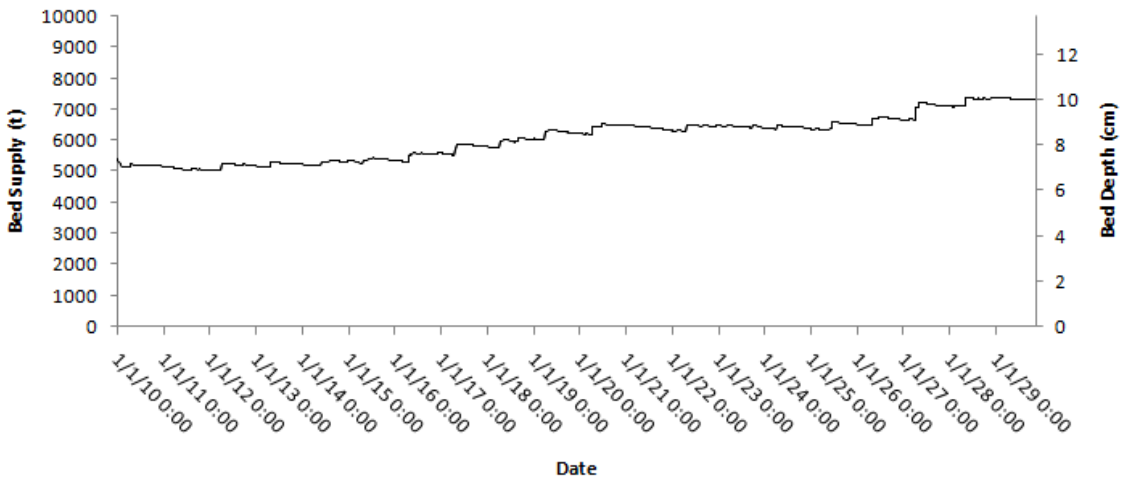


Figure 46 continued.

0.4 km²/yr Urbanization Rate with Upland Sediment Controls



0.4 km²/yr Urbanization Rate without Upland Sediment Controls



0.8 km²/yr Urbanization Rate with Upland Sediment Controls

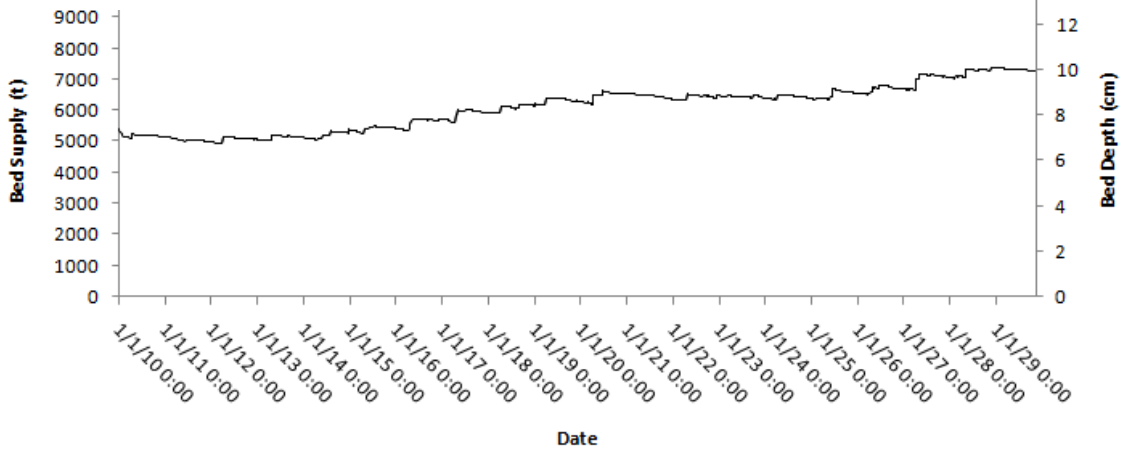


Figure 46 continued.

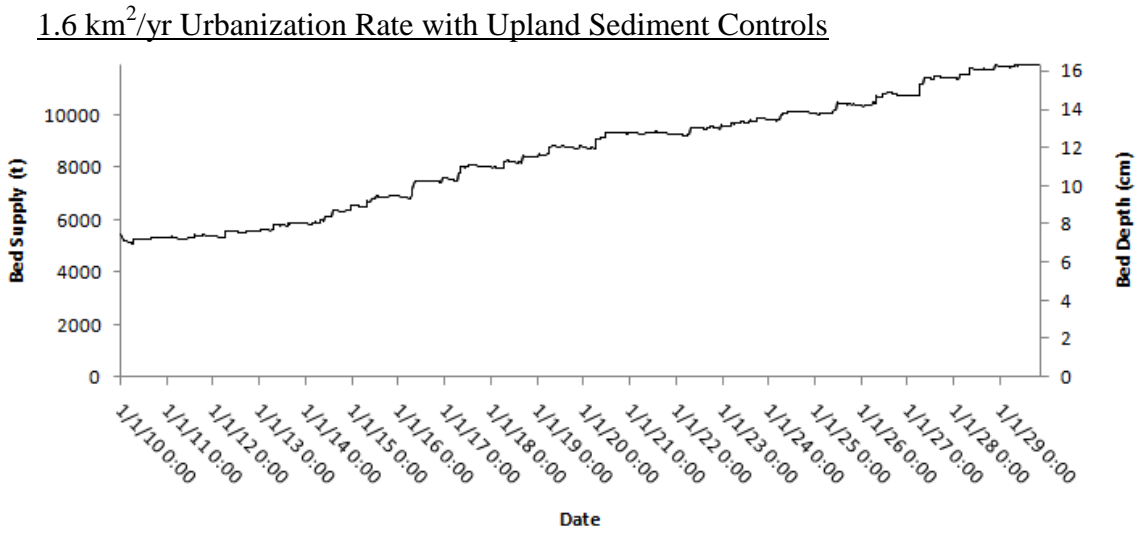
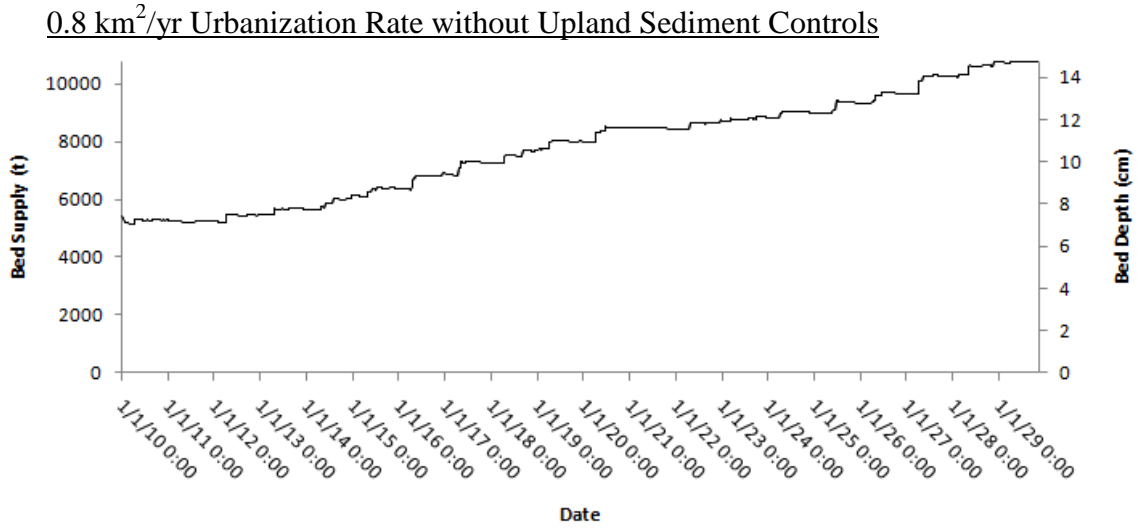


Figure 46 continued.

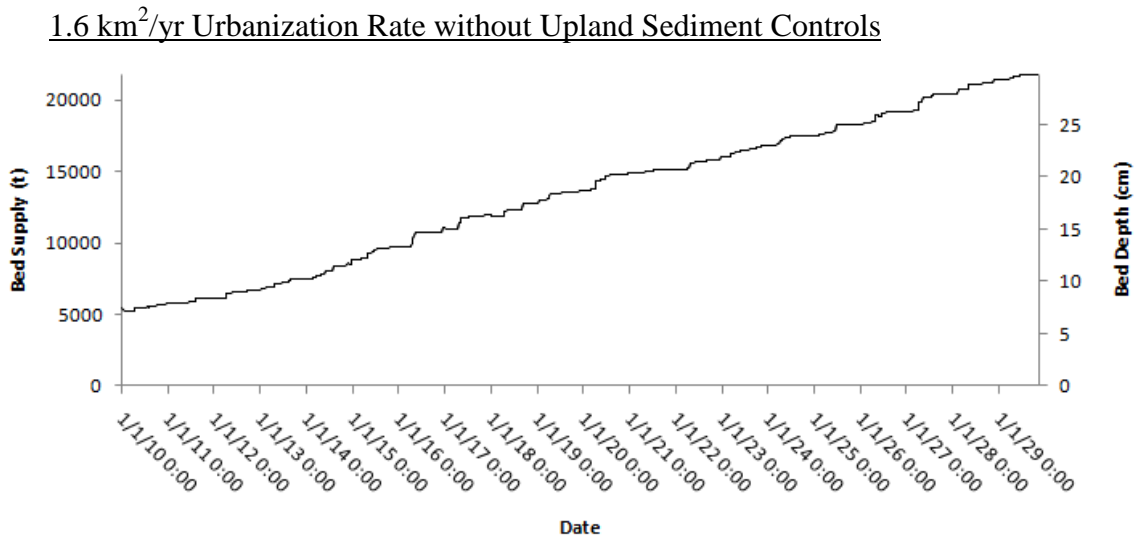


Figure 46: *Figure of bed supply for simulation runs.*

8.4 Discussion

The simulation run with no new urbanization area is representative of the study watershed under present conditions for the next 20 years assuming there is no new urban development. This simulation shows that the model is under predicting annual sediment yield for the simulation period compared with that of the calibration/validation period. Annual sediment yield for the calibration/validation period under equilibrium bed conditions is approximately 3,986 metric tons per year, and is approximately 1,862 metric tons for the 20 year simulation period with no additional urban area. This discrepancy is most likely due to the new HSPF model calibration used for the simulation runs. The new calibration cause an over simulation of low flowrates events and under simulated high flow rates. The transport capacity coefficients in the sediment model were decreased for low flow events and increased for high flow events to compensate. The reduction in the baseflow transport capacity most likely caused the reduced yield.

The shear stress coefficient was also reduced accordingly to match the observed sedigraphs, and the exponent used in the Upland/Tributary equation was reduced to create an equilibrium bed condition for the calibration period. This reduction in the shear stress coefficient and reduction of the transport capacity of high flow events most likely caused the elimination of direct bed and bank erosion as seen in Figure 45 and Table 28. However, another cause may be the limited calibration/validation data. The three year calibration/validation period has very low summer flow rates for the year 2008. No bank erosion occurred for this period, and bed erosion was minimal with the majority of sediments for this period coming from the SFGL. This period of minimal sediment erosion due to low flow rates helps explain why the calibration/validation results are different from that of the 20 year simulation run with no additional urban area. More calibration data may be needed to verify that sediment transport model is actually under-predicting sediment flux over a long period simulation and if the 2008 year is representative.

An interesting result of this study is that the bed grows as urbanization increases. This trend can be seen by observing the bed supply for the simulation runs with and without simulated control structures. The bed grows because sediment supply from the uplands/tributary source increases as streamflow increases. This process increases the total mass of suspended sediments in the stream channel. Transport capacity increases with streamflow as well, but if the sediment contribution from the upland/tributary source increases disproportionately higher than the transport capacity then deposition will begin to occur in the channel and erosion processes will cease. This process is the cause of the decrease in the erosion of SFGL sediments when comparing the simulation runs with and

without sediment control structures. This trend implies that a balance exists between erosion and deposition processes in the channel and erosion and transport processes in the uplands. These processes work in concert to create an equilibrium bed, and small changes to the uplands can have pronounced changes to the channel. When comparing the simulation runs with an urbanization rate of $0.4 \text{ km}^2/\text{yr}$ with and without sediment controls, the additional annual contribution of 115 metric tons per year from the upland/tributary source changed the bed from a quasi-equilibrium state to an aggrading bed state.

The key to bed degradation in this series of model simulations is SFGL erosion. The SFGL sediment generation component is the single most important bed erosion mechanism, and this mechanism is active when the SFGL is not at maximum supply. The SFGL generation component assumes that bioturbation of the bed steadily rebuilds the SFGL sediment supply by removing mass from the bed supply and placing the mass into the SFGL sediment supply. While excess shear stresses from storm peaks create a rapid spike of SFGL erosion, SFGL generation occurs as long as SFGL has not reached its maximum supply limit. During the simulation run with present conditions, 213 metric tons of sediment per year is removed from the bed supply and placed in the SFGL supply during SFGL generation. This mass increases to 268 metric tons per year during the simulation run with an urbanization rate of $0.4 \text{ km}^2/\text{yr}$ and sediment controls, and 285 metric tons for the simulation run with an urbanization rate of $0.8 \text{ km}^2/\text{yr}$ and sediment controls. For the simulation run with an urbanization rate of $1.6 \text{ km}^2/\text{yr}$ and sediment controls, SFGL generation increases to 318 metric tons. When comparing to the simulation runs with no sediment controls, the SFGL generation rates decrease slightly

from the increase in sediment contribution from the upland/tributary source which satisfies a larger fraction of the transport capacity and reduces SFGL erosion, and therefore reduces SFGL generation.

Deposition and erosion increase with increasing urban area. Sediment yield also increases with increasing urban area. The storm peaks increase rapidly and then fall rapidly during urban simulations. This causes a rapid increase in transport capacity, which increases erosion, but also a rapid decrease in transport capacity, which stops erosion and causes deposition.

The fraction of eroded material coming from the SFGL sediment and biological storage decrease at urban area increases. This decrease is because of the aggrading bed condition. The contribution of sediment from the Upland/Tributary source is greater than the increase in transport capacity caused from increasing urban area, so a larger fraction of the transport capacity is satisfied from the Upland/Tributary source and the fraction of material eroding from the SFGL storages decreases. Total generated biological material increased with increasing urban area. This is attributed to the increasing eroded mass of SFGL sediments with increasing urban area. More SFGL sediments are eroded, so more SFGL sediment are generated. It should be noted that only the fraction of eroded biological material reduces with increasing area, the total eroded mass of SFGL biofilm and yield at the outlet of SFGL biofilm material increases with increasing urban area.

Several general trends can be inferred from this analysis. The presence of low flow SFGL Flushing Events will continually degrade the bed through bioturbation. Annual or semi-annual High Flow Depositional Events will deposit to the bed and build back the bed supply. Increasing urban area will increase the flow rates to the channel

which will increase the contribution of sediments from the Upland/Tributary source. The Upland/Tributary source contribution will be of a greater magnitude than the increase in fluvial transport capacity caused by the increased flow rate, and these additional sediments will deposit and start to drown out the Low Flow SFGL Flushing Events. This analysis implies that controlling the mass of sediment that enters the stream corridor from the uplands is not satisfactory. Silt fences, hay bales, and other erosion control structures that simply filter out sediments but do not mitigate flows are not enough to reduce the yield of sediments at the watershed outlet. Peaking flow rates increase the transport capacity and fluvial shear in the stream corridor resulting in more SFGL flushing events, increase erosion from in-stream sources, and increase the bioturbation and biological activity within the corridor by exposing buried sediments. A balance exists not just between in-stream processes, but also upland erosion and transport processes.

Chapter 9: Conclusions

The health of stream ecosystems are very much dependent upon upland and in-stream sediment erosion, transport, and deposition processes. This presented research works towards the coupling of a computationally simple yet representative watershed scale erosion and sediment transport model which includes multiple in-stream sediment processes to be used for the study of upland and in-stream sediment erosion, transport, and deposition processes. It is expected that the coupling these models is so that in-stream processes, such as streambank erosion, can be more accurately modeled at the watershed scale. The objective of this thesis was to gain a better understanding of in-stream sediment transport processes at the watershed scale by using a modeling tool that can simulate multiple in-stream sediment processes under present watershed conditions and under varying urbanization rates.

Based on these results, several conclusions can be drawn including: 1) The importance of SFGL as mechanism for bed degradation, 2) The identification of Low Flow SFGL Flushing Events, 3) The identification of High Flow SFGL Flushing Events, 4) The annual cycle of bed storage, including the degradation of the bed through SFGL bioturbation throughout the year (from Low Flow SFGL Flushing Events), and the annual or semi-annual depositional event which rebuilds the bed supply (from High Flow Depositional Events), 5) The importance of SFGL as a mechanism for biofilm development, 6) The balance between erosion and deposition processes to create an equilibrium bed, 7) The impact of upland and tributary erosion on in stream processes.

The SFGL is the single most important factor contributing to bed erosion and biofilm development. Low Flow SFGL Flushing events continually degrade and erode

the SFGL, and, because of this constant deficit between the current SFGL supply and the maximum SFGL supply, bed material is constantly being removed from the bed storage and placed in the SFGL storage through bioturbation and the biofilm storage is continually growing. Because the bed is constantly degrading through the process of Low Flow SFGL flushing events, a quasi-equilibrium bed is created from the annual or semi-annual High Flow Depositional event which deposits mass quantities of sediments. Increasing urban area increases flow rates in the channel which increases the transport capacity in the channel and the contribution of sediment from the upland/tributary source. The current analysis shows that increasing urban area will only increase the frequency of High Flow Deposition events and decrease the effectiveness of Low Flow SFGL Flushing events. If urbanization continues at the current rate, channel flowrates can be expected to increase at least 75% and sediment flux at the outlet can be expected to increase over 150% in 20 years.

This analysis implies that controlling the mass of sediment that enters the stream corridor from the uplands is not satisfactory. Silt fences, hay bales, and other erosion control structures that simply filter out sediments but do not mitigate flows are not enough to reduce the yield of sediments at the watershed outlet. Peaking flow rates increase the transport capacity and fluvial shear in the stream corridor resulting in more SFGL flushing events, increase erosion from in-stream sources, and increase the bioturbation and biological activity within the corridor by exposing buried sediments. A balance exists not just between in-stream processes, but also upland erosion and transport processes, all of which must be considered when developing permeable land into impervious area and when developing sediment control structures.

Future improvements to this coupled modeling tool include the process based modeling of the upland/tributary sources, creating a seasonally variable infiltration parameter in the upland model, and creating a dynamic urbanization rate scenario for the model. Results from this thesis provide insight into the effect of urbanization on stream flows, the erosion, transport, and deposition of SFGL streambed and streambank material, the nature of biofilm development, and the long term trends of bed storage. Further long term research need to be done to verify the trends derived from this modeled data, but this Thesis has provided a useful modeling tool to be used for the understand of sediment transport processes at the watershed scale.

Appendix A

%Diff is the percent difference.

Δt is the time step (s).

a is the reference level (m).

$A^{(j)}_{(i)}$ is the area of the cross section (m^2).

$a_{(k)}$ is a coefficient for the erosion equation.

$B^{(j)}_{(i)}$ is the width of the channel (m).

$b_{(k)}$ is an exponent for the erosion equation (unitless).

C_1 is a factor to account for frozen ground effects (unitless).

C_a is a reference concentration and a is a reference level (mg/l).

C_{frozen} is a coefficient to account for frozen ground, if any.

C_{GWI} is groundwater outflow recession parameter (s^{-1}).

C_{GW2} is a user input parameter that can be used make groundwater outflow to storage relation nonlinear (m^{-1}).

C_{GWrec} is a daily recession constant of groundwater flow (unitless).

$C_{GWSlope}$ is a user input parameter index to groundwater slope (m).

C_{intfw} is an interflow inflow parameter supplied by the user (unitless).

C_{LZET} is the lower zone evapotranspiration parameter (unitless).

C_{tc} is a transport capacity calibration coefficient ($m^{1/2} \cdot s^2 / kg^{1/2}$).

$C_{\tau(1)}$ is the shear stress coefficient to account for the difference between the bed and bank shear (unitless).

$C_{\tau(2)}$ is the flow acceleration coefficient (unitless).

D is the arbitrary water depth chosen for this integration (m).

$D^{(j)}_{(i)}$ is the deposited mass of sediments (kg).

$D^{(j)}_{(i)}$ is the total deposition for the time step (kg).

$D^{(j)}_{(i)(bed)}$ is the deposition to the bed (kg).

$D^{(j)}_{sfgl(i)}$ is the deposition associated with the SFGL (kg/s.m²).

D_E is the empirical relationship between outflow depth and detention storage (m).

$D_{evap(i)}$ is the evapotranspiration for the time step (m).

D_{GW} is the baseflow for the permeable land segment (m).

D_{GW} is the outflow depth for ground water (m).

$D_{I(i)}$ is the interflow outflow for the time step i (m).

D_{INTFW} is the interflow for the permeable land segment (m).

D_{lzeval} is the maximum lower zone evapotranspiration (m).

D_{out} is the total outflow for the time step i .

D_R is the direct runoff from the land segment (m).

D_R is the depth of runoff (m).

$D_{sfglbio(i)}^{(j)}$ is the depositing material that comes from eroded biofilm (kg).

$D_{sfglsed}^{(j)}(i)$ is the sediment fraction of depositing material to the surface fine grained lamina (kg).

$E^{(j)}_{(i)(bank)}$ is the eroded mass from the bank for a time step (kg).

$E^{(j)}_{(i)(bed)}$ is the erosion from the bed (kg).

$E^{(j)}_{(i)(k)}$ represents the mass of eroded sediment (kg).

$E^{(j)}_{(i)(l)}$ is the summation of the eroded mass for every source with the source order (l) (kg).

$E^{(j)}_{(i)(l)}$ represents the eroded mass for the sediment source for the time step (kg).

$E'_{d(i)}^{(j)}$ is the lateral bank recession (m).

$E_d^{(j)}(i)$ is the bank retreat for the time step (m).

$E_d^{(j)}(i)$ is the depth of eroding bank material (m).

$E_{sfgsedl}^{(j)}(i)$ is the erosion of biofilm (kg).

$E_{sfgsel}^{(j)}(i)$ is the erosion of sediments from the SFGL (kg).

$E_v^{(j)}(i)$ is the evaporation from the reach during the time-step (m^3).

$f(IRC)_1$ and $f(IRC)_2$ are empirical functions.

$F^{(j)}(i)(k)$ is the fraction of eroded material from a particular sediment source .

$G_{sfgl(sed)}$ is the removal of fine sediments from the bed and into the SFGL from bioturbation (kg).

$G_{sfglsed}$ is the generation of sediment to the SFGL from bioturbation (kg).

$G_{sfglsed}$ is the generation of the biofilm over time from biological growth (kg).

$H^{(j)}(i)$ is the water depth (m).

$H^{(j)}(i)$ is the water depth for the time step (m).

$H^{(j)}(i)$ is the average of the flow depth (m)

$H^{(j)}(i+1/2)$ is the flow depth at the end of the interval (m).

$H^{(j)}(i-1/2)$ is the flow depth at the beginning of the interval (m).

$H_{bankfull}^{(j)}(i)$ is the bankfull depth (m).

I is the nominal infiltration rate supplied by the user (m/s).

I_{avg} is the average infiltration capacity over the land segment (m/s).

$I_{deep(i)}$ is the deep percolation for the time step (m).

$I_{in(i-1/2)}$ is the interflow inflow rate at the start of the timestep (m/s).

I_{lower} is the infiltration to the lower zone (m).

I_{max} is the maximum infiltration capacity for the land segment (m/s).

I_{min} is the minimum infiltration capacity for the land segment (m/s).

IRC is the interflow recession constant (unitless).

κ is the dimensionless von Karman constant equal to approximately 0.40.

$I_s(i)$ is the storage of the interflow at the start of the interval (m).

k_p is a deposition coefficient based on the concentration profile (unitless).

k_s is the flood wave coefficient (unitless).

k_s is the flood wave coefficient (unitless).

k_{ss} is the routing coefficient (unitless).

L is the length of the overland flow plane (m).

L_{reach} is the length of the stream reach (m).

$L_{reach(j)}$ is the length of the stream reach for the cell (m).

n is Manning's coefficient.

NS is the Nash-Sutcliffe coefficient.

O_{avg} is the average observed value for the time period,

O_j is the observed value for the time period.

$P^{(j)}_{(i)}$ is the precipitation into the stream-reach throughout the time step (m^3).

$P^{(j)}_{(i)}$ is the wetted perimeter of the cross section (m).

$P^{(j)}_{(i)(k)}$ is the fraction of material from a sediment source.

$P_{rate(i)}$ is the moisture supply rate to the surface (m/s).

$P_{s(i)}$ is the precipitation for the time step (m).

$Q^{(j)}_{ssin(i)}$ is the sediment flow rate into the stream reach during the time step (kg/s).

$Q^{(j)}_{ssout(i)}$ is the sediment flow rate out of the reach during the time step (kg/s).

$Q_{in}^{(j)}_{(i)}$ is the flow rate into the stream-reach from upstream and upland sources throughout the time step (m^3/s).

$Q_{out}^{(j)}_{(i+1/2)}$ is the flow rate out of the reach at the end of the time step (m^3/s).

$Q_{out}^{(j)}_{(i-1/2)}$ is the flow rate out of the reach at the beginning of the time step (m^3/s).

$R^{(j)}_{(i)}$ is the hydraulic radius of the fluid (m).

$R^{(j)}_{(i)}$ is the hydraulic radius of the fluid at the sediment source (m).

R^2 is the coefficient of determination.

$R_{infiltr}$ is the ratio of the maximum to the mean infiltration capacity for the land segment (m/m).

$R_{l_{fract}}$ is the fraction of lower zone inflow.

R_{LZSN} is the ratio of the lower zone storage to the lower zone nominal storage

R_{SUR} is a ratio used to determine the separation of surface runoff, interflow, and infiltration (unitless).

R_{UZSN} is the ratio of the upper zone storage to the upper zone nominal storage.

S is the slope of the overland flow plane (m/m).

$S^{(j)}$ is the energy slope which is assumed to be the slope of the channel bed (m/m).

$S^{(j)}_{(i)(k)}$ is the sediment supply of the erosion source (kg).

$S^{(j)}_{(i-1)(bed)}$ is the supply of bed sediments from the previous time step (kg).

$SA_{(k)}$ is the surface area of the sediment source (m²).

$SA_B^{(j)}_{(i)}$ is the surface area of the entire bankfull depth (m²).

$SA_E^{(j)}_{(i)}$ is the surface area of the eroded bank (m²).

S_{avg} is the average simulated value for the time period.

$S_{GW(i-1/2)}$ is the active groundwater storage at the start of the time step (m).

S_i is the simulated value for the time period.

$S_{LZS(i)}$ is the lower zone storage (m).

S_{LZSN} is the nominal lower zone storage supplies by the user (m).

S_{LZSN} is the parameter to account for the upper zone nominal storage (m).

$SS^{(j)}_{(i+1/2)}$ is the mass of sediment in suspension at the end of the time step (kg).

$SS^{(j)}_{(i-1/2)}$ is the mass of sediment being transported by the reach at the start of the time step (kg).

$SS^{(j)}_{(i-1/2)}$ is the mass of sediment in suspension at the start of the time step (kg).

$S_{sfglbio(i-1)}^{(j)}$ is the supply of biofilm in the SFGL from the previous time step (kg).

$S_{sfglbio(max)}^{(j)}$ is the maximum supply of biological material in the SFGL (kg).

$S_{sfglsed}^{(j)}_{(i-1)}$ is the supply of sediment in the SFGL from the previous time step (kg).

$S_{sfglsed(max)}^{(j)}$ is the maximum supply of the surface fine grained lamina (kg).

$S_{SUR(i)}$ is the storage of water on the land segment (m).

$S_{SURN(i)}$ is the equilibrium storage of water on the land segment for the current moisture supply rate.

$S_{UZS(i)}$ is the upper zone storage (m)

S_{UZSN} is the nominal lower zone storage supplies by the user (m).

$T_c^{(j)}(i)$ is the average transport capacity across the reach during the time step (kg).

$T_c^{(j)}(i)$ is the transport capacity of the reach (kg).

$T_{cr}^{(j)}(i)(l-1)$ is the residual transport capacity satisfied from the previous sediment source (kg).

$T_{cr}^{(j)}(i)(l)$ is the residual transport capacity for the sediment source (kg).

$T_{cr}^{(j)}(i)(l)$ is the residual transport capacity for the source order (kg).

$U^{(j)}(i+1/2)$ is the velocity at the end of the time step (m/s).

$U^{(j)}(i-1/2)$ is the velocity of the streamflow at the beginning of the time step (m/s).

U^* is the shear velocity in (m/s).

$V^{(j)}(i+1/2)$ is the volume of water in the stream-reach at the end of the time step (m³).

$V^{(j)}(i-1/2)$ is the volume of water in the stream-reach at the beginning of the time step (m³).

$W^{(j)}_{reach(j)}$ is the width of the channel for the current time step (m).

$W^{(j)}_{reach(j-1)}$ is the width of the channel for the previous time step (m).

w_s is sediment fall velocity in (m/s).

y is the depth increment (m).

z^* is the Rouse number.

ΔS_i is the change in the soil moisture storage for the time step (m).

Δt is the time step (s).

θ is the bank angle (m).

ρ is the density of the fluid (g/m³)

ρ_B is the density of the bank material (kg/m^3).

τ_{cr} is the critical shear stress for the erosion source (N/m^2).

τ_f is the shear stress of the fluid at the centroid of the erosion source (N/m^2).

$\tau_f^{(j)}(i)$ is the shear stress of the fluid at the location of the sediment source (N/m^2).

ω_s is the settling velocity of the <63 micron fraction (m/s).

References

- Abed, N.A., and Whiteley, H.R. (2002). *Calibration of the hydrological simulation program FORTRAN (HSPF) model using automatic calibration and geographical information systems*. Hydrological Processes, Vol. 16, pp. 3169-3188.
- Ackerman, D., Schiff, K.C., and Weisberg, S.B. (2005). *Evaluating HSPF in an arid, urbanized watershed*. Journal of the American Water Resources Association, April 2005, pp. 477-486.
- Adams, E., and Elliott, S. (2006). *Physically based modelling of sediment generation and transport under a large rainfall simulator*. Hydrological Processes, Vol. 20, pp. 2253-2270.
- Adesodun, et. al. (2006). *Structural stability and carbohydrate contents of an ultisol under different management systems*. Soil and Tillage Research 60(3).
- Ahmadi, S., Amin, S., Keshavarzi, A.R., and Mirzamostafa, N. (2006). *Simulating Watershed outlet sediment concentration using the ANSWERS model by applying two sediment transport capacity equations*. Biosystems Engineering, Vol. 94, pp. 615-626.
- Aksoy, H., and Kavvas, M.L. (2005). *A review of hillslope and watershed scale erosion and sediment transport models*. Catena, Vol. 64, pp. 247-271.
- Allen, P.M., Arnold, J.G., and Skipwith, W. (2008). *Prediction of channel degradation rates in urbanizing watersheds*. Hydrological Sciences, Vol. 35, pp. 1013-1029.
- Bergman, M.J., Green, W., and Donnangelo, L.J. (2002). *Calibration of storm loads in the South Prong watershed, Florida, using BASINS/HSPF*. Journal of American Water Resources Association. Vol. 38, pp. 1423-1436.
- Bicknell, B.R., Imhoff Jr., J.C., Jobs, T., and Donigian Jr., A.S. (2001). *Hydrological Simulation Program—FORTRAN (HSPF. Version 12 User's Manual*, Athens GA.: U.S. Environmental Protection Agency.
- Bockelmann, B.N., Fenrich, E.K., Lin, B., and Falconer, R.A. (2004). *Development of an ecohydraulics model for stream and river restoration*. Ecological Engineering, Vol. 22, pp. 227-235.
- Borah, D.K., and Bera, M. (2003). *Watershed-scale hydrologic and nonpoint-source pollution models: review of mathematical bases*. American Society of Agricultural Engineers, Vol. 46, pp. 1553-1566.

- Brun, S.E., and Band, L.E. (2000). *Simulating runoff behavior in an urbanizing watershed*. Computers, Environment, and Urban Systems, Vol. 24, pp. 5-22.
- Cancienne, R.M., Fox, G.A., and Simon, A. (2008) *Influence of seepage undercutting on the stability of root-reinforced streambanks*. Earth Surface Processes and Landforms, Vol. 33, pp. 1769-1786.
- Chang, H. H. (1988). *Fluvial Processes in River Engineering*. Krieger Publishing Company: Malabar, Florida.
- Chapra, Steven. (1997). *Water Resources and Environmental Engineering*. United States of America: McGraw Hill.
- Cho, J. Barone, V.A. and Mostaghimi, S. (2009). *Simulation of land use impacts on groundwater levels and streamflow in a Virginia watershed*. Agricultural Water Management, 96:1-11.
- Chow, Ven Te. Applied Hydrology. (New York: McGraw-Hill, 1988), 132-135.
- Coulter, C.B., Kolka, R.K., and Thompson, J.A. (2004). *Water Quality in agricultural, urban, and mixed land use watersheds*. Journal of the American Water Resources Association, December 2004, pp. 1593-1601.
- Collins, A.L., Walling, D.E., and Leeks, G.J.L. (1998). *Use of composite fingerprints to determine the provenance of the contemporary suspended sediment load transported by rivers*. Earth Surface Processes and Landforms, 23, 31-52.
- Davis, C. M. (2008). "Sediment fingerprinting using organic matter tracers to study streambank erosion and streambed sediment storage processes in the South Elkhorn Watershed." M.S. Dissertation, University of Kentucky, Lexington, Kentucky.
- Decho (1990). *Microbial exopolymer secretions in ocean environments: their role(s) in food webs and marine processes*. Oceanography Marine Biology Annual Review 28:73-153
- Diaz-Ramirez, J.N., L.R. Perez-Alegria, and W.H. McAnally. (2008). *Hydrology and sediment modeling using BASINS/HSPF in a tropical island watershed*. American Society of Agricultural and Biological Engineers, Vol. 51(5): 1555-1565.
- Dietrich, C.R., Green, T.R., and Jakeman, A.J. (1999). *An analytical model for stream sediment transport: application to Murray Murrumbidgee and river reaches, Australia*. Hydrological Processes, Vol. 13, pp. 763-776.

- Donigian, A.S. Jr. (2002). *Watershed Model Calibration and Validation: The HSPF Experience*. In Proc. WEF National TMDL Science and Policy. Phoenix, Arizona: Water Environment Federation.
- Dou, G.R. (1974). *Similarity theory and its application to the design of total sediment transport model*. Research Bulletin of Nanjing Hydraulic Research Institute, Nanjing, China.
- Stone, M., and Droppo, I.G. (1994). *In-Channel Surficial Fine Grained Sediment Lamina. PartII: Chemical Characteristics and Implications for Contaminant Transport in Fluvial Systems*. Hydrological Processes, Vol 8, 113-124.
- Droppo, I.G., Leppard, G.G., Flannigan, D. T., Liss, S.N. (1997) *The freshwater floc: a functional relationship of water and organic and inorganic floc constituents affecting suspended sediment properties*. Water, Air, and Soil Pollution. 99: 43-54.
- Droppo, I.G., and Amos, C.L. (2001). *Structure, stability, and transformation of contaminated lacustrine surface fine-grained laminae*. Journal of Sedimentary Research, Vol. 71, No. 5, pp 717-726.
- Duan, J.G., and Nanda, S.K. (2006). *Two-dimensional depth-averaged model simulation of suspended sediment concentration distribution in a groyne field*. Journal of Hydrology, Vol. 327, pp. 426-437.
- Einstein, H. A. (1950). *The Bed Load Function for Sediment Transportation in Open Channels*. Technical Bulletin 1026, US Department of Agricultural.
- Federal Interagency Stream Restoration Working Group (FISRWG). 1998. *Stream Corridor Restoration: Principles, Processes, and Practices*. Federal Interagency Stream Restoration Working Group (FISRWG). GPO Item No. 0120-A; SuDocs No. A 57.6/2:EN 3/PT.653. ISBN-0-934213-59-3
- Fox, J.F., and Papanicolau, A.N., (2008). *An un-mixing model to study watershed erosion processes*. Advances in Water Resources, 31, pp 96-108.
- Fox, J.F., and Papanicolau, A.N., (2008). *Application of the spatial distribution of nitrogen stable isotopes for sediment tracing at the watershed scale*. Journal of Hydrology 385, pp 46-55.

- Fraley, L.M., Miller, A.J., and Welty, C. (2009). *Contribution of in-channel processes to sediment yield of an urbanizing watershed*. Journal of the American Water Resources Association, Vol. 45, pp. 748-766.
- Garny, K., Horn, H., and Neu, T.R. (2008). *Interaction between biofilm development, structure and detachment in rotating annular reactors*. Bioprocess Biosystems Engineering, Vol. 31, pp. 619-629.
- Garny, K., Neu, T.R., and Horn, H. (2009). *Sloughing and limited substrate conditions trigger filamentous growth in heterotrophic biofilms—measurements in flow-through tube reactor*. Chemical Engineering Science, Vol. 64, pp. 2723-2732.
- Green, T.R., Beavis, S.G., Dietrich, C.R., and Jakeman, A.J. (1999). *Relating stream-bank erosion to in-stream transport of suspended sediment*. Hydrological Processes, Vol. 13, pp. 777-787.
- Guy, B.T., Dickenson, W.T., Sohrabi, T.M., and Rudra, R.P. (2009) *Development of an empirical model for calculating sediment-transport capacity in shallow overland flows: model calibration*. Biosystems Engineering, Vol. 103, pp. 245-255.
- Hanson, G. J., and Simon, A., (2001). *Erodibility of Cohesive sediments in the loess area of the Midwestern USA*. Hydrological Processes 15, pp, 23-38.
- Hardy, R.J., Bates, P.D., and Anderson, M.G. (2000). *Modelling suspended sediment deposition on a fluvial floodplain using a two-dimensional dynamic Finite Element model*. Journal of Hydrology, Vol. 229, pp. 202-218.
- Hessel, R., and Jetten, V. (2007). *Suitability of transport equations in modeling soil erosion for a small Loess Plateau catchment*. Engineering Geology, Vol. 91, pp. 56-71.
- Hunter, H.M, and Walton, R.S. (2008). *Land-use effects on fluxes of suspended sediment, nitrogen and phosphorus from a river catchment of the Great Barrier Reef, Australia*. Journal of Hydrology, Vol. 356, pp. 131-146.
- Jakeman, A.J., Green, T.R., Beavis, S.G., Zhang, L., Dietrich, C.R., and Crapper, P.F. (1999). *Modelling upland and instream erosion, sediment and phosphorus transport in a large catchment*. Hydrological Processes, Vol. 13, pp. 745-752.
- Jarritt, N.P., and Lawrence, D.S.L. (2006). *Simulating fine sediment delivery in lowland catchments: model development and application of INCA-sed*. Soil Erosion and Sediment Redistribution in River Catchments, 2006, pp. 207-214.
- Jarritt, N.P., and Lawrence, D.S.L. (2007). *Fine sediment delivery and transfer in lowland catchments: modeling suspended sediment concentrations in response to hydrological forcing*. Hydrological Processes, Vol. 21, pp. 2729-2744.

- Jeon, J., Yoon, C.G., Donigian Jr., A.S., and Jung, K. (2007) *Development of the HSPF-Paddy model to estimate watershed pollutant loads in paddy farming regions*. Agricultural Water Management, Vol. 90, pp. 75-86.
- Johnson, M.S., Coon, W.F., Mehta, V.K., Steenhuis, T.S., Brooks, E.S., and Boll, J. (2003). *Application of two hydrologic models with different runoff mechanisms to a hillslope dominated watershed in the northeastern US: a comparison of HSPF and SMR*. Journal of Hydrology, Vol. 284, pp. 57-76.
- Julian, J.P., and Torres, R. (2006). *Hydraulic erosion of cohesive riverbanks*. Geomorphology, Vol. 76, pp. 193-206.
- Kalin, L., Govindaraju, R.S., and Hantush, M.M. (2003). *Effect of geomorphologic resolution on modeling of runoff hydrograph and sedimentograph over small watersheds*. Journal of Hydrology, Vol. 276, pp. 89-111.
- Kentucky Division of Water (KYDOW). (2006). *2006 Integrated Report to Congress on Water Quality in Kentucky: Volume II*. Accessed November 17, 2007. <<http://www.water.ky.gov/sw/swmonitor/305b/>>.
- Kies, L. et. al. (1996) *On the role of algae and their exopolymers in the formation of suspended particulate matter in the Elbe estuary*. Archives Hydrobiologica Special Issues on Advanced Limnology. 47: 93-103
Kemper and Rosenau, 1986
- Kinsey-Henderson, A.E., Post, D.A., and Prosser, I.P. (2005). *Modelling sources of sediment at sub-catchment scale: an example from Burdekin catchment, North Queensland, Australia*. Mathematics and Computers in Simulation, Vol. 69, pp. 90-102.
- Kuhnle, R.A., Bingner, R.L., Foster, G.R., and Grissinger, E.H. (1996). *Effect of land use changes on sediment transport in Goodwin Creek*. Water Resources Research, Vol. 32, pp. 3189-3196.
- Langendoen, E. J., Simon, A.; Thomas, R. E. (2001). Proceedings of the 2001 Wetlands Engineering and River Restoration Conference, p 1233-1243,
- Langendoen, E.J., and Simon, A., (2008). Modeling the Evolution of Incised Streams. II: Streambank Erosion. Journal of Hydraulic Engineering. 134 (7), pp, 905-915.
- Lau, Y.L., and Liu, D. (1993). *Effect of flow rate on biofilm accumulation in open channels*. Water Resources, Vol. 27, pp. 355-360.

- Lartiges, et. al. (2001). *Composition, Structure, and Size Distribution of Suspended Particulates from the Rhine River*. *Water Research* 35(3): 808-816.
- Lehmann, A., Castella, E., and Lachavanne, J.B. (1997). *Morphological traits and spatial heterogeneity of aquatic plants along sediment and depth gradients, Lake Geneva, Switzerland*. *Aquatic Botany*, Vol. 55, pp. 281-299.
- Letcher, R.A., Jakeman, A.J., Calfas, M., Linforth, S., Baginska, B., and Lawrence, I. (2002). *A comparison of catchment water quality models and direct estimation techniques*. *Environmental Modeling & Software*, Vol. 17, pp. 77-85.
- Lian, Y., Chan, I., Singh, J., Demissie, M., Knapp, V., and Xie, H. (2007). *Coupling of hydrologic and hydraulic models for the Illinois River basin*. *Journal of Hydrology*, Vol. 334, pp. 210-222.
- Liu, W.C., Hsu, M.H, and Kuo, A.Y, (2002), *Modelling of hydrodynamics and cohesive sediment transport in Tanshui River estuarine system, Taiwan*. *Marine Pollution Bulletin* (44).
- Liu, D., Lau, L., Chau, Y.K., and Pacepavicius, G.J. (1993). *Characterization of biofilm development on artificial substratum natural water*. *Water Resources*, Vol. 27, pp. 361-367.
- Long, J.L.A., House, W.A., Parker, A., and Rae, J.E. (1998). *Micro-organic compounds associated with sediments in the Humber rivers*. *The Science of the Total Environment*, Vol. 210-211, pp. 229-253.
- Luo, B., Li, J.B., Huang, G.H. and Li, H.L. (2006). *A simulation-based interval two-stage stochastic model for agricultural nonpoint source pollution control through land retirement*. *Science of the Total Environment*, 361:38-56.
- Lui, W., Hsu, M., and Kuo, A.Y. (2002). *Modelling of hydrodynamics and cohesive sediment transport in Tanshui River estuarine system, Taiwan*. *Marine Pollution Bulletin*, Vol. 44, pp. 1076-1088.
- Madej, M.A., Sutherland, S.G., Lisle, T.E., and Pryor, B. (2009). *Channel responses to varying sediment input: a flume experiment modeled after Redwood Creek, California*. *Geomorphology*, Vol. 103, pp. 507-519.
- Merritt, W.S., Letcher, R.A., and Jakeman, A.J. (2003). *A review of erosion and sediment transport models*. *Environmental Modeling & Software*, Vol. 18, pp. 761-799.
- Millar, R.G., and Quick, M.C. (1997). *Development and testing of riverbank-stability analysis*. *Journal of Hydraulic Engineering*, November 2007, pp. 1051-1053.

- Millar, R.G., and Quick, M.C. (1998). *Stable width and depth of gravel-bed rivers with cohesive banks*. Journal of Hydraulic Engineering, 124(10) , pp. 1005-1013.
- Mishra, A., Kar, S., and Singh, V.P. (2007). *Determination of runoff and sediment yield from a small watershed in sub-humid subtropics using the HSPF model*. Hydrological Processes, Vol. 21, pp. 3035-3045.
- Mohamoud, Y.M. (2007). *Enhancing hydrological simulation program- FORTRAN model channel hydraulic representation*. American Water Resources Association, Vol. 43, pp. 1280-1292.
- Morris, G. L. and Fan, J. (1997). *Reservoir Sedimentation Handbook*. McGraw-Hill.
- Mosselman, E. (1998). *Morphological modeling of rivers with erodible banks*. Hydrological Processes, Vol. 12, pp. 1357-1370.
- Motha, J.A., Wallbrink, P.J., Hairsin, P.B., and Grayson, R.B. (2004). *Unsealed roads and suspended sediment sources in an agricultural catchment in south-eastern Australia*. Journal of Hydrology, Vol. 286, pp. 1-18.
- Nakato, T. (1984). *Numerical Integration of Einstein's Integrals*. Journal of Hydraulic Engineering. ASCE 110(12). Pp 1863-1868. December 1984.
- Nelson, D.W., Sommers, L.E. (1982). *Total carbon, organic carbon and organic matter*. Methods of Soil Analysis, A.L. Page, R.H Miller, and D.R. Keeney, eds., American Society of Agronomy, Wisconsin, USA, 539-579.
- Nelson, E.J., and Booth, D.B. (2002). *Sediment sources in an urbanizing, mixed land-use watershed*. Journal of Hydrology, Vol. 264, pp. 51-68.
- Owens, P.N., Walling, D.E., Carton, J., Meharg, A.A., Wright, J., and Leeks, G.J.L. (2001). *Downstream changes in the transport and storage of sediment-associated contaminants (P, Cr and PCBs) in agricultural and industrialized drainage basins*. The Science of the Total Environment, Vol. 266, pp. 177-186.
- Panday, S., and Huyakorn, P.S. (2004). *A fully coupled physically-based spatially-distributed model for evaluating surface/subsurface flow*. Advances in Water resources, Vol. 24, pp. 361-382.
- Papanicolaou, A.N., and Hildale, R. (2002). *Turbulence characteristics in gradual channel transition*. ASCE J. Engineering Mechanics, 128(9), 948-960.
- Papanicolaou, A.N., Elhakeem, M., Krallis, G., Prakash, S., and Edinger, J. (2008). *Sediment transport modeling review—current and future developments*. Journal of Hydraulic Engineering, January 2008, pp. 1-14.

- Richardson, J., I.G. Jowett. (2002). *Effects of sediment on fish communities in East Cape streams, North Island, New England*. New Zealand Journal of Marine and Freshwater Research. Vol 36. 431-442.
- Rouse, H. (1937). *Modern Conceptions of the Mechanics of Fluid Turbulence*. Trans. ASCE 102, pp. 463-505.
- Sanford, L.P., and Maa, J.P.Y. (2001). *A unified erosion formulation for fine sediments*. Marine Geology, Vol. 179, pp. 9-23.
- Shields Jr., F.D., Simon, A., and Dabney, S.M. (2009). *Streambank dewatering for increased stability*. Hydrological Processes, Vol. 23, pp. 1537-1547.
- Simon, A. (2008). *Fine sediment loadings to Lake Tahoe*. Journal of the American Water Resources Association, Vol. 44, pp. 618-639.
- Simon, A., and Collison, J.C. (2002). *Quantifying the mechanical and hydrologic effects of riparian vegetation on streambank stability*. Earth Surface Processes and Landforms, Vol. 27, pp. 527-546.
- Simon, A., and Thomas, R.E. (2002). *Processes and forms of an unstable alluvial system with resistant, cohesive streambeds*. Earth Surface Processes and Landforms, Vol. 27, pp. 699-718.
- Simon, A., Curini, A., Darby, S., and Langendoen, E.J. (2000). *Bank and near-bank processes in an incised channel*. Geomorphology, Vol. 35, pp. 193-217.
- Simon, A., Pollen-Bankhead, N., Mahacek, V., and Langendoen, E. (2009). *Quantifying reductions of mass-failure frequency and sediment loadings from streambanks using toe protection and other means: Lake Tahoe, United States*. Journal of American Water Resources Association, Vol. 45, pp. 170-186.
- Singh, J., Knapp, H.V., Arnold, J.G., and Demissie, M. (2005). *Hydrological modeling of the Iroquois River watershed using HSPF and SWAT*. American Water Resources Association, April 2005, pp. 343-360.
- Smith, B.P.G, Naden, P.S., Leeks, G.J.L., and Wass, P.D. (2003). *The influence of storm events on fine sediment transport, erosion and deposition within a reach of the River Swale, Yorkshire, UK*. The Science of the Total Environment, Vol. 314 – 316, pp 451–474.
- Smith, H.G., and Dragovich, D. (2008). *Sediment budget analysis of slope-channel coupling and in-channel sediment storage in an upland catchment, southeastern Australia*. Geomorphology, Vol. 101, pp. 643-654.

- Spiro and Stigliani, 2003. *Chemistry and the Environment*. Prentice Hall: New Jersey.
- Sponza, D.T. (2002). *Extracellular polymer substances and physiochemical properties of flocs in steady and unsteady-state activated sludge systems*. *Process Biochemistry* 37:983-998.
- Staley, N., Bright, T., Zeckoski, R.W., Benham, B.L., and Brannan, K.M. (2006). *Comparison of HSPF outputs using ftables generated with field survey and digital data*. American Water Resources Association, October 2006, pp. 1153-1162.
- Stehr et. al. (1995). *Exopolymers: An ecological characteristic of a floc-attached, ammonia-oxidizing bacterium*. *Microbial Ecology* 30(2)
- Stone, M., and Droppo, I.G. (2004). *In-channel surficial fine-grained sediment laminae (Part II): chemical characteristics and implications for contaminate transport in fluvial systems*. *Hydrological Processes*, Vol. 8, pp. 113-124.
- Thoms, M. C. 1987. *Channel sedimentation within the urbanized River Tame, UK*. *Regulated Rivers: Research and Management* 1:229–246.
- Thornton, D.C. (2002). *Diatom aggregation in the sea: mechanisms and ecological implications*. *European Journal of Phycology* 37:149-161.
- Trimble, S.W. (1997). *Contribution of stream channel erosion to sediment yield from an urbanizing watershed*. *Science*, Vol. 278, pp. 1442-1444.
- Turkington, A.V., Phillips, J.D., and Campbell, S.W. (2005). *Weathering the landscape evolution*. *Geomorphology*, Vol. 67, pp. 1-6.
- Tzoraki, O., and Nikolaidis, N.P. (2007). *A generalized framework for modeling the hydrologic and biogeochemical response of a Mediterranean temporary river basin*. *Journal of Hydrology*, Vol. 346, pp. 112-121.
- U.S. Environmental Protection Agency (1999). *Protocol for Developing Sediment TMDLs*. EPA 841-B-99-004. Office of Water (4503F), United States Environmental Protection Agency, Washington D.C. 132 pp.
- U.S. Environmental Protection Agency, Office of Water (2000). *BASINS Technical Note 6, Estimating Hydrology and Hydrologic Parameters for HSPF*. EPA-823-R00-012.
- U.S. Environmental Protection Agency, Office of Science and Technology. (2004). *The incidence and severity of sediment contamination in surface waters of the United States*, EPA 823-R-04-007.
- Van Oost, K., Quine, T. A., Govers G., De Gryze, S., Six, J., Harden, J. W.,

- Ritchie, J. C., McCarty, G. W., Heckrath, G., Kosmas, C., Giraldez, J. V., Marques da Silva, J. R., Merckx, R., (2007). *The Impact of Agricultural Soil Erosion on the Global Carbon Cycle*. Science (318), October 2007, pp 626-629.
- Viney, N.R., and Sivapalan, M. (1999). *A conceptual model of sediment transport: application to the Avon River basin in Western Australia*. Hydrological Processes, Vol. 13, pp. 727-743.
- Walling, D.E., and Amos, C.M. (1999). *Source, storage, and mobilisation of fine sediment in a chalk stream system*. Hydrol. Process., 13, 323-340.
- Walling, D.E. (2005). *Tracing suspended sediment sources in catchments and river systems*. Sci. of the Tot. Environ., 344, 159-184.
- Walling, D.E., Collins, A.L., Jones, P.A., Leeks, G.J.L., and Old, G. (2006). *Establishing fine-grained sediment budgets for the Pang and Lambourn LOCAR catchments, UK*. Journal of Hydrology, Vol. 130, pp. 126-141.
- Watts, C.D., Naden, P.S., Cooper, D.M., and Gannon, B. (2003). *Application of a regional procedure to assess the risk to fish from high sediment concentrations*. The Science of the Total Environment, Vol. 314 –316, pp. 551–565.
- Wilkinson, S.N., Prosser, I.P., Rustomji, P., and Read, A.M. (2009). *Modeling and testing spatially distributed sediment budgets to relate erosion processes to sediment yields*. Environmental Modeling & Software, Vol. 24, pp. 489-501.
- Wolman, M.G., 1967. *A Cycle of Sedimentation and Erosion in Urban River Channels*. Geografiska Annaler 49A:385-395.
- Worner, et. al. (2002). *Aggregate Associated Bacteria and Heterotrophic Flagellates in the River Elbe – Their Relative Significance along the Longitudinal Profile from 46 km to 583 km*. International Review of Hydrobiology. 87:255-266.
- Wood, P.J., and Armitage P.D., (1997). *Biological Effects of Fine Sediments on the Lotic Environment*. Environmental Management Vol. 21, No. 2, pp. 203–217
- Wu, Y., Falconer, R.A., and Uncles, R.J. (1998). *Modelling of water flows and cohesive sediment fluxes in the Humber Estuary, UK*. Marine Pollution Bulletin, Vol. 37, pp. 182-189.
- Wynn, T.M., Henderson, M.B., and Vaughan, D.H. (2008). *Changes in streambank erodibility and critical shear stress due to subaerial processes along a headwater stream southwestern Virginia, USA*. Geomorphology, Vol. 97, pp 260–273.

- Xu, Z., Godrej, A.N., and Grizzard, T.J. (2007). *The hydrological calibration and validation of a complexly-linked watershed—reservoir model for the Occoquan watershed, Virginia*. Journal of Hydrology, Vol. 345, pp. 167-183.
- Yan, L.J., Yu, X.X., Lei, T.W., and Qu, L.Q. (2008). *Effects of transport capacity and erodibility on rill erosion processes: a model study using the Finite Element method*. Geoderma, Vol. 146, pp. 114-120.
- Zhang, F., Yeh, G.T., Parker, J.C., Brooks, S.C., Pace, M.N., Kim, Y.J., Jardine, P.M., and Watson D.B., (2007), *A reaction-based paradigm to model reactive chemical transport in groundwater with general kinetic and equilibrium reactions*. Journal of Contaminant Hydrology (92), pp 10-32.
- Zhang, F., Yeh, G.T., Parker, J.C., and Jardine, P.M., (2008), *A reaction based river/stream water quality model: Model development and numerical schemes*. Journal of Hydrology(348), pp 496-509.
- Zappou, C. (2001). *Review of urban storm water models*. Environmental Modeling & Software, Vol. 16, pp. 195-231.
- Zimmerman-Timm, Heike. (2002). *Characteristics, Dynamics and Importance of Aggregates in Rivers – An invited review*. International Review of Hydrobiology. 87(2-3): 197-240.

Vita

Joseph Paul Russo

Place of Birth: Louisville Kentucky

Date of Birth: May 29, 1984.

Education

Bachelor of Science Civil Engineering	University of Kentucky Lexington, KY	August 2007 GPA 3.3
--	---	------------------------

Honors

Member of Chi Epsilon, Civil Engineering Honor Society

William N. and Ocie M. Downey Scholarship Recipient 2004-2007

University of Kentucky Civil Engineering Fellowship Recipient 2007-2009

Work History

Student Intern	Radcliff City Hall Storm Water Department	Summer 2005 and 2006
----------------	--	----------------------

Research Assistant	Dr. Jimmy Fox Water Resources UK Civil Engineering	2007-2009
--------------------	--	-----------

Publications and Presentations

Phillips, Jonathan, Sarah McCormack, Jidan Duan, Joseph Russo, Anne Schumacher, Ganesh Tripathi, Ruth Brockman, and Adam Mays. Origin and Interpretation of Knickpoints In the Big South Fork River Basin, Kentucky-Tennessee. Geomorphology. In review, June 2009.

Fox, J.F., Davis, C.M., Russo, J.P., Martin, D. Nitrogen stable isotope temporal variability for fine sediment transported from a lowland watershed. *Journal of Hydrology*, In Review.

Russo, J.P. and Fox, J.F. Investigation of land-use change and hydrologic forcing upon streambank erosion and in-stream sediment processes using a watershed model and sediment tracers. American Society of Civil Engineers Environmental Water Resources Institute 2009 Congress, Kansas City, Missouri, 15-19 May 2009.

Russo, J.P. and Fox, J.F. Investigation of land-use change and hydrologic forcing upon streambank erosion and in-stream sediment processes using a watershed model and sediment tracers. Kentucky Water Resources Annual Symposium, Lexington, KY, March 2, 2009.

Fox, J., Davis, C., Russo, J. and Martin, D. Nitrogen isotopes to study the variability of sediment transported from a lowland watershed in the Bluegrass. Kentucky Water Resources Annual Symposium, Lexington, KY, March 2, 2009.

Russo, J. and Fox, J.F. Study of sediment processes in the South Elkhorn Watershed using HSPF. Kentucky Water Resources Annual Symposium, Lexington, KY, March 17, 2008.